

Bioanalytical applications of real-time ATP imaging via bioluminescence

by

Jason Alan Gruenhagen

A dissertation submitted to the graduate faculty
in partial fulfillment of the requirements for the degree of

DOCTOR OF PHILOSOPHY

Major: Analytical Chemistry

Program of Study Committee:
Edward S. Yeung, Major Professor
Marc D. Porter
Robert S. Houk
Victor S.-Y. Lin
Donald Beitz

Iowa State University

Ames, Iowa

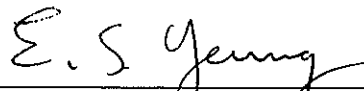
2003

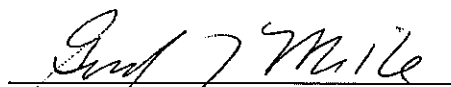
Graduate College
Iowa State University

This is to certify that the doctoral dissertation of

Jason Alan Gruenhagen

has met the dissertation requirements of Iowa State University


Major Professor


For the Major Program

To my parents who always supported and believed in me,
and my wife who has helped make all of my dreams come true.

TABLE OF CONTENTS

ABSTRACT	vi
CHAPTER 1. GENERAL INTRODUCTION	1
Dissertation Organization	1
Introduction Overview	1
ATP	1
Fluorescence Microscopy	6
Our Goal	14
References	15
CHAPTER 2. INVESTIGATION OF G PROTEIN-INITIATED, CA²⁺-DEPENDENT RELEASE OF ATP FROM ENDOTHELIAL CELLS	19
Abstract	19
Introduction	20
Experimental Section	23
Results	27
Discussion	33
Acknowledgements	36
References	37
CHAPTER 3. MONITORING REAL-TIME RELEASE OF ATP FROM MOLLUSCAN CENTRAL NERVOUS SYSTEMS	66
Abstract	66
Introduction	66
Experimental Section	69
Results and Discussion	71
Conclusions	75
Acknowledgements	76
References	76
CHAPTER 4. REAL-TIME IMAGING OF RELEASE OF ENCAPSULATED ATP FROM MCM-41-TYPE MESOPOROUS NANOSPHERES	106
Abstract	106
Introduction	107
Experimental Section	110
Results and Discussion	113
Conclusions	120
Acknowledgements	121
References	121

CHAPTER 5. GENERAL CONCLUSIONS	137
ACKNOWLEDGEMENTS	140

ABSTRACT

The research discussed within involves the development of novel applications of real-time imaging of adenosine 5'-triphosphate (ATP). ATP was detected via bioluminescence from the firefly luciferase-catalyzed reaction of ATP and luciferin. The use of a microscope and an imaging detector allowed for spatially resolved quantitation of ATP release. Employing this method, applications in both biological and chemical systems were developed.

First, the mechanism by which the compound 48/80 induces release of ATP from human umbilical vein endothelial cells (HUVECs) was investigated. Numerous enzyme activators and inhibitors were utilized to probe the second messenger systems involved in release. Compound 48/80 activated a G_q -type protein to initiate ATP release from HUVECs. Ca^{2+} imaging along with ATP imaging revealed that activation of phospholipase C and induction of intracellular Ca^{2+} signaling were necessary for release of ATP. Furthermore, activation of protein kinase C inhibited the activity of phospholipase C and thus decreased the magnitude of ATP release. This novel release mechanism was compared to the existing theories of extracellular release of ATP.

Bioluminescence imaging was also employed to examine the role of ATP in the field of neuroscience. The central nervous system (CNS) was dissected from the freshwater snail *Lymnaea stagnalis*. Electrophysiological experiments demonstrated that the neurons of the *Lymnaea* were not damaged by any of the components of the imaging solution. ATP was continuously released by the ganglia of the CNS for over eight hours and varied from ganglion to ganglion and within individual ganglia. Addition of the neurotransmitters K^+ and serotonin increased release of ATP in certain regions of the *Lymnaea* CNS.

Finally, the ATP imaging technique was investigated for the study of drug release systems. MCM-41-type mesoporous nanospheres were loaded with ATP and end-capped with mercaptoethanol functionalized CdS nanocrystals. Aggregates of nanospheres were bathed in imaging solution, and ATP bioluminescence was monitored to investigate the release kinetics of the nanosphere drug delivery systems. Addition of disulfide bond-cleaving molecules induced uncapping of the nanospheres and subsequently, the release of ATP. Increasing the concentration of the uncapping molecule decreased the temporal maximum and increased the magnitude of release of encapsulated ATP from the nanospheres. Furthermore, the release kinetics from the nanospheres varied with the size of the particle aggregates.

CHAPTER 1. GENERAL INTRODUCTION

Dissertation Organization

This dissertation begins with a general introduction to the fields pertinent to the research presented within. The subsequent chapters are presented as three complete scientific manuscripts including all relevant supporting material. The final chapter contains general conclusions and future aspirations for the work discussed throughout.

Overview

As science evolves into the twenty-first century, the divisions between the fields of chemistry, biochemistry, and biology have become indistinguishable. Moreover, there is an ever-increasing interdependence among scientists from each of these fields. This is exemplified in the study of adenosine 5'-triphosphate (ATP). In this chapter, an overview of ATP, its metabolic functions, and its role as a cellular messenger are presented. Following which, a brief discussion of fluorescence microscopy instrumentation and applications is undertaken. Finally, the application of fluorescence microscopy to the study of ATP is discussed.

ATP

Discovery

ATP was first identified in 1929 by two research groups independently: by Fiske and Subbarow in the United States¹ and by Lohmann in Germany². The structure of ATP was

elucidated three years later³. In that same year, Lohmann and Meyerhoff estimated the energy involved in the breakdown of the rich phosphate-anhydride linkages of ATP⁴. Further studies revealed that ATP was a product of glycolysis⁵, and thus, the central role of ATP in metabolism began to take shape. In 1941, Lipmann hypothesized that ATP was the primary molecule for chemical energy storage and proposed a cycle of ATP production and utilization existed within the cell⁶. In the years that followed, the theories of Lohmann and Lipmann became widely accepted, and the roles of ATP cellular function was solidified.

Functions of ATP

ATP serves numerous vital functions in the cell. First and foremost, it is the central molecule in metabolism. Molecules used as energy sources, for instance glucose, are broken down in the cell, and the energy obtained from them is stored in the phosphate-anhydride bonds of ATP⁷. For example, ATP is created via phosphorylation of adenosine 5'-diphosphate (ADP) in glycolysis. In the Krebs's cycle, guanosine 5'-triphosphate (GTP), which is interchangeable with ATP (see below), is synthesized from guanosine 5'-diphosphate. Furthermore, nicotinamide adenine dinucleotide (NADH) and flavin adenine dinucleotide (FADH₂) are formed in the Krebs's cycle. These molecules are oxidized in the mitochondria. The energy from their oxidation is used to establish a proton gradient across the inner mitochondrial membrane. The primary role of this gradient is to drive the synthesis of ATP by ATP synthase. A similar mechanism is employed in the photosynthetic pathway to couple absorption of light to the synthesis of ATP⁸. The synthesized pool of cellular ATP is utilized to energetically drive numerous cellular processes. For example, the majority of phosphorylation reactions, which are catalyzed by kinases, use ATP as the phosphate donor.

Additionally, ion and molecule transport occurs against charge and concentration gradients through ATPase enzymes, using the breakdown of ATP to ADP and phosphate as the driving force. These generated gradients are used for second messenger signaling (Ca^{2+}) and neurotransmission (K^+ and Na^+) among other cellular processes⁷.

In addition to its role in metabolism, ATP also maintains the proper concentrations of other nucleotides (NTPs). ATP is interchanged into the other NTPs, which are incorporated into DNA and RNA. Furthermore, NTPs serve other imperative functions in cellular homeostasis. For example, GTP couples the activation of many receptors to their induced cellular effects via G-proteins. A third function of ATP is its involvement in various cellular syntheses as a reactant. It is directly incorporated into RNA by RNA polymerases. For synthesis of DNA, ATP is converted to deoxy-ATP prior to incorporation by DNA polymerases. The adenosine of ATP is also incorporated into a number of coenzymes, including FADH_2 , adenosine-3',5'-cyclic monophosphate, NADH, and nicotinamide adenine dinucleotide phosphate⁷.

ATP as a cellular messenger

In the same year that ATP was discovered, Drury and Szent-Gyorgyi reported that extracellular ATP had drastic effects in the cardiovascular system⁹. Throughout the next 50 years, the consequences of extracellular ATP application on numerous cell types were studied. While the majority of these effects were attributed to adenosine¹⁰ and adenosine 5'-monophosphate (AMP)¹¹, by 1972 the distinct consequences of extracellular addition of ATP, ADP, AMP, and adenosine had been established¹².

In 1978, Burnstock established nomenclature for distinguishing adenosine and ATP receptors¹³. Adenosine receptors were termed P1 purinergic receptors; four of these receptors have been identified to date. P2 purinergic receptors, which are the ATP and ADP sensitive receptors, are more numerous and diverse than the P1 type. In 1994, Abbracchio and Burnstock classified P2 purinergic receptors into P2X and P2Y subtypes¹⁴. P2X receptors are ligand-gated ion channel receptors, while P2Y receptors are G protein coupled receptors. Seven P2X and six P2Y receptors have been identified and characterized to date. P2X receptors have been identified mainly in neurons and muscle cells. They respond to nM - μ M concentrations of ATP directly activating depolarizing currents. A few other general trends have been recognized for P2X receptors: 1) they have little selectivity for the various monovalent cations, and 2) they are activated and inactivated on the order of milliseconds. P2Y receptors, conversely, are quite diverse in both the effect of their activation and the agonists to which they respond. The P2Y receptors are classified further into their subtypes based on their response to various agonists, including ATP, ADP, their derivatives, and even the pyrimidine nucleotide UTP¹⁵. Today, they are being reclassified based on their protein sequences¹⁶. P2Y receptors have been identified in nearly every type of cell investigated (see reference 15 for a thorough listing). Activation of the receptors initiates numerous intracellular signaling pathways. All P2Y receptors have been linked to generation of intracellular Ca^{2+} increases via activation of phospholipase C (PLC). Increased Ca^{2+} levels initiate numerous cellular functions, most notably exocytosis and smooth muscle contraction. Secondary consequences of ATP stimulation of PLC include activation of protein kinase C and phospholipase A_2 and production of nitric oxide. Various P2Y receptor subtypes are reportedly also associated with inhibition of adenylate cyclase, which catalyzes production of

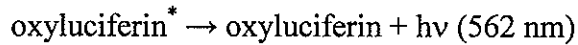
cAMP. Alternatively, the P2Y₁₁ has been linked to activation of adenylate cyclase and therefore production of cAMP¹⁷. cAMP controls various cellular processes by signaling for the phosphorylation and dephosphorylation of numerous enzymes. For example, cAMP controls the cellular production and breakdown of glycogen⁸. Numerous other pathways have been linked to P2Y receptor activation and are discussed in ref 17.

Detection of ATP

The actions of extracellular ATP on cells have been widely documented, as have the presence of the receptors that initiate them. However, the source of ATP release *in vivo* has remained less clear. This likely stems from the lack of suitable methods for monitoring real-time release of ATP on a single cell level. Several methods for detection of ATP have been developed utilizing high performance liquid chromatography (HPLC)¹⁸⁻²¹. Both intracellular and extracellular ATP levels can be detected via lysis or direct sampling of extracellular solution, respectively. Other less common methods for detection of ATP include ³²P radioactivity assays²², ³¹P NMR²³⁻²⁴, enzyme-coupled fluorescence assays for flow injection analysis²⁵, atomic force microscopy²⁶, and patch clamp studies employing a mutant ATP-sensitive K⁺ channel²⁷.

Bioluminescent Detection of ATP

The most common method for the detection of ATP is via the luciferase bioluminescence assay. The reaction employed in the assay is catalyzed by the firefly (*Photinus pyralis*) enzyme luciferase and is shown below.



Along with luciferase, Mg^{2+} is necessary for this reaction. In the reaction, oxyluciferin is formed in an excited state and then quickly relaxes to its ground state releasing a photon. The complete reaction is extremely fast, with the first photons being produced 25 ms after mixing of the components. When a non-saturating concentration of ATP is present, light emission reaches a maximum at 300 ms²⁸. The luciferase reaction is also very efficient, having a quantum efficiency of 0.88. Thus, 88 % of ATP molecules which react with luciferin lead to the production of a photon. This compares well with other common bioluminescence reactions. For example, the quantum efficiency of peroxidase-catalyzed reaction of luminol and hydrogen peroxide is twenty times lower than that of luciferase²⁹. For these reasons, detection of ATP via bioluminescence is very sensitive. ATP concentrations in the low fmole region are routinely detected employing commercially available kits. These kits have been applied in numerous situations, including quantifying intracellular ATP concentrations³⁰⁻³¹ and release of ATP from cultured cells³²⁻³⁴. However, without the concurrent use of an imaging scheme, ATP can only be detected on bulk samples and cannot be monitored in real-time.

Fluorescence Microscopy

Overview

Imaging techniques provide the ability to monitor many samples simultaneously, but separately. When coupled to sensitive and selective detection schemes, these methods afford

the ability to monitor a particular analyte continuously. In the field of biosciences, fluorescence microscopy is an indispensable imaging technique.

Instrumentation

The fluorescence microscope consists of four main components: the light source, wavelength selection optics, microscope objective, and detector. Mercury lamps are the most common source in fluorescence microscopy as they emit strongly over the entire visible and UV regions of the spectrum. The proper excitation wavelength is isolated by inserting a bandpass filter into the light path of the lamp. This filter selects only the wavelength of light necessary for excitation of the fluorescence probe of interest. The excitation light is focused onto the sample through the microscope objective lens. Emitted fluorescence is collected by the same microscope objective. A dichroic mirror is commonly employed to separate the excitation and emission photons. The excitation light enters the microscope 45° incident on the dichroic. This light is reflected 90° and proceeds through the objective to the sample. Since it has longer a wavelength, fluorescence collected from the sample is transmitted through the dichroic mirror to the detector. Another bandpass filter is placed just in front of the detector to eliminate any excitation light or stray light which passed through the dichroic mirror³⁵. Many of the recent advancements in fluorescence microscopy have involved its detectors. Thus, they are discussed in greater detail in the following two sections.

Single Element Detectors

Detection schemes applicable for fluorescence microscopy can be broadly classified as either single- or multi-element. The photomultiplier tube (PMT) is the most commonly employed

single element detector. It has the highest sensitivity of any detector used for fluorescence microscopy. Fluorescence photons collected by the microscope are focused onto the photocathode of the PMT. An incident photon causes ejection of an electron from the photocathode. This electron is accelerated to the first dynode of the PMT by an applied electric field. Upon striking this dynode, the electron induces expulsion of several new electrons because of its high kinetic energy from acceleration. This process continues for all of the dynodes until the photons reach the anode, where the current from the collected electrons is measured. The PMT is extremely sensitive due to the multiplication of signal by the dynodes and the low dark current associated with its operation³⁶. However, the PMT is still a single-element detector and thus cannot offer significant spatial resolution unless coupled with a scanning microscope. For this reason, PMTs are most commonly utilized in confocal microscopy.

Multi-Element Detectors

Utilizing multi-element detectors affords excellent spatial information in fluorescence microscopy. Of the numerous multi-element detectors that exist today, the silicon intensified target (SIT) and charge coupled device (CCD) cameras find the most widespread application. For a SIT, photons are collected on a photocathode where they induce release of an electron, similar to that of the PMT. This electron is accelerated through an electric field where it impacts the silicon target of the SIT. Here electron-hole pairs are formed and stored until they are read out by a sweeping electron beam. SITs yield excellent sensitivity and dynamic range but suffer from two especially severe drawbacks. SITs are prone to target damage if exposed to excessive photons. Moreover, SITs suffer from incomplete readout leading to

residual signal being present in subsequent images³⁷. For these reasons, SITs generally have been replaced by CCDs in fluorescence microscopy. CCDs are solid-state detectors first developed by Boyde and Smith at Bell Labs in 1969. However, they were mainly employed in astronomy until the pioneering work by Denton and colleagues in the early 1980s³⁸⁻³⁹. Photons incident on the CCD create electron-hole pairs upon striking the silicon collection areas. The electrons created are stored in minute voltage-defined areas or pixels of the silicon surface. The stored electrons are then shifted toward and to the output node where they are measured as current. While the CCD does not suffer from the same problems as does the SIT, significant drawbacks of CCDs still exist. For one, CCDs usually contain 100,000 – 1,000,000 individual pixels which need to be individually quantified. Since photons incident on the camera must be blocked during this time, the data acquisition rate suffers. However, this problem was alleviated by the development of frame-transfer cameras. Frame transfer involves transferring an entire image to a separate (read-out) set of pixels. These pixels are quantified while new data are acquired on the original set of pixels. A further disadvantage of CCDs is that they do not have any signal multiplication as do PMTs and SITs and thus lack sensitivity for low level signals. To overcome this limitation, an intensifier plate was integrated into the CCD. Photons incident on this intensified CCD (iCCD) strike the photocathode of the image intensifier and induce expulsion of an electron. This electron is accelerated in the presence of an electric field through a channel towards the CCD collection pixels. The electron collides with the walls of the channel, ejecting several new electrons. This process occurs numerous times within the channel creating many electrons from a single photon. Finally, upon striking the fluorescence screen at the end of the image intensifier, an electron causes a photon to be emitted, which is then collected by

the CCD pixels. ICCDs allow for detection of extremely low light levels, approaching the detection limit of a PMT. However, with the use of an image intensifier comes a loss in spatial resolution, since coupling an image intensifier channel to a single CCD pixel has been unsuccessful to date. Instead there is usually slight cross-talk amongst a few pixels from a single intensifier channel^{37,40}. A relatively new development in CCD detection is the use of an image intensifier during data read-out rather than collection. Roper Scientific utilized electron acceleration through a series of dynodes prior to quantitation at the output node⁴¹. Though still in its infancy, this amplification scheme has shown great potential in the field of CCDs.

Cell Calcium

One of the most common applications of fluorescence microscopy is monitoring intracellular calcium (Ca^{2+}) concentrations. Ca^{2+} is an extremely important mediator of cell function. It is maintained at low concentrations in the cytoplasm of a cell. Ca^{2+} is instead stored inside the endoplasmic reticulum and mitochondria of the cell as well as in the extracellular matrix between cells. Upon stimulated release into the cytoplasm, Ca^{2+} activates numerous cellular pathways while inhibiting others. Essential bioprocesses such as exocytosis, initiation of embryonic development in a newly formed zygote, and muscle contraction are all Ca^{2+} -dependent⁸. Thus, monitoring cellular Ca^{2+} levels has been of acute interest to scientists.

Ca^{2+} Indicator Dyes

The development of synthetic Ca^{2+} -sensitive dyes ushered in the widespread application of cellular imaging in live cells. Tsien and coworkers developed the first such indicator, Quin-

²⁴². This compound was followed by the development of superior indicators such as indo-1 and fluo-3⁴³. These compounds, which are not fluorescent in their uncomplexed form, become highly fluorescent in the presence of Ca^{2+} . Fura-2 is a Ca^{2+} indicator which has found widespread use recently because it allows for quantitation. By measuring the ratio of fluorescence at 340 and 380 nm, the ratio of uncomplexed to complexed fura-2 can be attained. This ratio is quantitative for Ca^{2+} over a large range of concentrations. One difficulty with all of these Ca^{2+} indicators is that they are negatively-charged and thus cannot pass through the phospholipid membrane of a cell. Hence, microinjection is the only plausible method for obtaining sufficient levels of the indicator in the cells. However, microinjection is time-consuming, difficult, and not amenable to all cell types⁴⁴. This obstacle was overcome by the development of acetoxymethyl (AM) ester forms of the above dyes. Since the AM ester indicators are neutral compounds, they can pass through the plasma membrane into the cytoplasm of a cell⁴⁵. There the AM ester is cleaved from the indicator by cellular phosphodiesterase enzymes. The resultant carboxyl form of the dye is again impermeable to the plasma membrane but this time is trapped inside the cell. The dye concentration builds up in the cell to levels much higher than that in the loading solution⁴⁴. Detection of Ca^{2+} /indicator fluorescence was first accomplished from a suspension of cells on a luminometer with a PMT detector. However, much of fluorescence microscopy now involves monitoring Ca^{2+} levels with a CCD. Through the proper choice of wavelength selecting optics, Ca^{2+} signaling can be obtained in real-time for numerous cells simultaneously. Thus, intercellular communication can be investigated by monitoring the Ca^{2+} response of cells to the stimulation of an adjacent cell. Alternatively, through use of a high magnification objective, Ca^{2+} release can be monitored spatially within a single cell.

Neurotransmitter Imaging

Neurotransmission represents one of the most important processes in the body. Likewise, it is also one of the most complex. Neuroscientists have acute interest in monitoring real-time, spatially-resolved release of neurotransmitters. However, most neurotransmitters, including glutamate, acetylcholine, epinephrine, norepinephrine, serotonin, and the oligopeptide transmitters, lack fluorophores for detection with traditional fluorescence microscopy. Numerous alternative methods for detection of neurotransmitters have been recently reported in the literature. Many of these applications are discussed in chapter 3 of this dissertation. Several advances in fluorescence microscopy for the detection of neurotransmitters have also been achieved over the past ten years. In general, these techniques have involved detection of native fluorescence from neurotransmitters. Because neurotransmitters lack the efficient fluorophores of dyes, lasers are employed as light sources for native fluorescence detection in fluorescence microscopy. In 1995, Tan and colleagues monitored uptake of serotonin by astrocytes by native fluorescence microscopy. They discovered that various areas within a singular astrocyte uptake and release different quantities of serotonin⁴⁶. In further studies, Lillard and Yeung investigated exocytosis from mast cells was stimulated with polymyxin. Serotonin was secreted in large initial bursts followed by a prolonged plateau level of release⁴⁷. With the development of iCCD for detection of lower light samples, other neurotransmitter detection schemes have arisen for fluorescence microscopy. Tong and Yeung reported the visualization of catecholamine release from chromaffin cells with native fluorescence using the 275 nm line of an Ar⁺ ion laser. Great heterogeneity was observed amongst various cells and within individual cells⁴⁸. Wang and coworkers developed a

method to detect glutamate in fluorescence microscopy. The enzyme glutamate dehydrogenase (GDH) was employed to catalyze the formation of NADH in the presence of glutamate. NADH, which is highly fluorescent, was detected with an iCCD. The release of glutamate from cultured neurons was detected upon stimulation with K^+ ,⁴⁹⁻⁵⁰.

Bioluminescent Imaging of ATP

Previously in our group, bioluminescent detection of ATP was coupled with real-time imaging on a microscope. Because detection of ATP was based on bioluminescence rather than fluorescence, neither a light source nor wavelength selection optics were necessary for these experiments. With no light source, the majority of the noise involved with standard fluorescence microscopy is removed, including both scattering of the source light and autofluorescence from the biological sample. Furthermore, the removal of the wavelength selection optics eliminates loss of signal light due to reflections at the filter surfaces. By using an iCCD cooled to -30°C to eliminate dark noise, detection of ATP was performed in a \sim zero noise environment. Thus, detection of standards down to 10 nM ATP was accomplished with their set up. This method was applied to the detection of ATP release from physically stimulated astrocytes. Furthermore, intracellular Ca^{2+} levels were monitored simultaneously with ATP imaging via laser-induced fluorescence on every other frame of data. From these analyses, an IP_3 -sensitive, Ca^{2+} -insensitive ATP release mechanism was elucidated. Furthermore, extracellularly released ATP was unequivocally shown to signal intracellular Ca^{2+} signaling in nearby astrocytes⁵¹. Since this first report of ATP detection via fluorescence microscopy, several other investigators have employed this scheme for analysis of ATP release in various environments⁵²⁻⁵⁴.

Chemical Imaging of ATP

The properties that make real-time imaging of ATP release appealing on the single cell level are also attractive in chemical imaging. Biocompatible mesoporous nanospheres are being designed to reversibly entrap drug compounds. Characterization of the encapsulation and release properties of these particles is imperative to their development. ATP is a potentially suitable probe molecule for these investigations. Nanospheres have dimensions on order of a single micron or less, compared to 10 μm for an average eukaryotic cell. Thus, an imaging technique would allow the simultaneous monitoring of release from numerous nanospheres individually. Furthermore, the high speed and sensitivity of ATP bioluminescence imaging with an iCCD allow for monitoring release on the second – millisecond timescale. ATP is also an excellent probe molecule because it is a biological compound and is employed in the treatment and diagnosis of numerous ailments⁵⁵.

Our Goal

The importance of ATP in bioanalytical sciences has been thoroughly underscored throughout this introduction. The ATP imaging technique developed in our lab by Wang and coworkers possesses several properties make it potentially useful in innumerable systems. Our goal was to investigate just a few of the possible applications of real-time ATP imaging for *in vitro* biopathway investigation, *in vivo* cellular signaling, and fundamental chemical analysis.

References

1. Fiske, C. H., Subbarow, Y. *Science* **1929**, *70*, 381-382.
2. Lohmann, K. *Naturwissenschaften* **1929**, *17*, 624-625.
3. Lohmann, K. *Biochem. Z.* **1932**, *254*, 381.
4. Myerhof, O., Lohmann, K. *Biochem. Z.* **1932**, *253*, 431.
5. Lohmann, K. *Biochem. Z.* **1934**, *271*, 120.
6. Lipmann, F. *Adv. Enzymol.* **1941**, *1*, 99.
7. Bridger, W. A., Henderson, J. F. *Cell ATP*; John Wiley and Sons: New York, 1983.
8. Voet, D., Voet, J. G. *Biochemistry*; 2nd ed. John Wiley and Sons: New York, 1995.
9. Drury, A., Szent-Gyorgyi, A. *J. Physiol.* **1929**, *68*, 213-237.
10. Lindler, F., Rigler, R. *Pflugers Arch.* **1931**, *226*, 697-708.
11. Hoffman, W. S. *J. Biol. Chem.* **1930**, *63*, 675.
12. Moir, T. W., Downs, T. D. *Am. J. Physiol.* **1972**, *222*, 1386-1390.
13. Burnstock, G. In *Cell Membrane Receptors for Drugs and Hormones: A Multidisciplinary Approach*; ed. Straub, R. W., Bolis, L., Raven: New York, 1978, 107-118.
14. Abbracchio, M. P., Burnstock, G. *Pharmacol. Ther.* **1994**, *64*, 445-475.
15. Dubyak, G. R., El-Moatassium, C. *Am. J. Physiol.* **1993**, *265*, C577-C606.
16. Kunapuli, S. P., Daniel, J. L. *Biochem. J.* **1998**, *336*, 513-523.
17. von Kugelgen, I., Wetter, A. *Naunyn-Schmiedeberg's Arch. Pharmacol.* **2000**, *362*, 310-323.
18. Brown, P. R., Krstulovic, A. M., Hartwick, R. A. *Adv. Chromatogr.* **1980**, *18*, 101-138.

19. Chapman, A. G., Westerberg, E., Siesjo, B. K. *J. Neurochem.* **1981**, *36*, 179-189.
20. Reiss, P. D., Zuurendonk, P. F., Veech, R. L. *Anal. Biochem.* **1984**, *140*, 162-71.
21. Formato, M., Masala, B., De Luca, G. *Clin. Chim. Acta* **1990**, *189*, 131-137.
22. Cogoli, J. M., Dobson, J. G. Jr. *Anal. Biochem.* **1981**, *110*, 331-337.
23. McLaughlin, A. C., Takeda, H., Chance, B. *Proc. Natl. Acad. Sci. U. S. A.* **1979**, *76*, 5445-5449.
24. Berkowitz, B. A., Balaban, R. S. *Magn. Reson. Med.* **1989**, *12*, 249-252.
25. Hansen, E. H., Gundstrup, M., Mikkelsen, H. S. *J. Biotechnol.* **1993**, *31*, 369-380.
26. Schneider, S. W., Egan, M. E., Jena, B. P., Guggino, W. B., Oberleithner, H., Geibel, J. P. *Proc. Natl. Acad. Sci. U. S. A.* **1999**, *96*, 12180-12185.
27. Gribble, F. M., Loussouarn, G., Tucker, S. J., Zhao, C., Nichols, C. G., Ashcroft, F. M. *J. Biol. Chem.* **2000**, *275*, 30046-30049.
28. McElroy, W. D., DeLuca, M. *Bioluminescence and Chemiluminescence: Basic Chemistry and Analytical Applications*; Academic Press: New York, 1981, 179-196.
29. Chiu, N. H. L., Christopoulos, T. K. *Clinical Chemistry* **1999**, *45*, 1954-1959.
30. Dellian, M., Walenta, S., Kuhnle, G. E., Gamarra, F., Mueller-Klieser, W., Goetz, A. E. *Int. J. Cancer* **1993**, *53*, 785-791.
31. Kretschmar, M., Nichterlein, T., Kuntz, P., Hof, H. *Diagn. Microbiol. Infect. Dis.* **1996**, *25*, 117-121.
32. Cotrina, M. L., Lin, J. H., Alves-Rodrigues, A., Liu, S., Li, J., Azmi-Ghadimi, H., Kang, J., Naus, C. C., Nedergaard, M. *Proc. Natl. Acad. Sci. USA* **1998**, *95*, 15735-15740.

33. Taylor, A. L., Kudlow, B. A., Marrs, K. L., Gruenert, D. C., Guggino, W. B., Schwiebert, E. M. *Am. J. Physiol.* **1998**, *275*, C1391-C1406.
34. Ostrom, R. S., Gregorian, C., Insel, P. A. *J. Bio. Chem.* **2000**, *275*, 11735-11739.
35. Herman, B. *Fluorescence Microscopy*; 2nd ed. Bios Scientific: New York, 1998.
36. Ingle, J. D. Jr., Crouch, S. R. *Spectrochemical Analysis*; Prentice Hall: Englewood, NJ, 1988.
37. Mason, W. T., ed. *Fluorescent and Luminescent Probes for Biological Activity*; Academic Press: London, 1993.
38. Sweedler, J. V., Bilhorn, R. B., Epperson, P. M., Sims, G. R., Denton, M. B. *Anal. Chem.*, **1988**, *60*, 282A-291A.
39. Epperson, P. M., Sweedler, J. V., Bilhorn, R. B., Sims, G. R., Denton, M. B. *Anal. Chem.*, **1988**, *60*, 327A-335A.
40. Periasamy, A., ed. *Methods in Cellular Imaging*; Oxford University Press: Oxford, 2001.
41. http://roperscientific.com/cascade_5_reasons.html
42. Tsien, R. Y. *Biochemistry* **1980**, *19*, 2396-2404.
43. Grynkiewicz, G., Poenie, M., Tsien, R. Y. *J. Biol. Chem.* **1985**, *260*, 3440-3450.
44. Rizzuto, R., Fasolato, C. eds. *Imaging Living Cells*; Springer –Verlag: Berlin, 1998.
45. Tsien, R. Y., Pozzan, T., Rink, T. J. *J. Cell. Biol.* **1982**, *94*, 325-334.
46. Tan, W., Parpura, V., Haydon, P. G., Yeung, E. S. *Anal. Chem.* **1995**, *67*, 2575-2579.
47. Lillard, S. J., Yeung, E. S. *J. Neurosci. Methods* **1997**, *75*, 103-109.
48. Tong, W., Yeung, E. S. *Appl. Spectrosc.* **1998**, *52*, 407-413.
49. Wang, Z., Yeung, E. S. *J. Chromatogr. B*, **1997**, *695*, 59-65.

50. Wang, Z., Yeung, E. S. *Appl. Spectrosc.* **1999**, *53*, 1502-1506.
51. Wang, Z., Haydon, P. G., Yeung, E. S. *Anal. Chem.* **2000**, *72*, 2001-2007.
52. Hashimoto, M., Shinozuka, K., Sasaki, T., Tanaka, N., Hossain, S., Kubota, Y., Tamura, K., Shido, O., Kunitomo, M. *Eur. J. Pharmacol.* **2001**, *416*, 179-183.
53. Newman, E. A. *J. Neurosci.* **2001**, *21*, 2215-2223.
54. Arcuino, G., Lin, J. H., Takano, T., Liu, C., Jiang, L., Gao, Q., Kang, J., Nedergaard, M. *Proc. Natl. Acad. Sci. U. S. A.* **2002**, *99*, 9840-9845.
55. Agteresch, H. J., Dagnelie, P. C., van den Berg, J. W., Wilson, J. H. *Drugs* **1999**, *58*, 211-232.

CHAPTER 2. INVESTIGATION OF G PROTEIN-INITIATED, CALCIUM-DEPENDENT RELEASE OF ATP FROM ENDOTHELIAL CELLS

A manuscript prepared for submission to The American Journal of Physiology

Jason A. Gruenhagen* and Edward S. Yeung

* Primary researcher and author

ABSTRACT

Extracellular ATP is an important mediator of communication among endothelial cells. ATP binds to purinergic receptors that regulate Ca^{2+} signaling, nitric oxide production, and cAMP levels. While the effects of extracellular ATP stimulation on endothelial cells are well documented, the source and mechanism by which ATP is released have not been examined thoroughly. In this study, we investigated G protein-stimulated release of ATP from human umbilical vein endothelial cells (HUVECs) using the G protein stimulant compound 48/80. Application of compound 48/80 resulted in dose-dependent ATP evolution from cultured HUVECs. This release of ATP was not cytotoxic as demonstrated by a lactate dehydrogenase (LDH) toxicity assay and the ability of the cells to load and retain the viability dye calcein following stimulation. Mastoparan also stimulated release of ATP, further suggesting the process was G-protein initiated. This G protein was insensitive to pertussis toxin (PTX) and appeared to be of the G_q -subtype. The ATP efflux was completely

abolished in the presence of EGTA and thapsigargin, signifying a strict Ca^{2+} dependence. Furthermore, compound 48/80-induced ATP release was significantly decreased in cells pretreated with the phospholipase C (PLC) inhibitor U73122. Thus, the release pathway appears to proceed through an increase in intracellular Ca^{2+} via PLC activation.

Additionally, the G protein-initiated release of ATP was attenuated by pretreatment of the cells with either phorbol ester or indolactam V, activators of protein kinase C. Finally, this release was not affected by treating HUVECs with nitric oxide synthase inhibitors or glybenclamide. We compared these results to the existing theories of cellular ATP release, and they correlated best with release via a non-specific plasma membrane channel.

INTRODUCTION

The role of ATP as an intercellular messenger has attracted widespread interest over the past ten years. The binding of ATP to purinergic receptors on the surface of cells initiates receptor-mediated responses. These purinergic receptors are classified into two categories: ion channel-coupled P2X type and G protein-coupled P2Y type. P2 receptors are further classified by their pharmacological and genetic properties (1, 2). Their activation initiates several different second messenger pathways in many types of cells, including neurons, smooth muscle cells, mast cells, and epithelial cells (3). The most thoroughly investigated of these pathways is the elevation of intracellular Ca^{2+} levels via activation of PLC and subsequent production of inositol (1,4,5) triphosphate (IP_3). IP_3 binds to receptors on the endoplasmic reticulum, releasing stored Ca^{2+} . Increasing intracellular Ca^{2+} initiates/regulates numerous cellular responses, such as insulin secretion in β -cells (4), synaptic transmission in neurons (5, 6), mast cell degranulation (7), and platelet aggregation at injury sites (8).

ATP signaling in endothelial cells appears to be important for proper endothelium function. Activation of endothelial cells by ATP *in vitro* has been shown to increase cytosolic Ca^{2+} levels and consequently to cause production of nitric oxide (NO) (9). NO regulates endothelium vascular tone, inhibits platelet aggregation, and reduces vascular smooth muscle proliferation in the cardiovascular system (10). Ca^{2+} signaling also activates secretion of von Willebrand factor from the Weibel-Palade bodies, the main exocytotic vesicle in endothelial cells (11). A number of other important effects occur in endothelial cells upon increase of intracellular Ca^{2+} , including release of prostacyclin and endothelin-1 and an enhancement in microvascular permeability (see reference 12 for a review).

While much is known about the stimulatory effects of ATP on endothelial cells, the source of this ATP is unclear. One possibility is secretion of ATP stored in exocytotic vesicles. A number of researchers have reported ATP being copackaged with either norepinephrine or acetylcholine in neuronal synaptic vesicles where it acts as a fast excitatory neurotransmitter (13 - 15). Vesicular release of ATP has also been observed in chromaffin cells and epithelial cells (15), but has yet to be reported in endothelial cells. The cytoplasm is the other obvious source for release. Under extreme circumstances, ATP may be liberated from a cell's cytoplasm following lysis. However, recent evidence suggests that release of ATP from the cytosolic pool may also occur in a regulated, non-cytotoxic manner. ATP is reported to be released from many cell types via ATP binding cassette proteins, such as the cystic fibrosis transmembrane conductance regulator (CFTR) chloride channel (16). The concept of this ion channel being able to pass a large highly charged molecule like ATP is at this time highly controversial, and numerous researchers have reported conflicting results on the matter (15, 17).

Mechanical stimulation also results in release of ATP in numerous cell lines (18 - 20). Stout et al. have recently postulated that ATP is released through connexin proteins in mechanically stimulated astrocytes (21). Connexins commonly form gap junctions between cells, but can also form channels to the extracellular matrix termed hemichannels (22). The presence of hemichannels and their ability to release small dye molecules has been known for some time. Cotrina and coworkers previously discovered that C6 glioma cells with increased connexin43 expression release larger amounts of ATP than do control cells (19). A recent report by Arcuino et al. lends support to this proposed release mechanism (23). They note that release of ATP from the cytoplasmic pool represents a viable method for cellular communication in nonexcitable cells. Furthermore, numerous surrounding cells can be influenced by the release of ATP in this manner, because the concentration of ATP in the cytoplasm is ~2 mM (23).

In this study, we performed experiments on human umbilical vein endothelial cells, a popular model for the investigation of endothelium function. The G protein agonist compound 48/80 was employed to stimulate release of ATP from HUVECs. Bioluminescence produced by the reaction of luciferin and ATP in the presence of firefly luciferase was monitored in real-time on a microscope equipped with an intensified CCD. Ca^{2+} imaging was conducted on the same set up and served in both experimental and control capacities. G protein initiated-ATP efflux from HUVEC cultures was dose-dependent and occurred concurrently with an increase in intracellular Ca^{2+} levels. Several of the key enzymes and second messengers involved in this ATP release mechanism were identified, and release in HUVECs was compared to other proposed pathways.

EXPERIMENTAL SECTION

Chemicals- Compound 48/80, thapsigargin, and EGTA were purchased from Sigma (St. Louis, MO). Firefly luciferase (from *Photinus pyralis*) and D-luciferin were obtained from both Sigma and R & D Systems (Minneapolis, MN). BAPTA AM, fluo-3 AM, calcein AM, and Pluronic F-127 were from Molecular Probes (Eugene, OR). U73122 (1-[6-((17 β)-3-methoxyestra-1,3,5(10)-trien-17-yl]amino)hexyl]-1H-pyrrole-2,5-dione) and U73343 (1-[6-((17 β)-3-methoxyestra-1,3,5(10)-trien-17-yl]amino)hexyl]-2,5-pyrrolidinedione) were purchased from both Calbiochem (La Jolla, Ca.) and Sigma. All other drugs were from Calbiochem. U73122, U73343, phorbol-12-myristate-13-acetate (PMA), Go6893, bisindolylmaleimide (BIM), indolactam V, thapsigargin, BAPTA AM, fluo-3 AM, and calcein AM were dissolved in dimethylsulfoxide (DMSO, Sigma) as stock solutions. BAPTA AM, fluo-3 AM, and calcein AM were diluted 1000-fold in buffer containing 0.1 % Pluronic F-127 (20% in DMSO) to aid in solubilization of the dye. All other drugs were diluted to the pretreatment concentration in imaging buffer. The concentration of DMSO in pretreatment solutions never exceeded 0.3%.

Cell Cultures- Human umbilical vein endothelial cells (HUVECs) were purchased from American Type Culture Collection (Manassas, VA). Cells were grown in Medium 199 (Life Technologies, Rockville, MD) supplemented with 10% fetal bovine serum, 100 U/ml penicillin, and 100 μ g/ml streptomycin. Cells were plated on 22 x 22 mm square coverslips coated with poly-L-lysine (Sigma) substrate. Teflon O-rings (Small Parts, Inc., Logansport, IN) were attached to coverslips with Sylgard 184 (Dow Corning, Midland, MI) prior to coating with poly-L-lysine and acted as solution chambers. Cells were grown at 37°C in an atmosphere of 95% air-5% CO₂. Prior to stimulation, cells were rinsed with buffer (135 mM

NaCl, 5 mM KCl, 2 mM MgCl₂, 2 mM CaCl₂, 10 mM HEPES (4-(2-hydroxyethyl)-1-piperazineethanesulfonic acid) and 10 mM glucose (pH = 7.3)). In experiments performed with buffers containing different concentrations of Ca²⁺, the ionic strength of the solution was maintained by varying the sodium concentration accordingly. Experiments were conducted only on confluent cultures. Experiments were performed on cultures between 15 and 25 total passages.

ATP Imaging- ATP imaging was performed on the stage of an inverted microscope (Axiovert 100 TV, Zeiss, Germany). Bioluminescence signal was collected with a Zeiss Apochromat 20X microscope objective (NA = 0.75) and detected with an intensified charge-coupled device (iCCD; EEV 576 x 384 pixels CCD chip, Roper Scientific, Trenton, NJ) attached to the camera mount of the microscope. Cells were incubated in 100 µl buffer containing 100 µg/ml firefly luciferase and 205 µM D-luciferin. Images were collected at a frequency of 1.33 Hz with 500 ms exposure times. All experiments were performed at room temperature. Stimulant was applied to the cells via a 10 µl Hamilton syringe in the first ten frames of the collected images. The camera offset was removed by subtracting an image file collected with the camera shutter closed.

Ca²⁺ Imaging- The same experimental set up was utilized for Ca²⁺ imaging as was used for ATP imaging. HUVECs were loaded for 50 min at room temperature with 8.85 µM fluo-3 AM in buffer with reduced Ca²⁺ (200 µM). The cells were then incubated, also at room temperature, for an additional 30 min in buffer to allow for complete de-esterification of the fluo-3. Excitation was accomplished using a Zeiss Atto Arc HBO 100 W mercury lamp with a 475 +/- 20 nm bandpass filter. Fluorescence emission was isolated via a 505 nm dichroic mirror and a 530 +/- 18 nm bandpass filter prior to detection with the iCCD. No

autofluorescence was detected at the wavelengths utilized. The exposure time of the iCCD and the power of the mercury lamp were varied based on the efficiency of the fluo-3 loading of each individual coverslip.

Cytotoxicity Assay- LDH assays (Sigma) were performed at room temperature on a UV-VIS absorbance spectrometer (HP 8452A Diode Array Spectrophotometer, Hewlett Packard, Palo Alto, CA). Coverslips were rinsed with buffer three times at 15-minute intervals. The final rinse from each coverslip was collected as a background sample. Compound 48/80, A23187, or buffer was added to each coverslip and then sampled after 10 minutes. The LDH content was determined by adding the assay solution (50 μ l) to each sample (100 μ l) and allowing the assay reaction to proceed for 25 min. The assay reaction involves the reduction of NAD^+ to NADH by LDH. NADH then reduces a colorless tetrazolium dye to its colored form. The reaction was halted with 1 M HCl (15 μ l), and the peak absorbance of each sample was evaluated from 480-500 nm to quantitate LDH. For control coverslips (buffer as stimulant), an additional step was performed. After the background and experimental samples were obtained, 20 μ M digitonin was added to the coverslip to achieve total lysis of the cells. Complete cell lysis was estimated by optically observing the morphological change of digitonin-stimulated cells. The digitonin-treated sample was diluted with buffer until its absorbance neared that of the compound 48/80 and A23187-treated samples. This sample was assayed identically to the others and served as the maximum releasable LDH.

Calcein Loading Efficiency- Calcein loading efficiency was carried out on the same fluorescence microscope setup as was used for Ca^{2+} imaging. Dishes containing HUVECs were stimulated with compound 48/80 or control (buffer). After 15 min, the cells were

rinsed and incubated in buffer containing 1 μM calcein AM for 45 min at room temperature and in buffer for 20 min at room temperature to allow for loading and complete de-esterification of calcein, respectively. Cell viability was expressed as the percent of cells able to load calcein.

Calcein Leakage- Again the same instrumental set-up was employed for calcein leak experiments as for Ca^{2+} imaging. Dishes of HUVECs were loaded with 1 μM calcein AM in buffer for 45 min at room temperature. After incubation in buffer for 20 min to allow de-esterification of the dye, compound 48/80 or buffer was added to the dishes. The number of cells exhibiting fluorescence was monitored prior to and following stimulation. The percent of calcein-loaded cells maintaining fluorescence was reported for both compound 48/80 and buffer-stimulated dishes.

Data Presentation/Analysis- Bioluminescence and fluorescence signal were obtained and processed with Winview32 software (Roper Scientific). The mean bioluminescence signal was calculated for each frame of data. The net ATP signal was calculated by subtracting the pre-stimulation average signal from the maximum ATP signal. Except in the dose response curve, ATP data are reported as the percent counts of the experimental versus the control (compound 48/80 stimulation of untreated dishes, unless otherwise noted). For temporal responses, the initiation and maximal times represent the 10% and 90% maximal signals. Calcium fluorescence images were analyzed by subtracting a pre-stimulation image from all post-stimulation images. A cell was deemed as having signal only if its fluorescence after stimulation was ten times the background standard deviation. Identical processing was performed for calcein images except that the post-stimulation image was subtracted from a pre-stimulation image for calcein leak experiments. Standard errors were determined for

LDH assay are depicted in Table 1A. Compound 48/80-induced release of LDH was almost two orders of magnitude lower than that obtained from cell lysis. Furthermore, the LDH levels obtained for compound 48/80 stimulation were not significantly different than those obtained for stimulation with A23187 or buffer. The possible cytotoxic effects of compound 48/80 were further examined with the cell viability dye calcein AM. HUVECs were able to load and maintain calcein dye both prior to and after exposure of HUVECs to 15 $\mu\text{g/ml}$ compound 48/80 (Table 1B). A second test for cytotoxicity using calcein is the ability of a cell to maintain the loaded dye upon stimulation. When 15 $\mu\text{g/ml}$ compound 48/80 was added to calcein-loaded HUVECs, 48.9 \pm 9.8 % of the cells failed to maintain calcein fluorescence (Table 1C). Taken together, the three assays suggest that upon stimulation with compound 48/80 the HUVEC membrane is permeable to calcein (622 Da) but not LDH (134 kDa). This permeability to calcein is not permanent and ceases upon removal of compound 48/80.

Next we attempted to confirm that a G protein was indeed the initiation site for compound 48/80-induced ATP release. Direct stimulation of HUVECs with another G protein stimulant, mastoparan, also produced significant release of ATP. As shown in Figure 2 (A and B), mastoparan produced 67.2 \pm 10.8 % (N = 3) as much ATP release as did compound 48/80. The onset of ATP release (38.4 \pm 5.8 s and 104.1 \pm 8.1 s, N = 4) was similar to that of compound 48/80-induced release. PTX, an inhibitor of G_i and G_o but not G_q proteins, was utilized to further investigate the involvement of G proteins in initiating release of ATP. As shown in Figure 2 (A and B), overnight incubation of HUVECs with PTX did not alter the magnitude of compound 48/80-evoked ATP efflux (95.2 \pm 13.9 % (N = 22) of buffer-pretreated HUVECs). Furthermore, PTX treatment did not significantly

affect the temporal onset (43.8 ± 3.0 s, $N = 22$) of G protein-initiated release of ATP. Thus a G_q protein is the probable initiation site for compound 48/80-induced ATP efflux.

Addition of compound 48/80 to HUVECs also stimulated increases in intracellular Ca^{2+} as depicted in Figure 3A. 83.7 ± 3.3 % of cells responded with increased Ca^{2+} levels upon addition of $15 \mu\text{g/ml}$ compound 48/80 ($N = 15$). The temporal onset and maxima of Ca^{2+} increase were 37.3 ± 1.5 s and 51.2 ± 1.9 s ($N = 42$). The temporal onset of both Ca^{2+} and ATP release were quite similar. Thus, the ATP and Ca^{2+} responses were further investigated to determine whether: 1) the Ca^{2+} increase was the result of ATP release, 2) the Ca^{2+} increase was necessary for the release of ATP, or 3) the two were simply two parallel results of the same stimulation. Thapsigargin (Tg), an inhibitor of Ca^{2+} ATPases, was employed to deplete intracellular Ca^{2+} stored within the ER, and $100 \mu\text{M}$ EGTA in Ca^{2+} -free buffer was used to remove the extracellular Ca^{2+} source. As depicted in Figure 3 (B and C), compound 48/80-stimulated cells pretreated for 20 min with both Tg and Ca^{2+} -free buffer did not release significant amounts of ATP (5.9 ± 2.7 % of control, $N = 6$). Also, the temporal onset of ATP release under these conditions was significantly delayed (initiation at 84.6 ± 10.7 s) for HUVECs that did exhibit ATP release. Ca^{2+} imaging confirmed that under Ca^{2+} -free conditions compound 48/80 did not cause significant Ca^{2+} increases (3.2 ± 2.3 % of cells responded, $N = 9$) in HUVECs as shown in Figure 3 (D and E). These data suggest that G protein-initiated release of ATP from HUVECs is strictly Ca^{2+} dependent.

Based on these results, the possibility that increasing intracellular Ca^{2+} levels alone was sufficient for initiating ATP efflux from HUVECs was investigated. Exposure of cells to the Ca^{2+} ionophore A23187 ($10 \mu\text{M}$) in buffer containing 4 mM $CaCl_2$ (double that of the

control imaging buffer) failed to stimulate significant release of ATP without the addition of compound 48/80. As shown in Figure 3 (B and C), A23187 caused 5.2 +/- 0.3 % (N = 3) of the ATP release as did 15 µg/ml compound 48/80, while buffer alone produced 4.5 +/- 1.7 % (N = 3). Ca^{2+} imaging demonstrated that intracellular Ca^{2+} was increased in 89.6 +/- 0.6 % (N = 3) of cells, as depicted in Figure 3 (D and E). Likewise, direct stimulation of HUVECs with 5 µM thapsigargin increased intracellular Ca^{2+} levels in 92.1 +/- 4.2 % (N = 3) of cells (Figure 3 (D and E)), but was unable to induce release of ATP (4.8 +/- 0.7 % (N = 3) versus release caused by compound 48/80), as illustrated in Figure 3 (B and C). These experiments provide evidence that ATP release from HUVECs was dependent not only on increased intracellular Ca^{2+} levels, but also on at least one other as of yet unidentified factor.

Next, experiments were conducted to determine whether the Ca^{2+} -based control of G protein-initiated ATP release in HUVECs was exerted through the well-established phospholipase C/IP₃ pathway. Prior to stimulation, cells were incubated for 30 min in imaging buffer containing either U73122 or U73343, an inhibitor of phospholipase C and its inactive analog, respectively. When stimulated with compound 48/80 under extracellular Ca^{2+} -free conditions, ATP release from HUVECs was significantly inhibited in cells pretreated with U73122 (12.7 +/- 3.4 % of cells pretreated with U73343, N = 6) as shown in Figure 4 (A and B). When extracellular Ca^{2+} was restored and EGTA was removed, U73122 still attenuated stimulated ATP release but to a lesser degree (20.9 +/- 8.9 % of U73343 treated cells, N = 4). Ca^{2+} imaging confirmed that intracellular Ca^{2+} signaling was reduced in compound 48/80-stimulated HUVECs pretreated with U73122 with and without extracellular Ca^{2+} present. As shown in Figure 4 (C and D), 64.6 +/- 10.6 % (N = 4) of cells responded with increased Ca^{2+} when cells were pretreated with U73122 compared to 81.4 +/- 4.1 % (N

= 8) of cells pretreated with U73343. Additionally, when Ca^{2+} was removed, only 25.0 +/- 10.6 % (N = 12) of U73122 treated cells responded with increased Ca^{2+} versus 67.7 +/- 16.0 % (N = 4) for U73343. The temporal initiation of ATP release was extended slightly in cells pretreated with U73122 (49.5 +/- 9.1 s and 49.4 +/- 12.3 s under Ca^{2+} -free conditions and Ca^{2+} -present conditions, respectively), for those cells in which release was detected (3 of 7 for U73122 under Ca^{2+} -free conditions and 5 of 7 for U73122 under Ca^{2+} -present conditions). Moreover, U73343 did not appear to affect ATP or Ca^{2+} signaling. The temporal response of compound 48/80-stimulated cells pretreated with U73343 with and without Ca^{2+} present were not significantly different than those obtained for buffer and EGTA treatment, respectively (data not shown). Together with the earlier experiments, these results suggest that G protein-activated release of ATP proceeds via activation of phospholipase C and subsequent increases in intracellular Ca^{2+} .

The protein kinase C dependence of G protein-initiated ATP release was also examined. Phospholipase C, which produces IP_3 , additionally generates diacylglycerol (DAG). When activated by DAG, protein kinase C modulates Ca^{2+} signaling in HUVECs (24) and thus could be involved in ATP release. As illustrated in Figure 5 (A and B), pretreatment with neither bisindolylmaleimide (BIM) nor Go6893, both inhibitors of PKC, altered the magnitude of compound 48/80-stimulated release of ATP (102.8 % +/- 4.9, N = 7 and 95.1 % +/- 8.9, N = 6 of controls, respectively). Likewise pretreatment with BIM or Go6893 did not significantly affect the temporal onset of ATP release. Hence, activation of PKC did not appear to be necessary for compound 48/80-induced release of ATP. Next, the effect of PKC activation on ATP efflux was studied using the PKC activators phorbol-12-myristate-13-acetate (PMA) and indolactam V. Figure 5 (C and D) shows the ATP release

for compound 48/80-stimulated HUVECs pretreated with PMA and indolactam V. As depicted, treatment with the PKC activators reduced the magnitude of stimulated ATP release from HUVECs (14.2 +/- 3.4, N = 7 and 56.8 +/- 9.9 %, N = 7 of control, respectively). The temporal initiation of ATP release was delayed in compound 48/80-stimulated HUVECs pretreated with PKC activators (59.9 +/- 8.6 s, N = 10 and 49.7 +/- 3.1 s, N = 7 for PMA and indolactam V, respectively) versus buffer only (41.2 +/- 1.8 s).

We then examined whether the production of nitric oxide was involved in G protein-initiated release of ATP in HUVECs. As mentioned earlier, increases in intracellular Ca^{2+} activate nitric oxide synthase (NOS). The results of experiments conducted with the NOS inhibitors L-NAME and L-NMMA are depicted in Figure 6 (A and B). The magnitude of compound 48/80-stimulated release of ATP was not significantly altered in either L-NAME or L-NMMA pretreated cells (96.0 +/- 6.7 %, N = 8 and 95.7 +/- 8.3 %, N = 7 of untreated cells, respectively). Additionally, the temporal onset of ATP release for inhibitor-treated cells was not significantly different than that of control cells. Thus it appears that nitric oxide production is not necessary for G protein-initiated release of ATP.

Finally, we wanted to determine if compound 48/80-induced release of ATP in HUVECs occurred via a CFTR-transmembrane ion channel. Glybenclamide blocks CFTR channels and is commonly employed to identify CFTR-coupled release. In HUVECs treated with 100 μM glybenclamide, compound 48/80-induced release of ATP was not significantly modified. As shown in Figure 7 (A and B), the magnitude of release was 96.3 +/- 10.3 % (N = 6) of control dishes and its onset occurred at 39.3 +/- 2.9 s. These results generally suggest that ATP release in this G protein-initiated pathway was not occurring through a CFTR channel.

DISCUSSION

This study investigated the pathway through which human umbilical vein endothelial cells release ATP when stimulated with the mast cell degranulator compound 48/80. Compound 48/80 probably initiates the release pathway by activating a G_q protein. G_q proteins have been previously identified in HUVECs (25) and link G protein-coupled receptors to the activation of phospholipase C and subsequently to increases in intracellular Ca^{2+} levels (26). Also, G_q proteins, in HUVECs and in general, are not pertussis toxin sensitive (27). The next step in the release pathway appeared to be the activation of PLC by the G_q protein. PLC produced IP_3 which caused release of Ca^{2+} from the ER, Ca^{2+} influx from the extracellular matrix, or both.

Upregulation of PKC significantly attenuated ATP release. PKC activation, by treatment of the cells with PKC activators for ~20-30 min, has been reported to inhibit PLC in many cell types, including endothelial cells (28 - 29). The rate and magnitude of release under conditions of PKC activation in our experiments were similar to those in U73122-treated HUVECs. This suggested that protein kinase C possibly downregulated phospholipase C in our system. This mechanism could possibly act in feedback inhibition of ATP release. For instance, extended activation of the compound 48/80-stimulated G protein would result in the continued activation of PLC. PLC produces both IP_3 and DAG, an activator of PKC. DAG would then stimulate PKC activity that would in turn result in the termination, or at least reduction, of ATP efflux.

A number of recent studies have been published which are especially interesting in light of the results obtained in this paper. Stout and coworkers reported ATP release through connexin hemichannels in mechanically stimulated astrocytes (21). They noted that cells

loaded with calcein blue dye (MW = 400 Da) released the dye upon mechanical stimulation. However, neither Oregon Green (MW = 1100 Da) nor LDH (MW = 134 kDa) was released under these same conditions. Moreover, the connexin channel inhibitor flufenamic acid attenuated the release of both calcein blue and ATP. Arcuino and colleagues undertook a similar study (23). They noted that ATP was released in astrocytes upon lowering extracellular Ca^{2+} levels. Fluorescence imaging revealed propidium (MW = 563 Da) and dicarboxy-dichlorofluorescein (MW = 445 Da) uptake also occurred upon stimulation. However, fluorescein-dextran conjugates (MW = 1.5 – 2,000 kDa) were unable to enter the astrocytes under identical conditions. Furthermore, connexin-deficient C6 glioma did not release ATP when stimulated. Like Stout and coworkers, Arcuino and colleagues hypothesized that connexin hemichannels may be the channel through which ATP efflux occurs. Finally, they also reported release of ATP from HUVECs and epithelial cells stimulated identically to the astrocytes. To date, the mechanism of nonspecific ATP release in astrocytes has not been identified. However, ATP release in both of these reports would correlate well with the pathway investigated here. We noted that HUVECs stimulated with compound 48/80 were still able to load and maintain calcein after compound 48/80 washout. However, we also observed that calcein preloaded into HUVECs was released upon stimulation with compound 48/80 while LDH was not. Moreover, compound 48/80 was also able to stimulate release of ATP from astrocytes. Like in HUVECs, this release of ATP was found to be Ca^{2+} -dependent (30). If the release mechanisms in HUVECs and astrocytes indeed occur through similar or identical pathways, these papers together could provide a framework for what perhaps could be a more general pathway. Certainly, a more detailed inquiry will be necessary to determine if this is indeed true.

We could not rule out exocytosis as the source of ATP release in our experiments. As is typically the case in exocytosis, we observed a strict dependence on Ca^{2+} in our system. If calcein were confined to the exocytotic vesicles and released upon stimulation, the leakage could be explained. However, calcein fluorescence was very uniform across the cell suggesting this was not the case. Furthermore, the magnitude of ATP release (estimated to be in the high nM – low μM levels) seemed more indicative of release from the cytoplasm where ATP is plentiful ($\sim 2 \text{ mM}$) (23). We found no data to suggest the release of ATP occurred through a CFTR or other ATP binding cassette proteins. ATP release stimulated by compound 48/80 was not inhibited by glybenclamide. This is in contrast to the majority of proposed CFTR-permeable ATP release mechanisms (17).

Release of ATP initiated by G protein activation in endothelial cells could potentially be an important pathway in the human body. As discussed earlier, released ATP causes the activation of several pathways in numerous cell types. Endothelial cells interact with many different cell types in the human body. These include smooth muscle cells around the blood vessels, glial cells in the brain, platelets and neutrophils in the blood, and other endothelial cells (31). Endothelial cells might influence the vasodilation/vasoconstriction of blood vessels by releasing ATP onto neighboring smooth muscle cells and onto other endothelial cells. ATP has been shown to induce the synthesis of NO, a major modulator of vascular smooth muscle tone, in endothelial cells (9). Therefore, release of ATP from endothelial cells might alter smooth muscle function both directly via activation of Ca^{2+} -linked purinergic receptors on the smooth muscle cells and indirectly by stimulating production of NO (10).

Glial cell/endothelial cell interactions are responsible for communication across the blood brain barrier (31). Activation of endothelial cells by either the glial cells or compounds carried in the blood could induce ATP efflux. ATP would then act on endothelial cell purinergic receptors to regulate the microvascular permeability via regulation of intracellular Ca^{2+} signaling and cAMP levels (32). In addition, released ATP might activate Ca^{2+} signaling in glial cells, which has been implicated in the modulation of neuronal synaptic transmission (5, 6). ATP release from endothelial cells also appears to be exceedingly important in inflammation and wound healing. As mentioned earlier, ATP-induced Ca^{2+} signaling in endothelial cells initiates production of NO. NO prevents adhesion of platelets and neutrophils to healthy endothelial cells (33). ATP released by endothelial cells also activates Ca^{2+} signaling in platelets and neutrophils. Activation of these cells induces their aggregation at wound sites, since damaged endothelial cells are unable to synthesize NO (33).

In summary, the activation of G proteins in human umbilical vein endothelial cells by compound 48/80 was investigated. It was discovered that ATP is released upon stimulation of the cells. This release, which was seemingly initiated via a G_q protein, was modulated by PLC and subsequent Ca^{2+} signaling. The release did not appear to occur through a CFTR ion channel, but seems to correlate well with nonspecific, cytoplasmic release mechanisms recently postulated.

ACKNOWLEDGEMENTS

The authors would like to thank Dr. Robert T. Doyle and Dr. Philip G. Haydon for their assistance in cell culturing. Additionally, the authors would also like to thank Dr. Craig A.

each condition based on the number of samples analyzed. A P value of <0.05 was considered significant as calculated by the Student's t-test for paired experiments.

RESULTS

Addition of the G protein stimulant compound 48/80 to confluent coverslips of HUVECs caused release of cellular ATP, as depicted in Figure 1 (A and B). ATP release was initiated 41.1 +/- 1.8 s (N = 30) after addition of 15 µg/ml compound 48/80. The ATP signal reached a maximum at 126.2 +/- 5.8 s and slowly decreased back to basal levels (10 – 15 min). For the injection displayed in Figure 1 (A and B), basal release of ATP was below our detection limits (<5 nM) while the maximal release was at approximately 600 nM ATP. Since a perfusion system was not utilized in these experiments, the slow decrease to basal levels could be a result of the continued presence of compound 48/80 and/or from ATP-induced ATP release from HUVECs. The dose-dependence of compound 48/80-stimulated release of ATP is shown in Figure 1C. ATP efflux was not detected at compound 48/80 concentrations lower than 5 µg/ml and plateaued at ~60 µg/ml compound 48/80 at around 4 µM ATP.

The toxicity of compound 48/80 to the HUVECs was also investigated. For this purpose, an LDH assay was employed. LDH is a large cytoplasmic protein whose release is a marker of the loss of cell membrane integrity. HUVEC plates were sampled prior to and following activation with compound 48/80, buffer, or the Ca²⁺ ionophore A23187. A23187 was utilized as a control stimulant since it activates HUVECs by increasing the cell's intracellular Ca²⁺ concentration, as does compound 48/80 (see below). Buffer-stimulated control plates were sampled further after lysing the cells with digitonin. The results of the

Aspinwall and Dr. Michael McCloskey for their helpful discussions and critical reviews of this manuscript. The Ames Laboratory is operated for the U. S. Department of Energy by Iowa State University under Contract No. W-7405-Eng-82. This work is supported by the Director of Science, Office of Basic Energy Sciences, Division of Chemical Sciences.

REFERENCES

1. von Kugelgen, I., Wetter, A. (2000) *Naunyn Schmiedebergs Arch. Pharmacol.* **362**, 310-323
2. Khakh, B. S., Burnstock, G., Kennedy, C., King, B. F., North, R. A., Seguela, P., Voigt, M., Humphrey, P. P. (2001) *Pharmacol. Rev.* **53**, 107-118
3. Brake, B. J., Julius, D. (1996) *Annu. Rev. Cell Div. Bio.* **12**, 519-541
4. Ashcroft, S. J. (1976) *Ciba Found. Symp.* **41**, 117-139
5. Araque, A., Sanzgiri, R. P., Parpura, V., Haydon, P. G. (1999) *Can. J. Physiol. Pharmacol.* **77**, 699-706
6. Jeremic, A., Jeftinija, K., Stevanovic, J., Glavaski, A., Jeftinija, S. (2001) *J. Neurochem.* **77**, 664-675
7. Lawson, D., Fewtrell, C., Raff, M. C. (1978) *J. Cell. Biol.* **79** 394-400
8. Evans, J. H., Sanderson, M. J. (1999) *Cell Calcium* **26**, 103-110
9. Ando, J., Ohtsuka, A., Korenaga, R., Sakuma, I., Kamiya, A. (1993) *Front. Med. Biol. Eng.* **5**, 17-21
10. Forstermann, U., Closs, E. I., Pollock, J. S., Nakane, M., Schwarz, P., Gath, I., Kleinert, H. (1994) *Hypertension* **23**, 1121-1131
11. Knop, M., Gerke, V. (2002) *Biochim. Biophys. Acta* **1600**, 162-167

12. Nilius, B., Droogmans, G. (2001) *Physiol. Rev.* **81**, 1415-1459
13. von Kugelgen, I., Goncalves, J., Driessen, B., Starke, K. (1998) *Adv. Pharmacol.* **42**, 120-125
14. Unsworth, C. D., Johnson, R. G. (1990) *Proc. Natl. Acad. Sci. U. S. A.* **87**, 553-557
15. Bodin, P., Burnstock, G. (2001) *Neurochem. Res.* **26**, 959-969
16. Cantiello, H. F. (2001) *Pflugers Arch.* **443**, S22-S27
17. Schwiebert, E. M. (1999) *Am. J. Physiol.* **276**, C1-C8
18. Grygorczyk, R., Hanrahan, J. W. (1997) *Am. J. Physiol.* **272**, C1058-C1066
19. Cotrina, M. L., Lin, J. H., Alves-Rodrigues, A., Liu, S., Li, J., Azmi-Ghadimi, H., Kang, J., Naus, C. C., Nedergaard, M. (1998) *Proc. Natl. Acad. Sci. USA* **95**, 15735-15740
20. Wang, Z., Haydon P. G., Yeung, E. S. (2000) *Anal. Chem.* **72**, 2001-2007
21. Stout, C. E., Costantin, J. L., Naus, C. C., Charles, A. C. (2002) *J. Biol. Chem.* **277**, 10482-10428
22. Goodenough, D. A., Paul, D. L. (2003) *Nat. Rev. Mol. Cell Biol.* **4**, 285-294
23. Arcuino, G., Lin, J. H., Takano, T., Liu, C., Jiang, L., Gao, Q., Kang, J., Nedergaard, M. (2002) *Proc. Natl. Acad. Sci. U. S. A.* **99**, 9840-9845
24. Vuong, P. T., Malik, A. B., Nagpala, P. G., Lum, H. (1998) *J. Cell Physiol.* **175**, 379-387
25. Clark, C. B., McKnight, N. L., Frangos, J. A. (2002) *Biochem. Biophys. Res. Commun.* **299**, 258-262
26. Exton, J. H. (1996) *Annu. Rev. Pharmacol. Toxicol.* **36**, 481-509
27. Strathmann, M., Simon, M. I. (1990) *Proc. Natl. Acad. Sci. U. S. A.* **87**, 9113-9117

28. Chen, B. C., Lin, W. W. (1999) *Br. J. Pharmacol.* **127**, 1908-1914
29. Chuprun, J. K., Rapoport, R. M. (1997) *J. Recept. Signal Transduct. Res.* **17**, 787-814
30. Gruenhagen, J. A., Yeung, E. S. In preparation
31. Cryer, A. ed. (1983) *Biochemical Interactions at the Endothelium*, Elsevier Science, Amerstam, Netherlands
32. Abbott, N. J. (2000) *Cell Mol. Neurobiol.* **20**, 131-147
33. Kunapuli, S. P., Daniel, J. L. (1998) *Biochem. J.* **336**, 513-523

Table 1. Cytotoxicity of compound 48/80-induced ATP release on HUVECs.

A)

Stimulant	LDH Release
Buffer	0.62 +/- 0.11
5 μ M A23187	0.97 +/- 0.51
25 μ g/ml Compound 48/80	1.15 +/- 0.13
40 mM Digitonin	100 +/- 6.16

B)

Stimulant	# of Cells Loading Calcein
Buffer	129.2 +/- 5.1
16.8 μ g/ml Compound 48/80	136.0 +/- 5.2

C)

Stimulant	% of Cells Leaking Calcein
Buffer	1.7 +/- 1.7 %
15 μ g/ml Compound 48/80	48.9 +/- 9.8 %

FIGURE CAPTIONS

Figure 1. Compound 48/80-induced release of ATP in HUVECs. ATP signal was monitored from cultured HUVECs stimulated with 15 $\mu\text{g/ml}$ compound 48/80. A, single frames of data are shown at various times after stimulation. B, concentration of ATP efflux following stimulation is plotted versus time after stimulation. C, the dose dependence of ATP release is depicted in a plot of the maximum ATP release versus compound 48/80 concentration. The overall curve is the combined data from five separate dose response curves obtained from HUVECs in different passages. All data points represent the combined data from at least five independent compound 48/80 injections, except for [compound 48/80] = 0 and 5 $\mu\text{g/ml}$, for which only three injections were performed.

Figure 2. G protein dependence of compound 48/80-induced release of ATP from HUVECs. HUVECs were stimulated with 10 μM mastoparan. HUVECs pretreated overnight with 250 ng/ml PTX or buffer were stimulated with 15 $\mu\text{g/ml}$ compound 48/80. Representative time courses of ATP release (A) along with plots of overall ATP release (B) are depicted.

Figure 3. Compound 48/80 induces increases in intracellular Ca^{2+} and Ca^{2+} -dependent release of ATP from HUVECs. Intracellular stores of Ca^{2+} were depleted by incubation of HUVECs with 250 nM thapsigargin for 20 minutes, and

extracellular Ca^{2+} was removed by bathing cells in buffer with Ca^{2+} removed and 100 μM EGTA added to remove any residual Ca^{2+} ions (Tg/EGTA). Compound 48/80 induced intracellular Ca^{2+} increases in HUVECs loaded with fluo-3. Single frames of Ca^{2+} imaging data are depicted at various times after stimulation with 15 $\mu\text{g}/\text{ml}$ compound 48/80 (A). Representative time courses of ATP release (B) and Ca^{2+} signaling (D) are depicted along with plots of overall ATP release (C) and Ca^{2+} signaling (E) for HUVECs stimulated with 15 $\mu\text{g}/\text{ml}$ compound 48/80 (Tg/EGTA and 48/80), 10 μM Ca^{2+} ionophore (A23187), 5 μM thapsigargin (Tg) or buffer. Inset for B: Zoomed-in look at the lack of ATP release caused by thapsigargin, A23187, and buffer.

Figure 4. Phospholipase C dependence of compound 48/80-induced release of ATP from HUVECs. HUVECs were pretreated for 20 min with either the PLC inhibitor U73122 (10 μM) or its inactive analog U73343 (10 μM). Removal of extracellular Ca^{2+} by pretreatment in Ca^{2+} -free buffer containing 100 μM EGTA was performed concurrently with 10 μM U73122 (U73122/EGTA) to further investigate the role of PLC on release of ATP. Representative time courses of ATP release (A) and Ca^{2+} signaling (C) are depicted along with plots of overall ATP release (B) and Ca^{2+} signaling (D) for cells stimulated with 15 $\mu\text{g}/\text{ml}$ compound 48/80.

- Figure 5. Protein kinase C-dependence of compound 48/80-induced release of ATP from HUVECS. HUVECS were pretreated for 30 min with 5 μ M BIM and 1 μ M Go6893, both PKC inhibitors (A and B), or with 1 μ M PMA or 1 μ M indolactam V (Indo), both PKC activators (C and D). Representative time courses of ATP release (A and C) are depicted along with plots of overall ATP release (B and D) for cells stimulated with 15 μ g/ml compound 48/80.
- Figure 6. Nitric oxide-dependence of compound 48/80-induced release of ATP from HUVECS. HUVEC dishes were pretreated for 30 min with either 100 μ M L-NAME, 10 μ M L-NMMA, or buffer. Representative time courses of ATP release (A) are depicted along with plots of overall ATP release (B) for cells stimulated with 15 μ g/ml compound 48/80.
- Figure 7. Glybenclamide pretreatment does not perturb compound 48/80-induced release of ATP from HUVECS. HUVECS were treated with 100 μ M glybenclamide (Glyb) or buffer prior to stimulation with 15 μ g/ml compound 48/80. Representative time courses of ATP release (A) are depicted along with plots of overall ATP release (B).

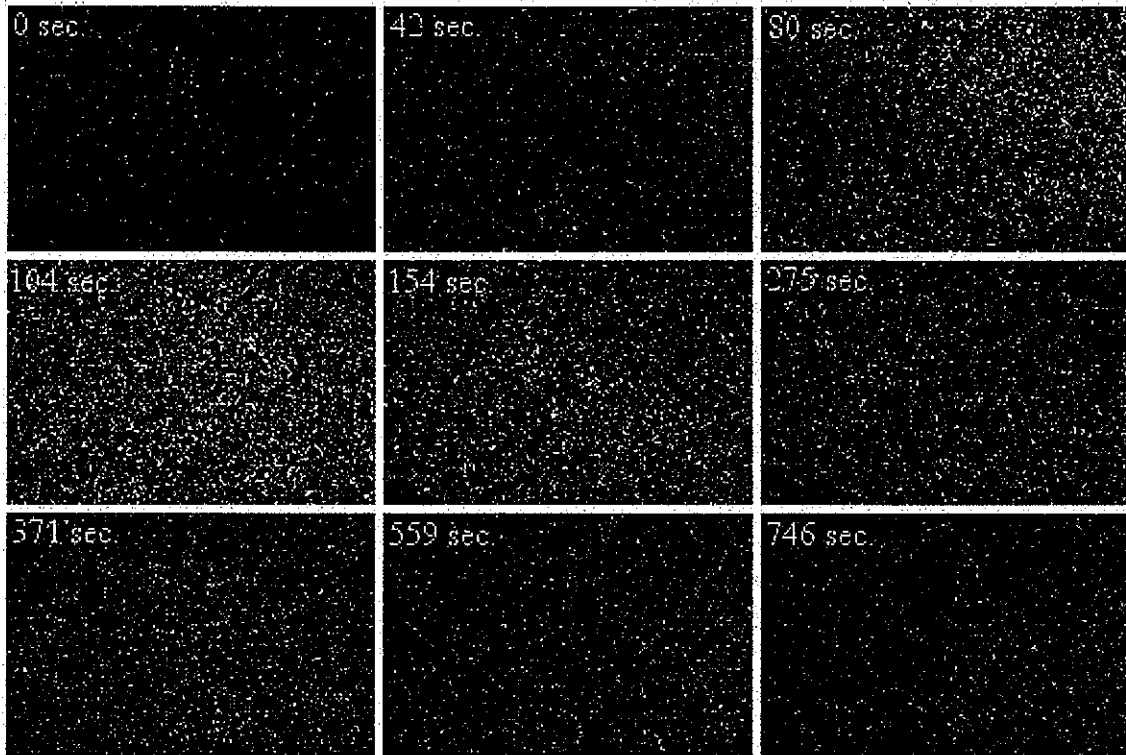


FIGURE 1A

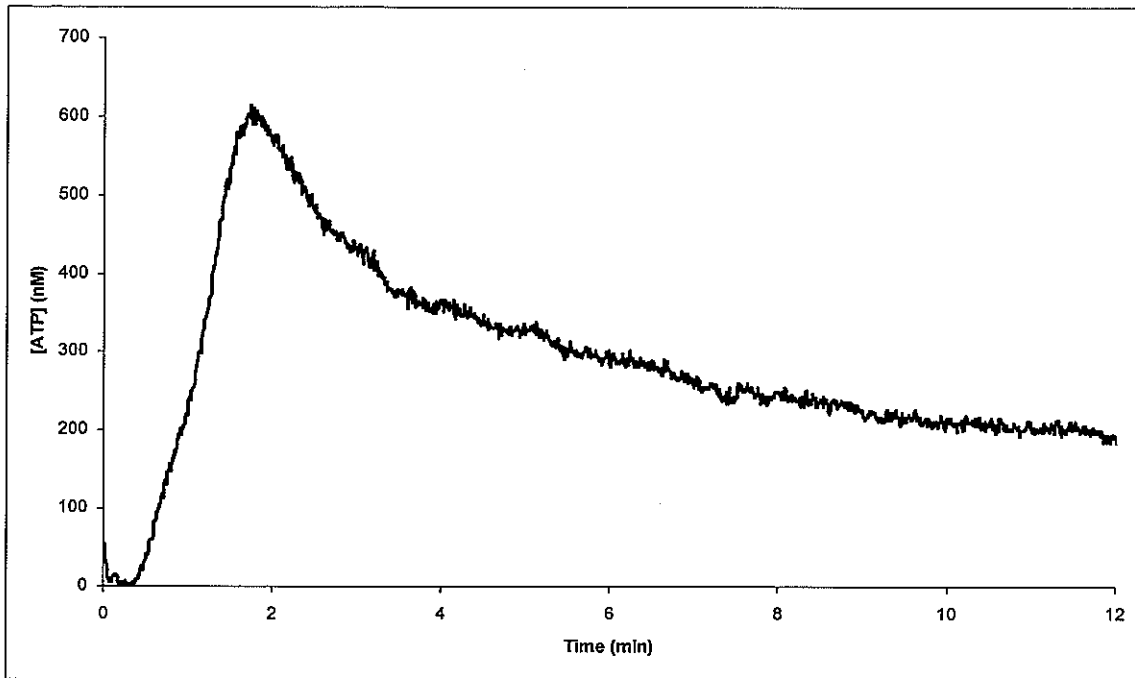


FIGURE 1B

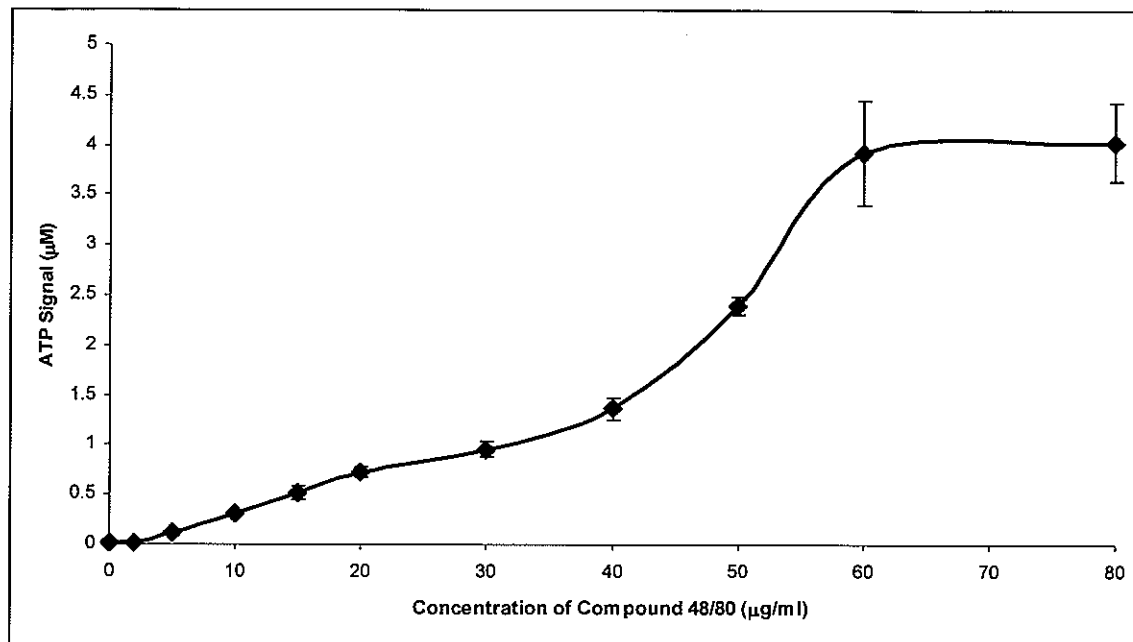


FIGURE 1C

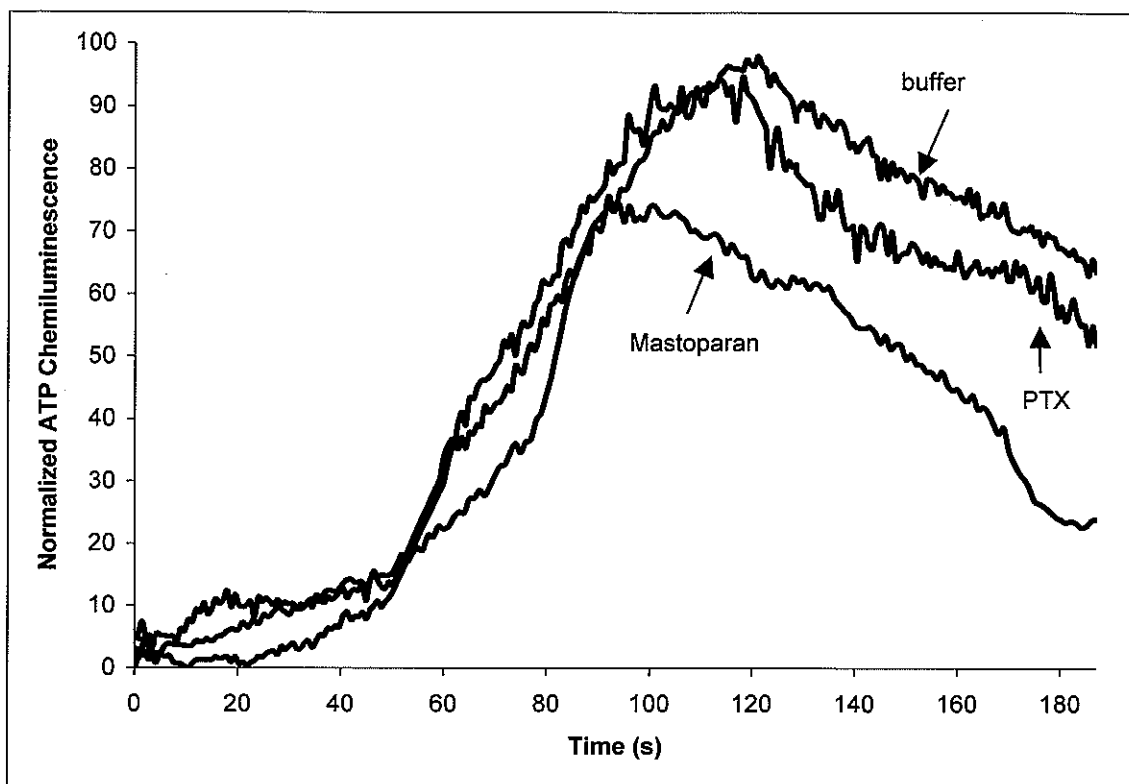


FIGURE 2A

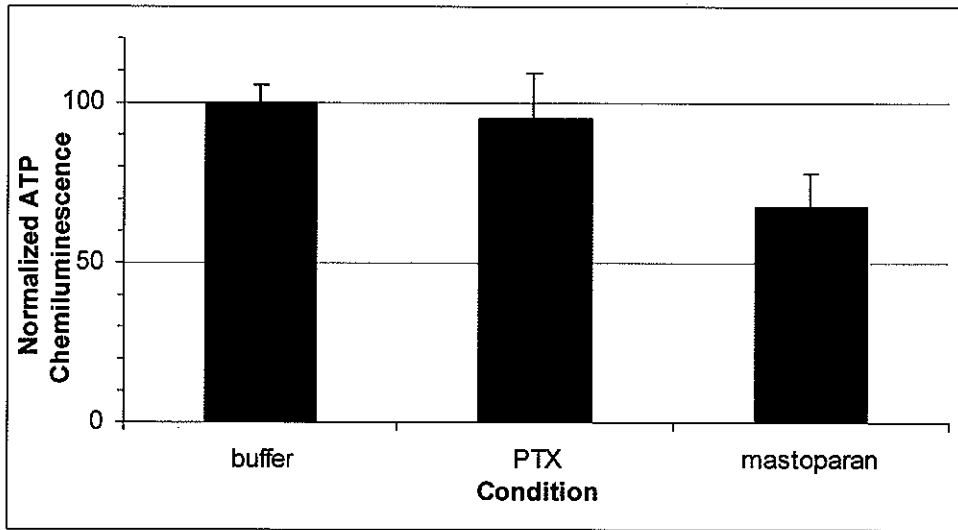
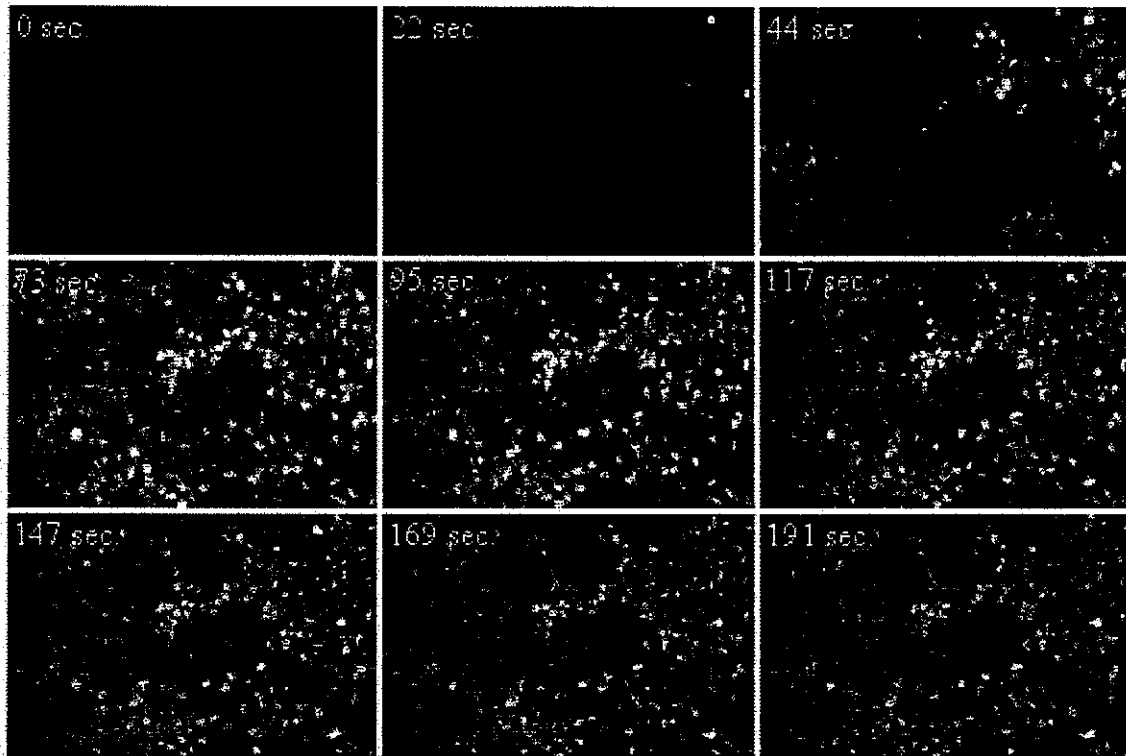
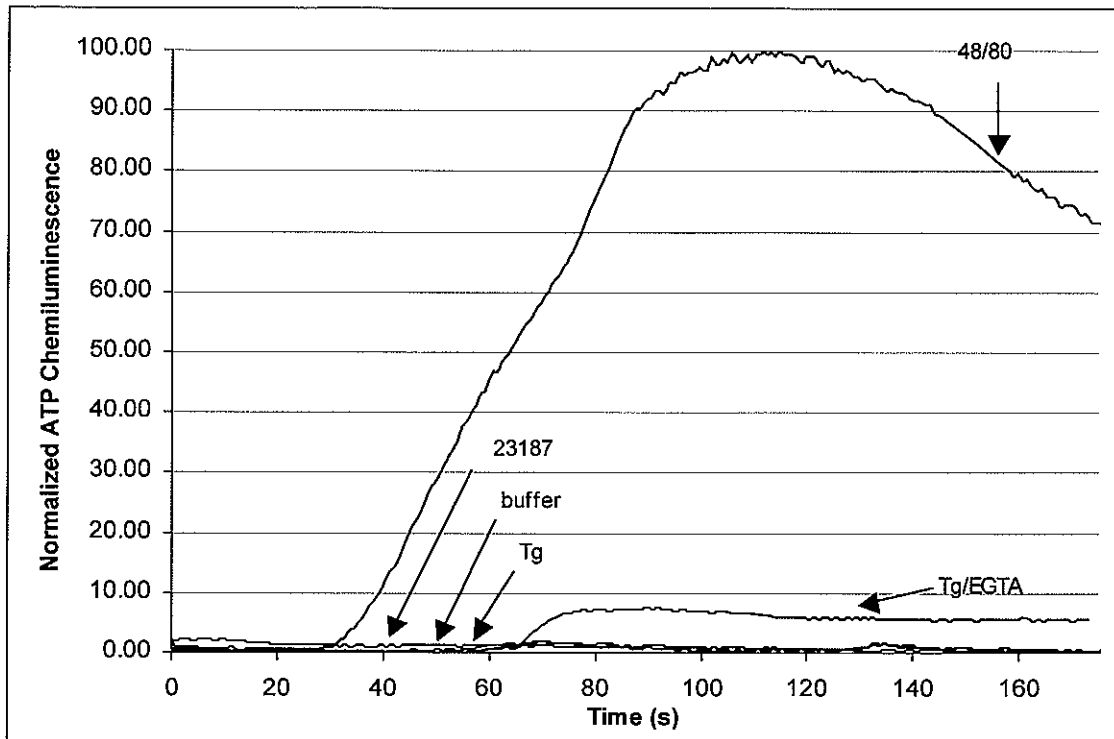


FIGURE 2B

**FIGURE 3A**



Inset:

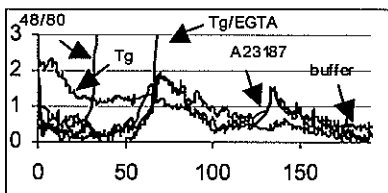


FIGURE 3B

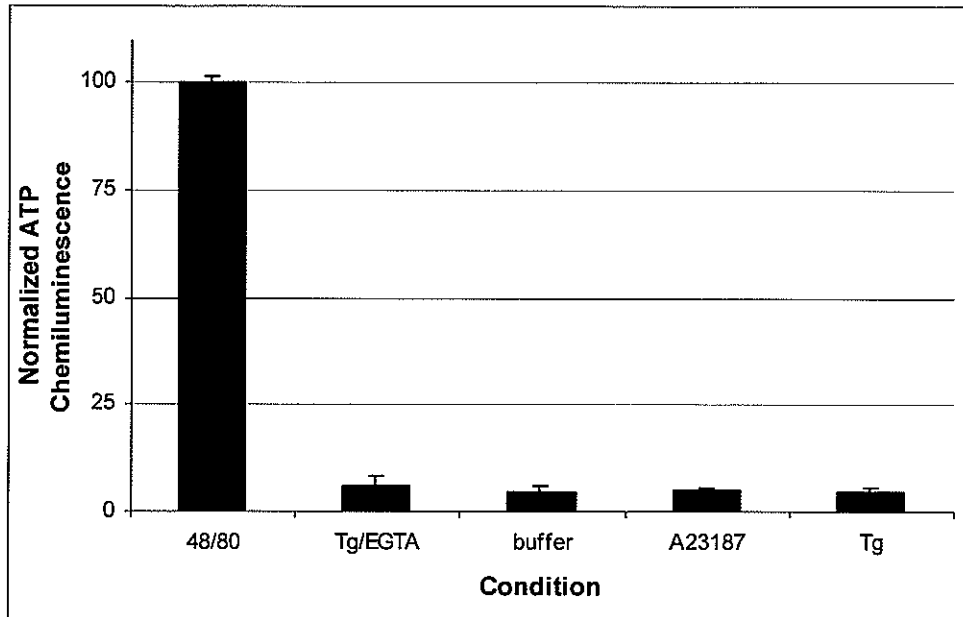


FIGURE 3C

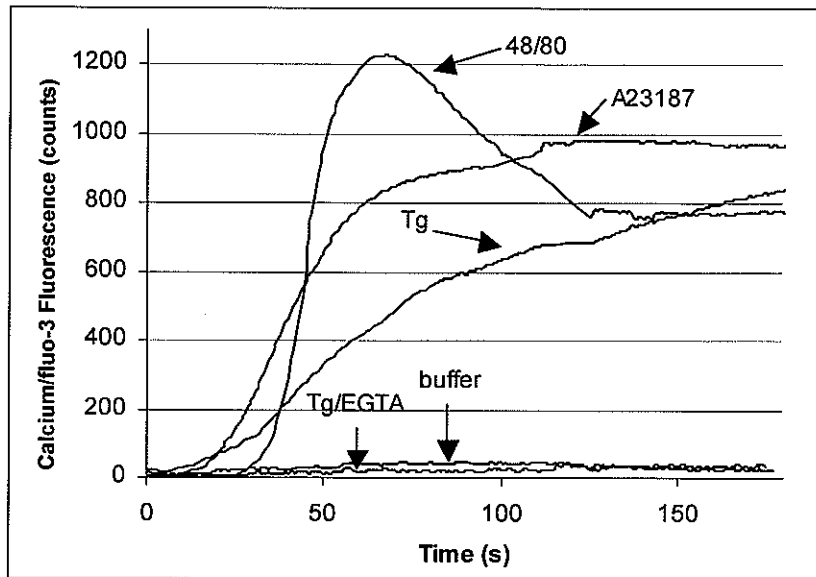


FIGURE 3D

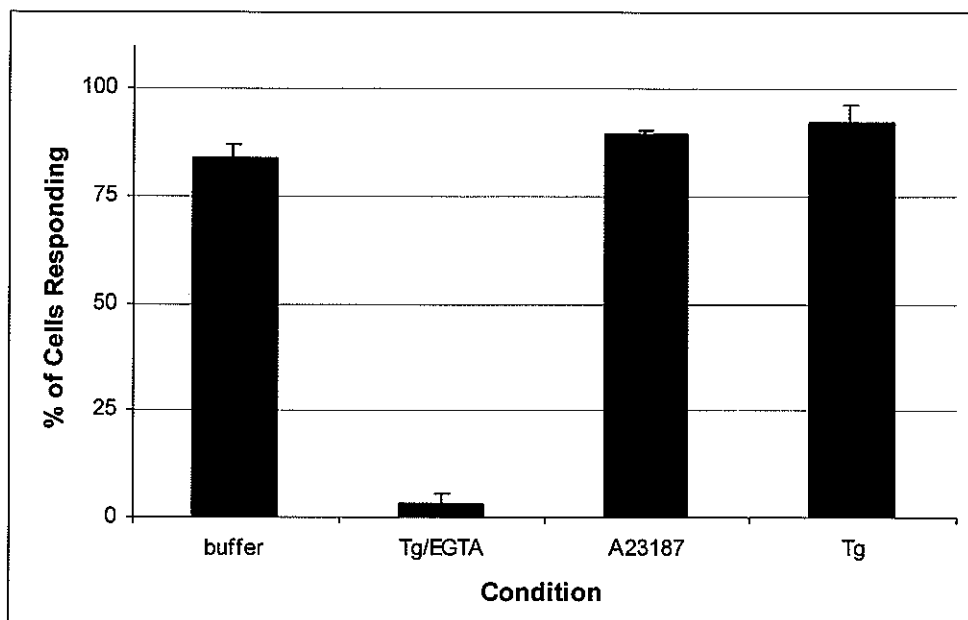


FIGURE 3E

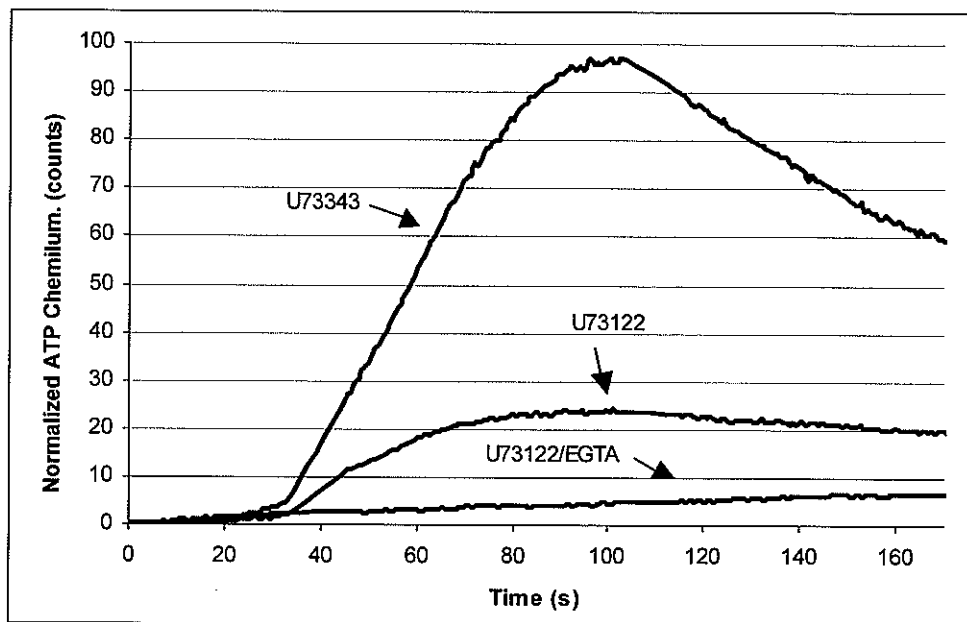


FIGURE 4A

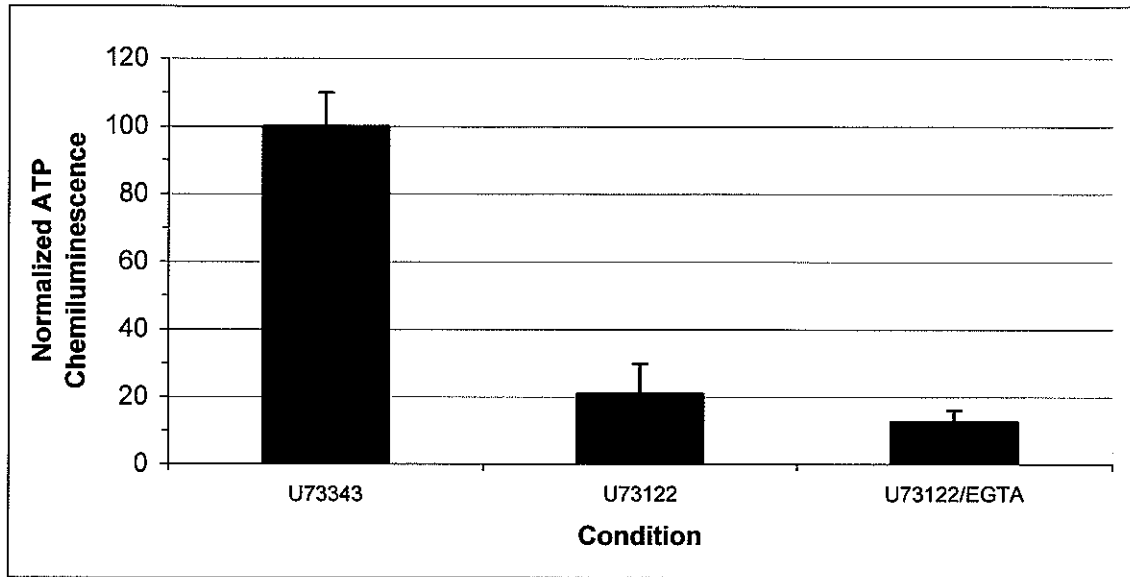


FIGURE 4B

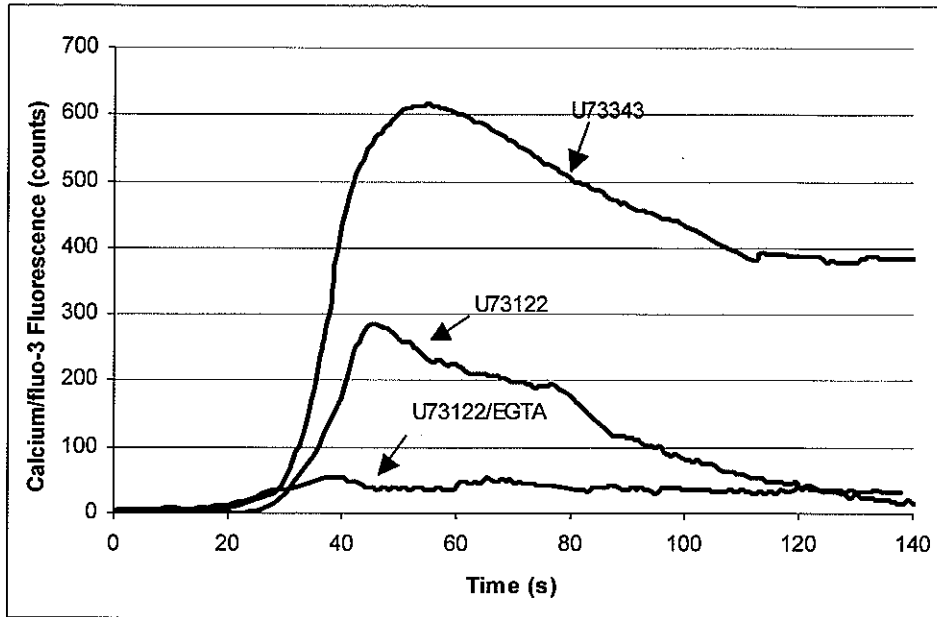


FIGURE 4C

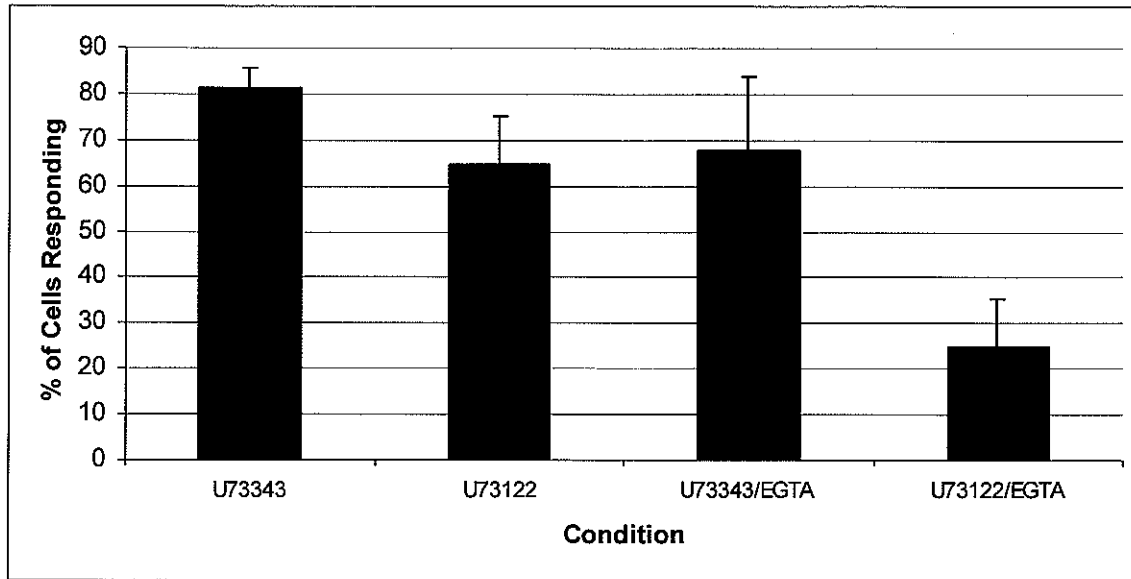


FIGURE 4D

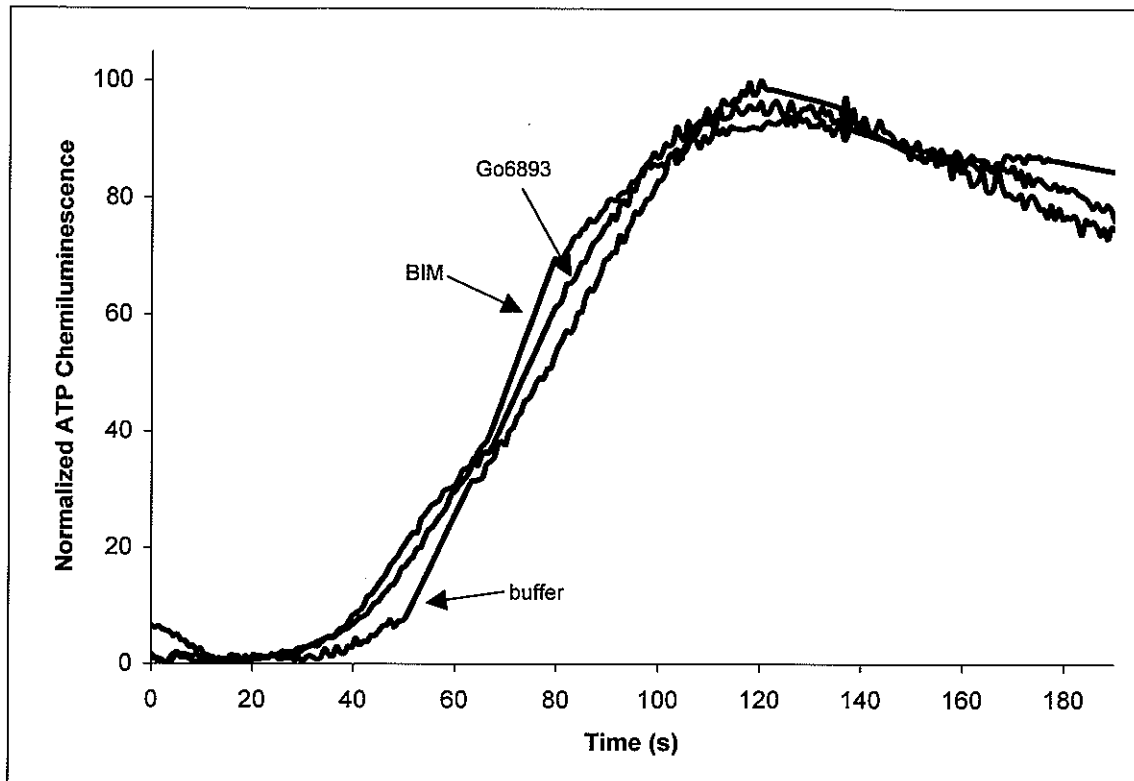


FIGURE 5A

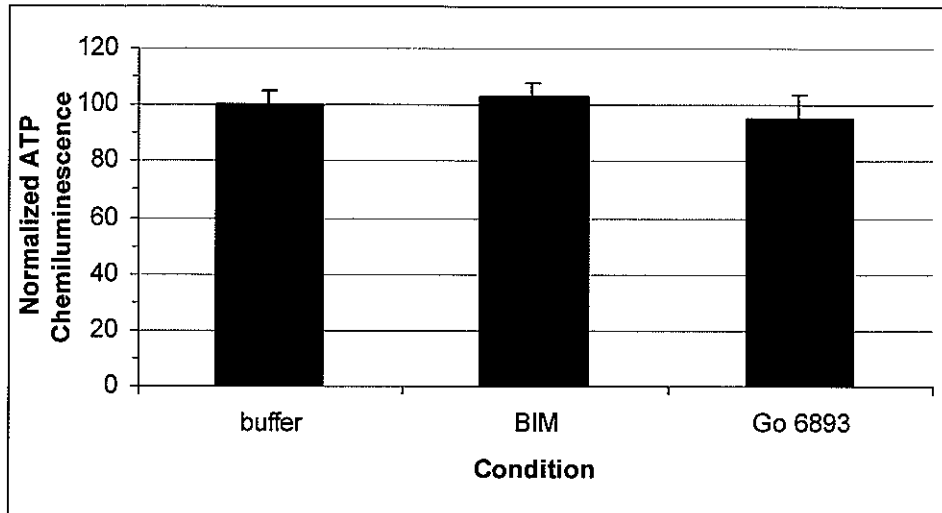


FIGURE 5B

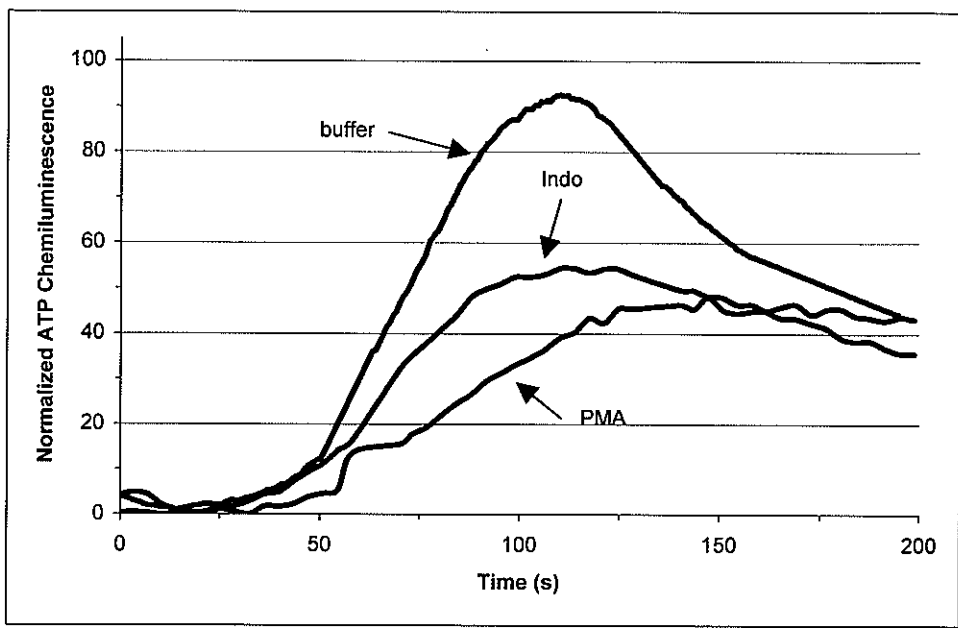


FIGURE 5C

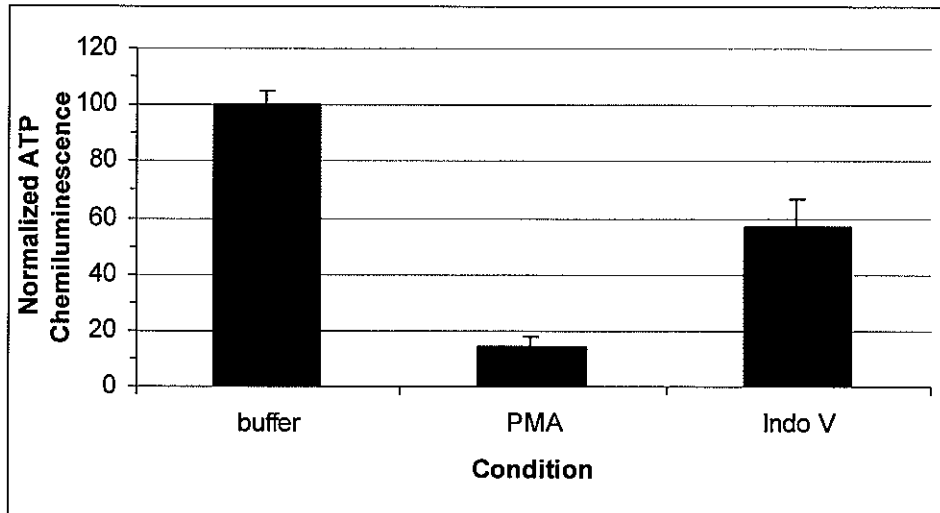


FIGURE 5D

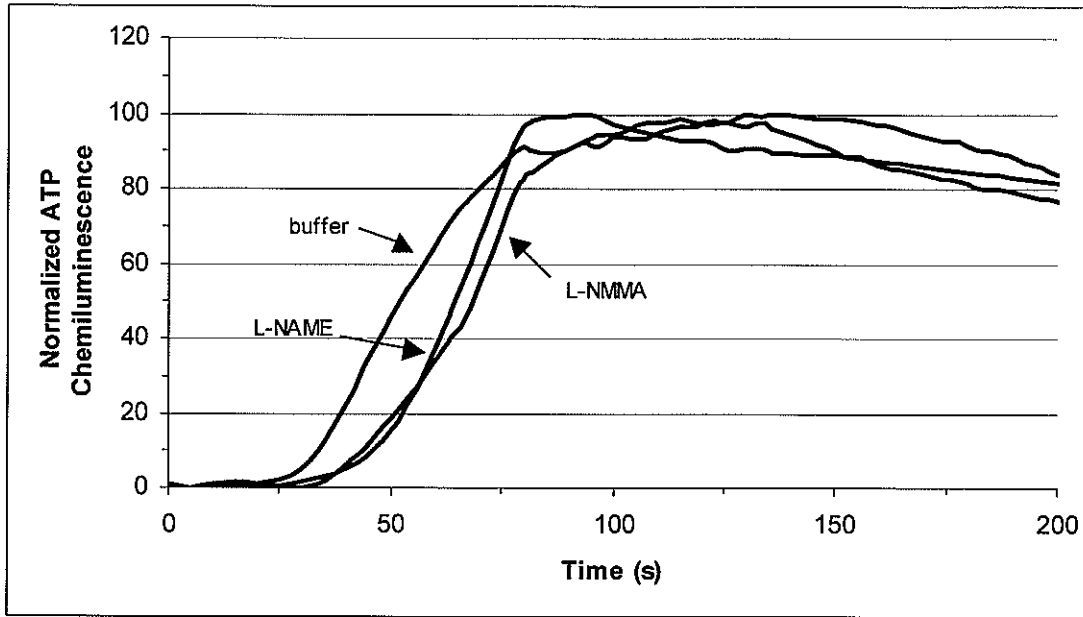
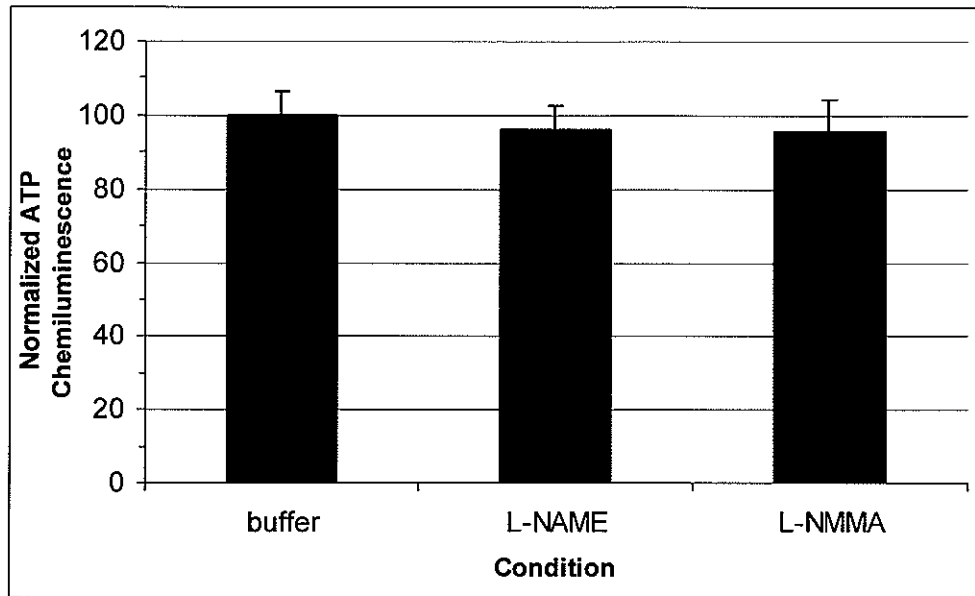


FIGURE 6A

**FIGURE 6B**

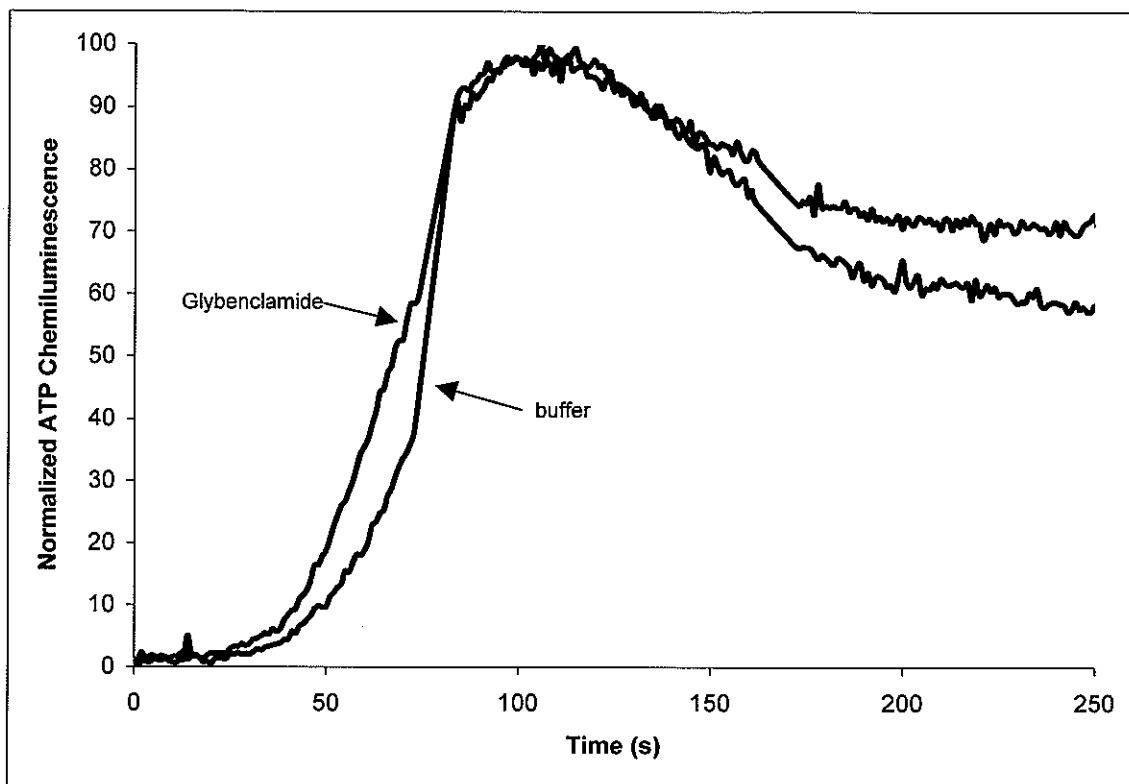


FIGURE 7A

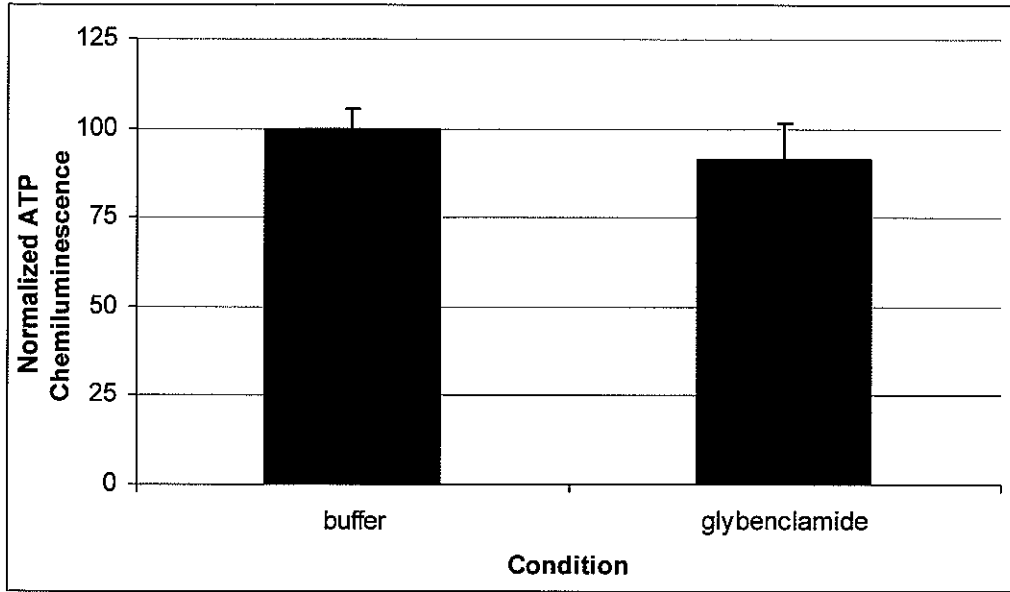


FIGURE 7B

CHAPTER 3. MONITORING REAL-TIME RELEASE OF ATP FROM MOLLUSCAN CENTRAL NERVOUS SYSTEMS

A manuscript prepared for submission to Analytical Chemistry

Jason A. Gruenhagen^{*}, Peter Lovell, Leonid L. Moroz, and Edward S. Yeung

^{*} Primary researcher and author

ABSTRACT

The further understanding of neuronal function is imperative for the prevention and treatment of neurofunctional disorders. To aid in this realization, novel methods for monitoring neuronal cell function must be developed and characterized. In this study, we report the application of real-time imaging of luciferase-catalyzed ATP bioluminescence for the investigation of ATP release from whole central nervous systems of the freshwater snail *Lymnaea stagnalis*. The large neurons of invertebrates, such as *Lymnaea*, are excellent models for the study of general neurobiology. Release of ATP from *Lymnaea* ganglia varied among the different ganglia as well as within individual ganglia. Furthermore, the magnitude of ATP release varied following the stimulation of neurons with common neurotransmitters.

INTRODUCTION

Neurotransmission is perhaps the most important and most complex of all cell processes. Proper neuron function depends not only on the physiology of the neurons

themselves, but also on the maintenance of the correct neuronal environment by glial cells and endothelial cells. Furthermore, great heterogeneity exists in the neuronal population themselves. Various neurons respond to and release numerous neurotransmitters, including glutamate, serotonin, catecholamines, dopamine, and several peptide transmitters¹⁻².

Additionally, the response of different neurons to these neurotransmitters can vary in both magnitude and temporal kinetics. The importance of neurotransmission is further exemplified by the variety of pathological disorders that involve improper brain homeostasis, including Parkinson's disease, Alzheimer's disease, multiple sclerosis, epilepsy, meningitis, and focal cerebral ischemia (strokes)². Clearly, further understanding of the neuronal environment and neurotransmission will yield additional knowledge and superior prevention and treatment methodologies for these disorders.

Traditionally, lesser organisms are utilized in the investigation of neuronal function. These model systems are employed because they typically contain fewer neurons resulting in less complex neuronal circuits¹. Mollusks are especially valuable in this regard. Mollusks lack a central brain, instead possessing several masses of neurons, termed ganglia. Within these ganglia, the large cell bodies (up to 150 μm in diameter) of individual neurons can be reliably identified from one preparation to the next. This enables the functional characterization of specific neurons in a variety of neuronal circuits such that individual neurons can be correlated with whole animal behavior output. Furthermore, their large size and surface location in the ganglia allow for relatively straightforward removal of individual neurons from the ganglia and placement in primary cell culture where the cells exhibit robust outgrowth and synaptogenesis.

Conventionally, radioligand binding, *in situ* hybridization histochemistry, Western blotting, and electrophysiology have been the most common techniques employed for the investigation of neuronal function³. While these techniques are extremely valuable, each maintains significant shortcomings. For instance, radioligand binding, *in situ* hybridization, and Western blotting allow for sensitive and specific direct detection of macromolecules, but lack the temporal resolution to study cells in real-time. Conversely, electrophysiology techniques yield real-time results through the measure of ion flux across membranes, but cannot yield significant spatial information of signals. Recently, analytical chemists as well as neuroscientists have recognized the vast potential for development of techniques for application in neuroscience. Typically, these methods are aimed at the detection of neurotransmitters in real-time with superior specificity. Current *in vivo* techniques include amperometric detection of dopamine and catecholamines release with carbon-fiber electrodes⁴⁻⁶; laser-induced fluorescence detection of amine-containing neurotransmitters sampled via microdialysis and separated with liquid chromatography⁷⁻⁸; amperometric detection of amine-containing neurotransmitters sampled via microdialysis and separated with capillary liquid chromatography⁹; MALDI-MS detection of peptides and proteins separated by CE¹⁰⁻¹²; and electrochemical detection of dopamine via both direct sampling with CE and detection at the cell body with microelectrodes¹³. Our own group has focused on the native fluorescence detection of release and uptake of serotonin¹⁴⁻¹⁶. These studies were performed on a microscope equipped with a CCD camera yielding superior spatial resolution, sensitivity, selectivity, and temporal resolution, simultaneously. With the development of the intensified CCD camera, detection of lesser optical signals has become possible. For instance, release of catecholamines from chromaffin cells was monitored by

capillary electrophoresis with laser induced fluorescence detection¹⁷. More recently, a method for the real-time detection of bioluminescence generated from the reaction of luciferin and ATP in the presence of firefly luciferase was developed in our group¹⁸.

ATP has been identified as an important messenger in the neuronal environment. It is released from neurons simultaneously with other neurotransmitters and acts as both a fast transmitter and a neuromodulator¹⁹⁻²⁵. Thus, application of our ATP detection technique, which has to date only been employed with cultured astrocytes and endothelial cells, to detection of ATP release in neuronal systems seemed feasible. Here we investigated the figures of merit for our ATP imaging for use in whole mollusk ganglia imaging. Next we present the detection of ATP released from the ganglia of the freshwater snail *Lymnaea stagnalis*. Release is assessed spatially within the organism and individual ganglia. Finally, we evaluate the effect of artificial neurotransmitter stimulation on release of ATP from *Lymnaea*.

EXPERIMENTAL SECTION

Chemicals. Firefly luciferase (from *Photinus pyralis*) was obtained from R & D Systems (Minneapolis, MN). NOC-18 and diethylamine-NONOate (DEA-NONOate) were purchased from Calbiochem (La Jolla, CA). All other chemicals were from Sigma (St. Louis, MO). Low ionic strength HEPES buffer contained 10 mM 4-(2-hydroxyethyl)-1-piperazineethanesulfonic acid (HEPES), 5 mM KCl, and 5 mM NaCl (pH = 7.75). *Lymnaea* HEPES buffer contained 10 mM HEPES, 40 mM NaCl, 1.7 mM KCl, 4.1 CaCl₂, and 1.5 mM MgCl₂ (pH = 7.75).

Specimen Preparation. Individual *Lymnaea stagnalis* (Gastropoda, Pulmonata, Basommatophora, Lymnaeidae) were acquired from an inbred population originally raised at the Free University Amsterdam. These animals were maintained in well aerated fresh water aquaria at room temperature and fed lettuce every other day. Animals with shell lengths of 20-30 mm were deshelled with small scissors and anesthetized for 10 minutes in 10% Listerine (v/v) solution in *Lymnaea* HEPES buffered saline. Animals were pinned down under saline in black sylgard dissection dishes and the ganglia were removed via a dorsal midline incision. Ganglia were pinned down on sylgard dishes under *Lymnaea* HEPES buffered saline and used for subsequent experiments.

ATP Imaging. ATP imaging was performed on the stage of a stereo dissection microscope (Nikon SMZ-2T). Bioluminescence signal was collected through the 1.6X objective lens and detected with an intensified charge-coupled device (iCCD; EEV 576 x 384 pixels CCD chip, Roper Scientific, Trenton, NJ) attached to the camera mount of the microscope. Samples were incubated in 1 ml buffer containing 100 $\mu\text{g}/\text{ml}$ firefly luciferase and 205 μM D-luciferin. Images were collected at a frequency of 0.80 Hz with 1000 ms exposure times. All experiments were performed at room temperature. Stimulants were applied to the cells via a micropipette just prior to data acquisition.

Data Presentation/Analysis. Bioluminescence signal was obtained and processed with Winview32 software (Roper Scientific). The number of pixels over a threshold value was calculated for each frame of data. The ATP concentrations were determined from a calibration curve obtained with the exact same imaging parameters. Standard errors were determined for each condition based on the number of samples analyzed. A P value of <0.05 was considered significant as calculated by the Student's t-test for paired experiments.

RESULTS AND DISCUSSION

Assessing ATP Imaging for Investigation of Mollusk Neurotransmission. We originally aimed to employ the giant sea slug, *Aplysia californica*, for investigation of release of ATP from mollusk ganglia. *Aplysia* neurons are very large (50 – 500 μm in diameter) compared to human neurons (< 10 μm in diameter)²⁶. Thus, these neurons would be ideal to establish whether ATP is released in neuronal environments. However, upon monitoring bioluminescence from ATP standards for luciferase contained in filtered seawater, we noted that the detection limit for ATP under these conditions was poor compared to our previous experiments. This results because the luminescence efficiency of the luciferase enzyme is reduced in solutions containing high salt content, especially Ca^{2+} ions²⁷. Another plausible model mollusk, *Lymnaea stagnalis*, is a freshwater organism and therefore requires a buffer with much lower ionic strength than filtered seawater. *Lymnaea* neurons are slightly smaller (50 – 100 μm in diameter²⁶) than those of *Aplysia* but are large enough to be applicable for this study. To identify which system would yield the best detection efficiency for ATP, we compiled calibration curves for bioluminescence detection of ATP in filtered seawater, a lower ionic strength balanced salt solution (*Lymnaea* HEPES buffer), and a low ionic strength HEPES buffer containing only MgCl_2 and NaCl . The low ionic strength HEPES buffer has been shown to give the best sensitivity for detection of ATP in our systems. As portrayed in Figure 1, *Lymnaea* HEPES buffer was a much better buffer for ATP detection than filtered seawater, but was slightly inferior to low ionic strength HEPES buffer. Because of the better sensitivity, we chose to utilize freshwater *Lymnaea* ganglia throughout this study.

We next examined whether any of the compounds potentially present in the *Lymnaea* sample would interfere with our ATP detection reaction. Cytidine 5'-triphosphate, guanosine 5'-triphosphate, uridine 5'-triphosphate, and adenosine 5'-diphosphate (ADP) are all present in high concentrations in cells along with ATP²⁸. If any of these compounds either reduced ATP bioluminescence or produced bioluminescence themselves, our method would be compromised. However, none of these compounds diminished the signal produced by injection of ATP standards. Furthermore, of these chemicals, only ADP caused any significant signal of its own in the presence of luciferin and luciferase. The signal from ADP was over two orders of magnitude smaller than that caused by the same concentration of ATP. Additionally, nitrites and nitrates are also prevalent in molluscan nervous systems²⁹. However, neither of these anions either caused bioluminescence itself or inhibited ATP bioluminescence. Additionally, mollusks ganglia contain numerous nitrenergic neurons, which produce large amounts of nitric oxide (NO, 100 nM)²⁶. To identify whether NO could interfere with our detection scheme we employed the NO donors, DEA-NONOate and NOC-18. DEA-NONOate, but not NOC-18, caused slight bioluminescence in standard experiments. A large concentration of NO was necessary to cause even a minute signal, and thus its interference was not considered significant. Finally, interference from the neurotransmitters employed as stimulants later in this study was assessed. Neither serotonin nor KCl caused bioluminescence in the presence of luciferin and luciferase. Likewise neither compound reduced the ability of ATP to produce bioluminescence. Thus, ATP imaging was satisfactory for use in the investigation of *Lymnaea* neurotransmission.

Release of ATP from the *Lymnaea* CNS. Through careful dissection of *Lymnaea*, a complete and functional central nervous system (CNS) can be isolated. When bathed in ATP

imaging solution immediately following isolation from the organism, all ganglia of the *Lymnaea* CNS release large amounts of ATP. Several studies have previously shown that glia cells release ATP when physically stimulated^{18,30-32}. This is likely the source for much of the observed ATP. As expected, the amount of ATP signal, and thus ATP release, from the sample decreased with time. After a period of ½ -1 hour the release of ATP from the CNS leveled off. Figure 2 (A and B) depict release of ATP from an isolated CNS four hours after its dissection and isolation, while Figure 2 (C and D) show release from the right pedal ganglion under higher magnification. This ATP signal persisted for over eight hours (the longest time that release was monitored from a single specimen). ATP release from physically stimulated astrocytes diminishes on the order of minutes¹⁸, suggesting that this extended release is associated with the neurons. Moreover, ATP release due to damaged or dead cells within the CNS would not likely be sustained nor would it remain stable for such a time period. Further evidence that ATP release from the *Lymnaea* CNS was authentic and not from cell damage was obtained from electrophysiology experiments. Isolated neurons were bathed in ATP detection solution while the membrane potential was monitored via a sharp intracellular electrode. Neither luciferin nor luciferase had any effect on membrane potential or on the ability to fire action potentials following depolarization (n=4 neurons, data not shown). These electrophysiological responses require the presence of stable and functional membranes and thus verify that release of ATP from the *Lymnaea* CNS is a natural event. Furthermore, to check that neurons are excited (depolarized) in response to serotonin or K⁺ perfusion, membrane potential was monitored during the application of these compounds. Both serotonin and high K⁺ depolarized the neurons and caused the firing of action potentials.

Spatially Isolated Release of ATP. Release from the right pedal ganglion of a *Lymnaea* CNS in Figure 2 (C and D) appeared to be limited spatially. Hence, we sought to identify if this was an isolated case or a general trend. Upon examination of other specimens, we found that release was not uniform, but varied within the ganglion in all cases. This was most evident in the visceral ganglion. Figure 3 (A and D) show two visceral ganglia from distinct *Lymnaea* specimens. The detected release of ATP from these ganglia is shown in Figure 3 (B and E). In both of these ganglia, a large amount of ATP is being released from a specific region within the specimen, while other regions of the sample display very little signal. Figure 3 (C and F) further illustrate this phenomenon by depicting the calculated ATP release for regions of high release, low release, and background. It is interesting that the releasing regions of both ganglia are in similar positions in the samples. However, without single cell resolution on our optical images, it is impossible to conclude whether release in both cases is coming from the same few or single cell.

Induced ATP Release via Addition of Neurotransmitters. We next sought further evidence that the release of ATP observed above was indeed from the neurons. If ATP does act as either a neuromodulator or neurotransmitter in *Lymnaea*, its release should be regulated by the activity of the cells. Thus neurotransmitters, which are either excitatory or inhibitory in neurons, should influence the amount of ATP released in the *Lymnaea* CNS. We first employed KCl to stimulate neuron activity. High KCl solutions depolarize neurons by altering the electrochemical gradient across the membrane and are commonly utilized to artificially mimic neurotransmitter-induced neuron firing. As depicted in Figure 4 (A – C), addition of KCl escalated release of ATP from the left pedal ganglion of this *Lymnaea* ganglion. Figure 4 (D – G) depict pre- and post-stimulation plots of ATP release from the

left pedal ganglion, the visceral ganglion, and a non-ganglion region. Since K^+ stimulation of neurons was effective in initiating accelerating release of ATP, we sought a more specific stimulus to examine. Serotonin was utilized since a number of neurons in the *Lymnaea* CNS are serotonin-sensitive³³. As with KCl, serotonin increased the magnitude of ATP release when artificially added to the *Lymnaea* CNS. Figure 5 (A and B) depict an optical image and ATP release from a right pedal ganglion. After addition of serotonin, the release of ATP from this ganglion was significantly augmented, as shown in Figure 5C. ATP signal plots for the pedal ganglion and a non-ganglion area are presented in Figure 5 (D and E) prior to and after serotonin addition. The right cerebral ganglion is visible in the extreme left side of these images. As displayed in Figure 5F, ATP release from this ganglion is unaffected by the addition of serotonin. Furthermore, the right pleural ganglion is visible in the upper left of the images and has a slightly enhanced level of ATP release after addition of serotonin. Thus, as expected, only particular cells in certain ganglia initiate release of ATP after stimulation.

CONCLUSIONS

In this report, we have applied our real-time ATP imaging technique to study release of ATP in the CNS. The freshwater snail *Lymnaea* was chosen as our model system because of the simplicity of its CNS, the large size of its neurons, and the high sensitivity of ATP imaging in *Lymnaea* buffer. Release from the various ganglia of *Lymnaea* was detected and varied spatially from ganglion to ganglion and within an individual ganglion. Furthermore, addition of neuroexcitatory compounds to the sample escalated release of ATP in certain regions of the CNS. Future inquiries with this technique involve attempting to identify the

specific regions or cells in ATP release and to link ATP release directly to synaptic transmission through simultaneous application of imaging and electrophysiology. Clearly, with its high spatial resolution, temporal resolution, selectivity, and sensitivity, this technique has the potential to further our understanding of neurotransmission.

ACKNOWLEDGEMENTS

The authors would like to thank Dr. Jinjian Zheng, Thomas J. Ha, Sami Jezzini, and Michaela Bodnarova for their assistance in sample isolation and their helpful discussions. The Ames Laboratory is operated for the U. S. Department of Energy by Iowa State University under Contract No. W-7405-Eng-82. This work is supported by the Director of Science, Office of Basic Energy Sciences, Division of Chemical Sciences.

REFERENCES

1. Wall, Z. W. *An Introduction to Molecular Neurobiology*; Sinauer Associates: Sunderland, MA, USA, 1992.
2. Walz, W. ed. *The Neuronal Environment: Brain Homeostasis in Health and Disease*; Humana Press: Totowa, NJ, USA, 2002.
3. Boulton, A. A., Baker, G. B., Bateson, A. N. eds. *In Vitro Neurochemical Techniques*; Humana Press: Totowa, NJ, USA, 1999.
4. Hochstetler, S. E., Puopolo, M., Gustincich, S., Raviola, E., Wightman, R. M. "Real-time amperometric measurements of zeptomole quantities of dopamine released from neurons" *Anal. Chem.* **2000**, *72*, 489-496.

5. Mundorf, M. L., Joseph, J. D., Austin, C. M., Caron, M. G., Wightman, R. M. "Catecholamine release and uptake in the mouse prefrontal cortex" *J. Neurochem.* **2001**, *79*, 130-142.
6. Phillips, P. E., Stuber, G. D., Heien, M. L., Wightman, R. M., Carelli, R. M. "Subsecond dopamine release promotes cocaine seeking" *Nature* **2003**, *422*, 614-618.
7. Zhou, S. Y., Zuo, H., Stobaugh, J. F., Lunte, C. E., Lunte, S. M. "Continuous *in vivo* monitoring of amino acid neurotransmitters by microdialysis sampling with on-line derivatization and capillary electrophoresis" *Anal. Chem.* **1995**, *67*, 594-599.
8. Bowser, M. T., Kennedy, R. T. "In vivo monitoring of amine neurotransmitters using microdialysis with on-line capillary electrophoresis" *Electrophoresis* **2001**, *22*, 3668-3676.
9. McKenzie, J. A., Watson, C. J., Rostand, R. D., German, I., Witowski, S. R., Kennedy, R. T. "Automated capillary liquid chromatography for simultaneous determination of neuroactive amines and amino acids" *J. Chromatogr. A* **2002**, *962*, 105-115.
10. Fuller, R. R., Moroz, L. L., Gillette, R., Sweedler, J. V. "Single neuron analysis by capillary electrophoresis with fluorescence spectroscopy" *Neuron* **1998**, *20*, 173-181.
11. Park, Y. H., Zhang, X., Rubakhin, S. S., Sweedler, J. V. "Independent optimization of capillary electrophoresis separation and native fluorescence detection conditions for indolamine and catecholamine measurements" *Anal. Chem.* **1999**, *71*, 4997-5002.
12. Rubakhin, S. S., Page, J. S., Monroe, B. R., Sweedler, J. V. "Analysis of cellular release using capillary electrophoresis and matrix assisted laser desorption/ionization-time of flight-mass spectrometry" *Electrophoresis* **2001**, *22*, 3752-3758.

13. Anderson, B. B., Ewing, A. G. "Chemical profiles and monitoring dynamics at an individual nerve cell in Planorbis corneus with electrochemical detection" *J. Pharm. Biomed. Anal.* **1999**, *19*, 15-32.
14. Tan, W., Parpura, V., Haydon, P. G., Yeung, E. S. "Neurotransmitter imaging in living cells based on native fluorescence detection" *Anal. Chem.* **1995**, *67*, 2575-2529.
15. Lillard, S. J., Yeung, E. S. "Temporal and spatial monitoring of exocytosis with native fluorescence imaging microscopy" *J. Neurosci. Methods* **1997**, *75*, 103-109.
16. Parpura, V., Tong, W., Yeung, E. S., Haydon, P. G. "Laser-induced native fluorescence (LINF) imaging of serotonin depletion in depolarized neurons" *J. Neurosci. Methods* **1998**, *82*, 151-158.
17. Yeung, E. S. "Following single cell dynamics with native fluorescence microscopy" *Anal. Chem.* **1999**, *71*, 522A-529A.
18. Wang, Z., Haydon, P. G., Yeung, E. S. "Direct observation of calcium-independent intercellular ATP signaling in astrocytes" *Anal. Chem.* **2000**, *72*, 2001-2007.
19. Wang, Z., Yeung, E. S. "Selective detection of neurotransmitters by fluorescence and chemiluminescence imaging" *Pure Appl. Chem.* **2001**, *73*, 1599-1611.
20. von Kugelgen, I., Allgaier, C., Schobert, A., Starke, K. "Co-release of noradrenaline and ATP from cultured sympathetic neurons" *Neuroscience* **1994**, *61*, 199-202.
21. Santos, P. F., Caramelo, O. L., Carvalho, A. P., Duarte, C. B. "Characterization of ATP release from cultures enriched in cholinergic amacrine-like neurons" *J. Neurobiol.* **1999**, *41*, 340-348.

22. Brown, P., Dale, N. "Spike-independent release of ATP from *Xenopus* spinal neurons evoked by activation of glutamate receptors" *J. Physiol.* **2002**, *540*, 851-860.
23. Jo, Y. H., Role, L. W. "Coordinate release of ATP and GABA at in vitro synapses of lateral hypothalamic neurons" *J. Neurosci.* **2002**, *22*, 4794-4804.
24. Santos, D. A., Salgado, A. I., Cunha, R. A. "ATP is released from nerve terminals and from activated muscle fibres on stimulation of the rat phrenic nerve" *Neurosci. Lett.* **2003**, *338*, 225-228.
25. Newman, E. A. "Glial cell inhibition of neurons by release of ATP" *J. Neurosci.* **2003**, *23*, 1659-1666.
26. Moroz, L. L. "Giant identified NO-releasing neurons and comparative histochemistry of putative nitrenergic systems in gastropod mollusks" *Microsc. Res. Tech.* **2000**, *49*, 557-569.
27. Stanley, P. E., McCarthy, B. J., Smither, R. eds. *ATP Luminescence: Rapid Methods in Microbiology*; Blackwell Scientific: Oxford, UK, 1989.
28. Tomiya, N., Ailor, E., Lawrence, S. M., Betenbaugh, M. J., Lee, Y. C. "Determination of nucleotides and sugar nucleotides involved in protein glycosylation by high-performance anion-exchange chromatography: sugar nucleotide contents in cultured insect cells and mammalian cells" *Anal. Biochem.* **2001** *293*, 129-137.
29. Cruz, L., Moroz, L. L., Gillette, R., Sweedler, J. V. "Nitrite and nitrate levels in individual molluscan neurons: single-cell capillary electrophoresis analysis" *J. Neurochem.* **1997**, *69*, 110-115.

30. Newman, E. A. "Propagation of intercellular calcium waves in retinal astrocytes and Muller cells" *J. Neurosci.* **2001**, *21*, 2215-2223.
31. Verderio, C., Matteoli, M. "ATP mediates calcium signaling between astrocytes and microglial cells: modulation by IFN-gamma" *J. Immunol.* **2001**, *166*, 6383-6391.
32. Stout, C. E., Costantin, J. L., Naus, C. C., Charles, A. C. "Intercellular calcium signaling in astrocytes via ATP release through connexin hemichannels" *J. Biol. Chem.* **2002**, *277*, 10482-10428.
33. Walcourt-Ambakederemo, A., Winlow, W. "5-HT receptors on identified Lymnaea neurones in culture: pharmacological characterization of 5-HT₂ receptors" *Gen. Pharmacol.* **1994**, *25*, 1079-1092.

34. FIGURE CAPTIONS

- Figure 1. Standard calibration curves for luciferase-catalyzed ATP bioluminescence in low ionic strength HEPES buffer (\blacktriangle), *Lymnaea* HEPES buffer (\blacksquare), and filtered seawater (X).
- Figure 2. Spatially resolved imaging of a *Lymnaea* CNS using a iCCD. (A) A compiled optical image of a whole CNS from 25 individual 100 ms images under low room light. (B) A compiled ATP bioluminescence image of the same whole CNS from 19 individual 1000 ms images. (C) A higher magnification compiled optical image of the right pedal ganglion of a *Lymnaea* specimen. The image is the average of 20 individual 100 ms images under low room light. (D) The corresponding compiled ATP bioluminescence image of the same ganglion averaged from 25 individual 1000 ms images.
- Figure 3. Spatially limited release of ATP from two visceral ganglia. Compiled optical images of visceral ganglia from two individual *Lymnaea* specimens. The images are the average of 20 (A) and 50 (B) individual 100 ms images under low room light. The corresponding compiled ATP bioluminescence images of the same ganglia averaged from 8 (B) and 20 (E) individual 1000 ms images. (C, F) Calculated individual frame ATP release from the outlined areas in A and D, respectively.

Figure 4. Stimulation of ATP release by addition of K^+ . (A) Compiled optical image of a *Lymnaea* CNS averaged from 50 individual 100 ms images under low room light. Corresponding compiled ATP bioluminescence images from the same CNS prior to (B) and following (C) addition 1 mM KCl. Images are the average of 8 and 20 individual 1000 ms images of ATP bioluminescence, respectively. Calculated ATP release plots from the left pedal ganglion (D), visceral ganglion (E), and non-ganglion, background area (F) prior to (■) and following (◆) stimulation. ATP release plots are calculated for the areas outlined in A.

Figure 5. Stimulation of ATP release by addition of serotonin. (A) Compiled optical image of the right pedal ganglion of a *Lymnaea* CNS averaged from 50 individual 100 ms images under low room light. Corresponding compiled ATP bioluminescence images from the same ganglion prior to (B) and following (C) addition of 100 μ M serotonin. Images are the average of 25 individual 1000 ms images of ATP bioluminescence. Calculated ATP release plots from the right pedal ganglion (D), non-ganglion, background area (E), and right cerebral ganglion (F) prior to (■) and following (◆) stimulation. ATP release plots are calculated for the areas outlined in A.

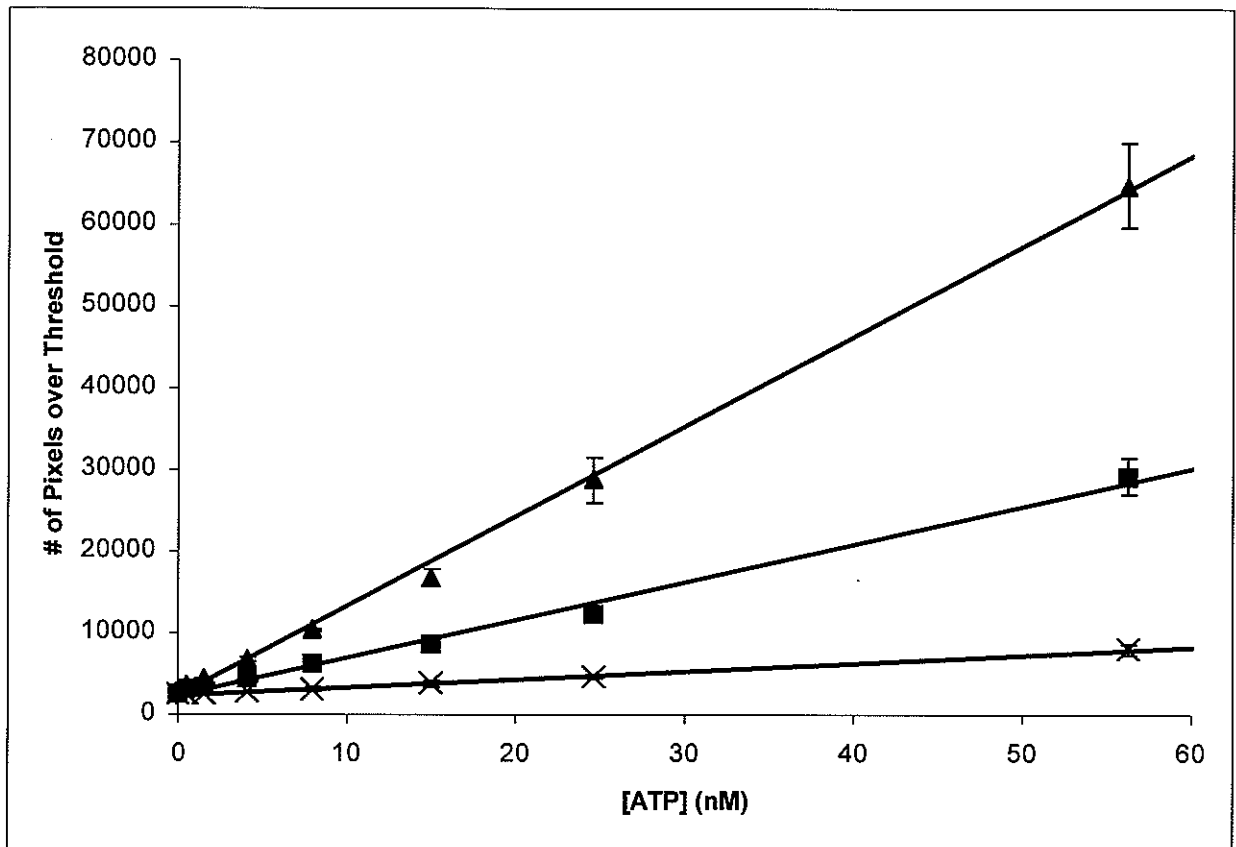


FIGURE 1

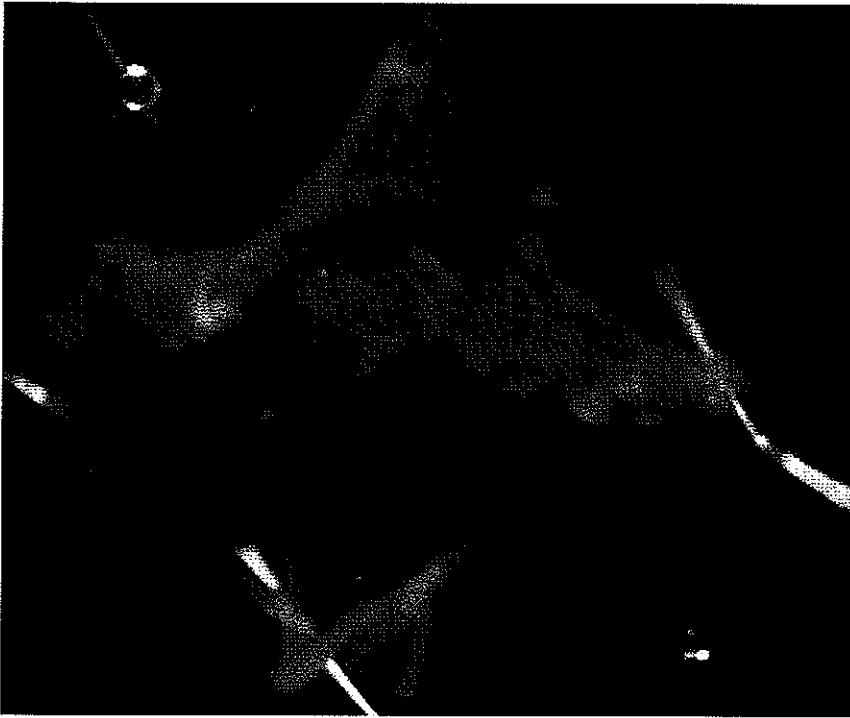


FIGURE 2A

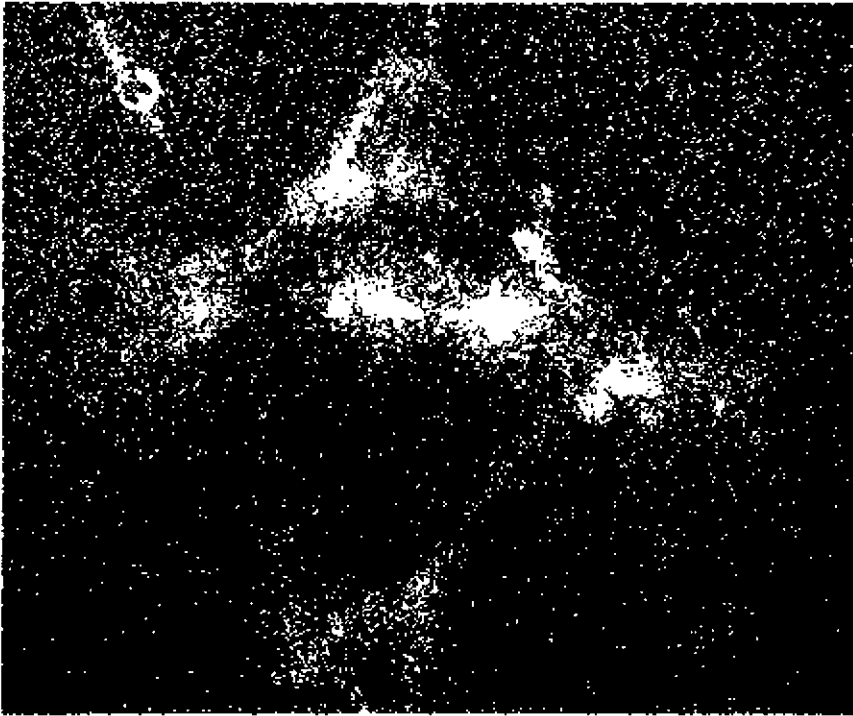


FIGURE 2B

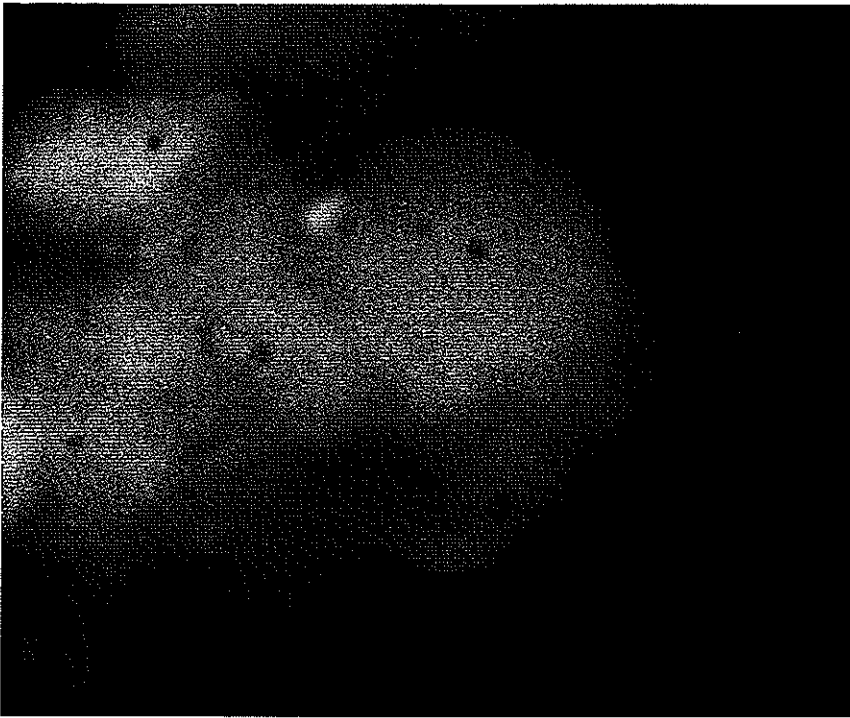


FIGURE 2C

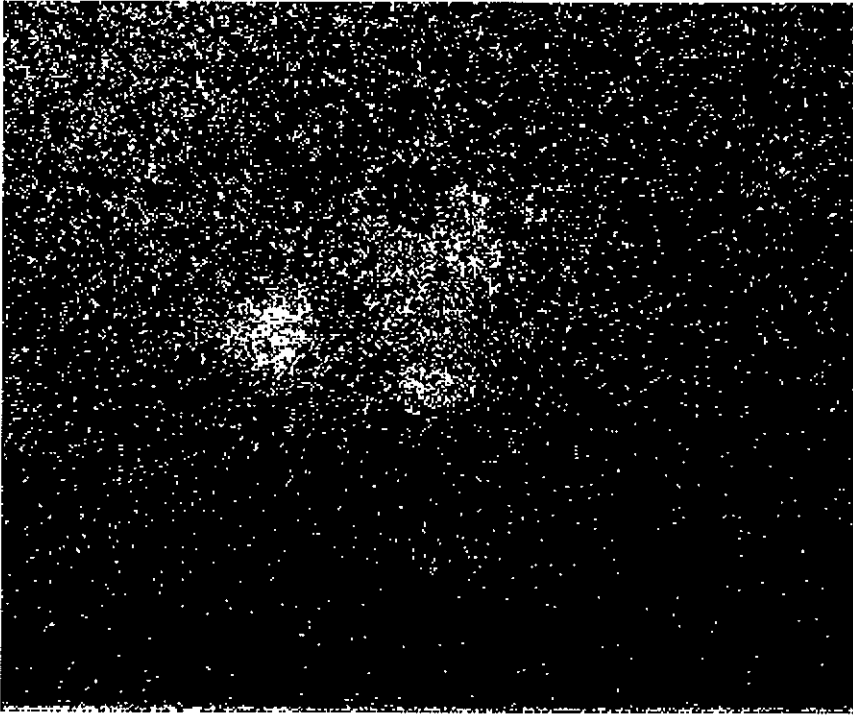


FIGURE 2D

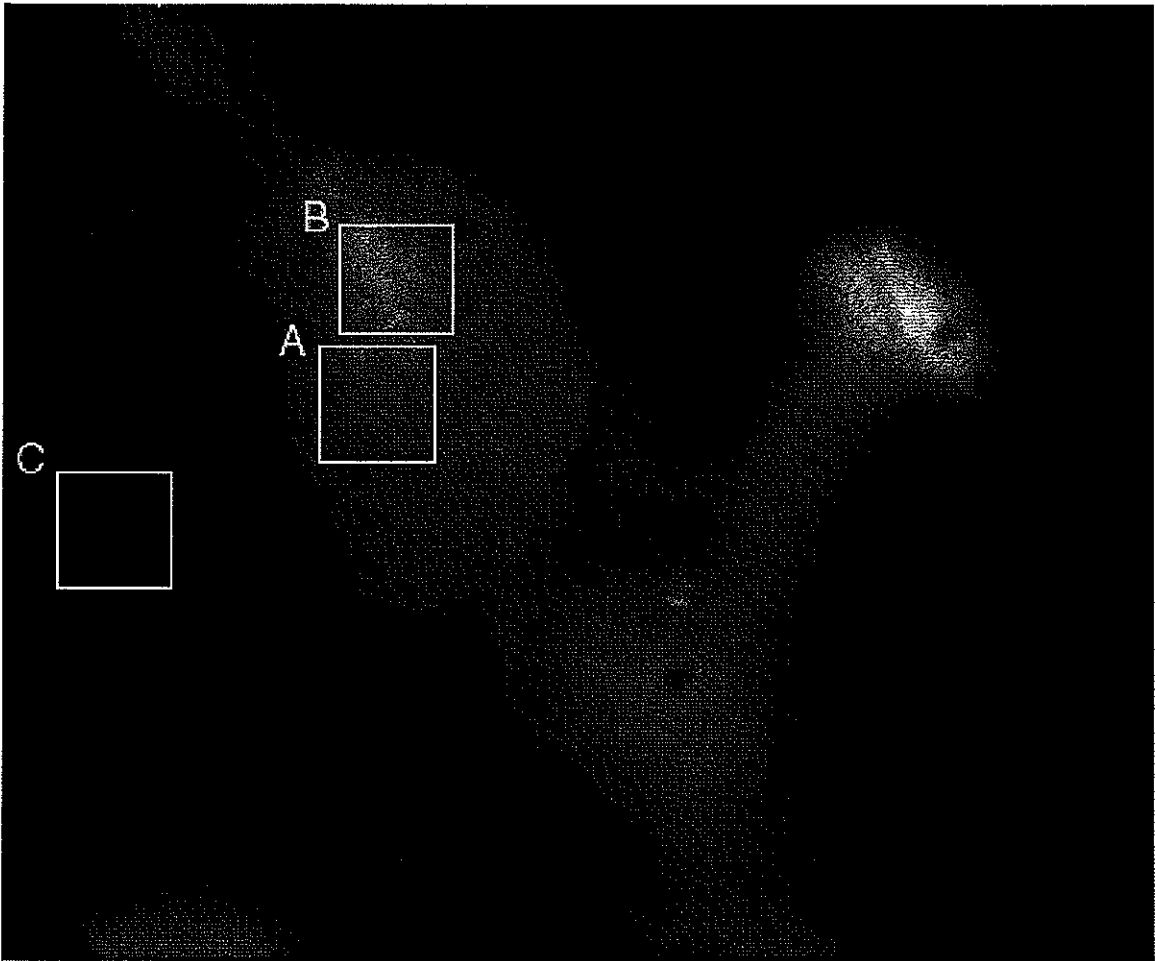


FIGURE 3A

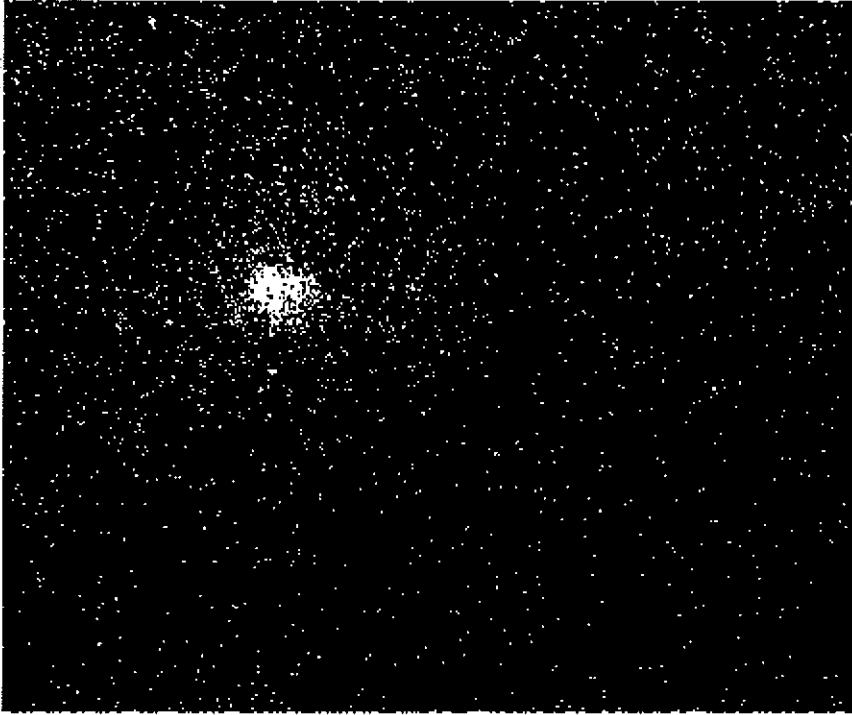


FIGURE 3B

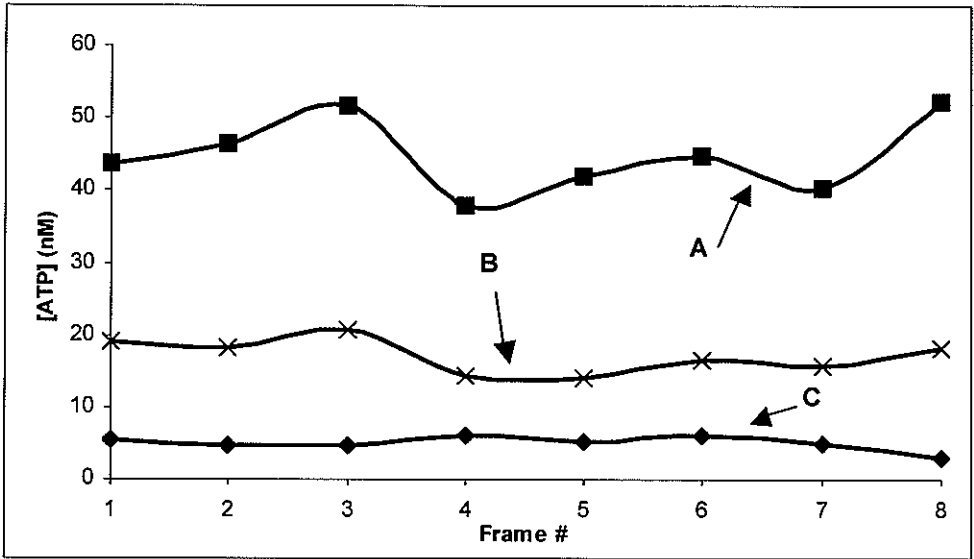


FIGURE 3C

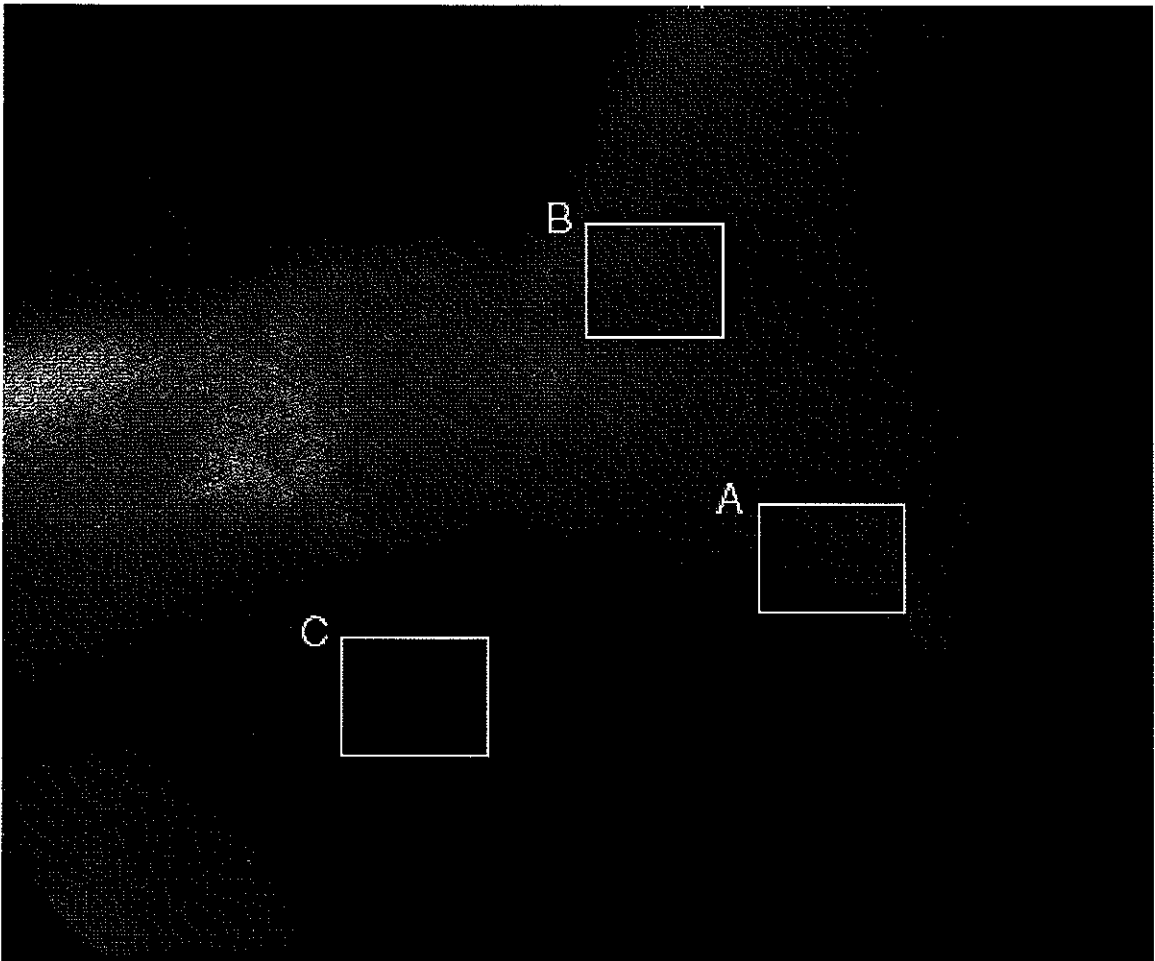


FIGURE 3D

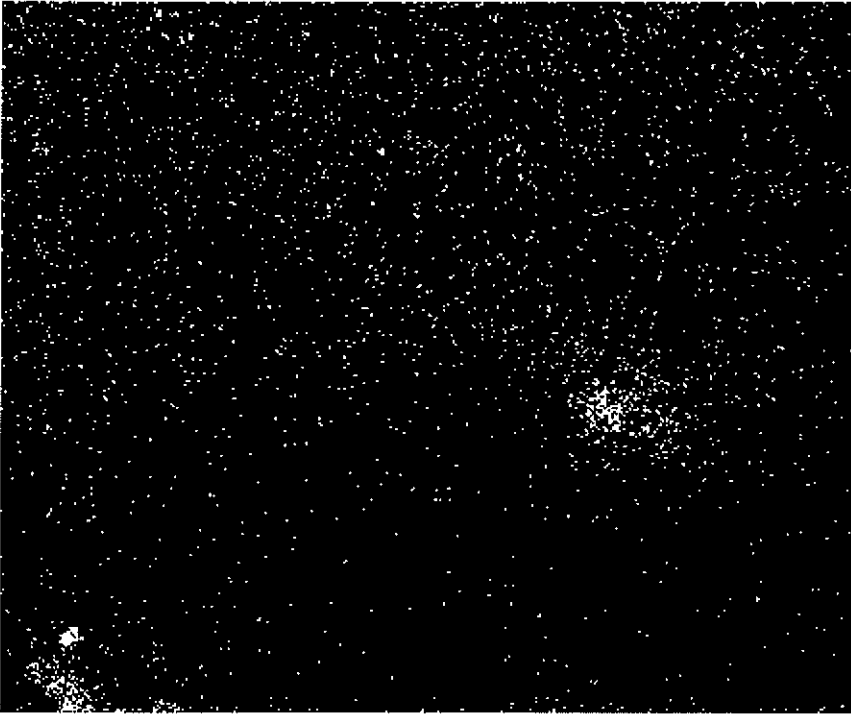


FIGURE 3E

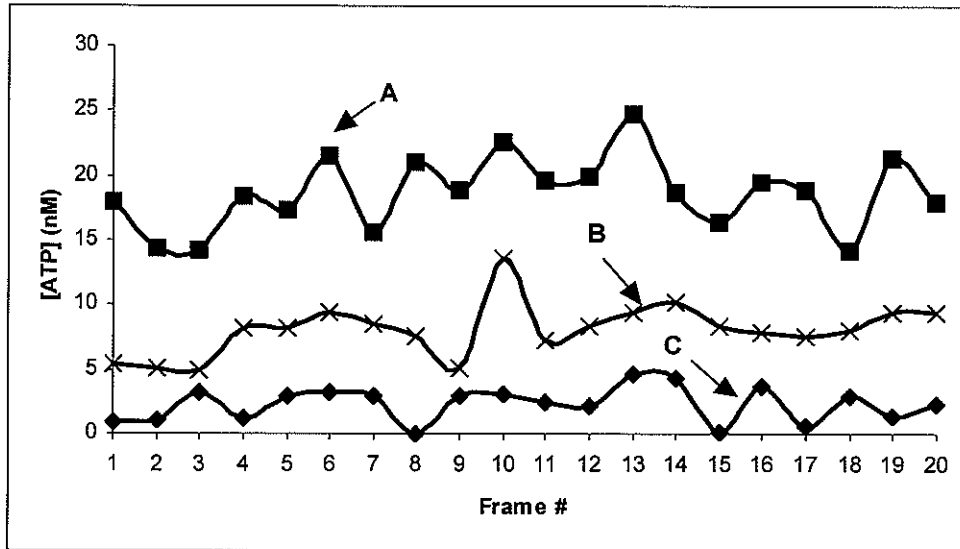


FIGURE 3F

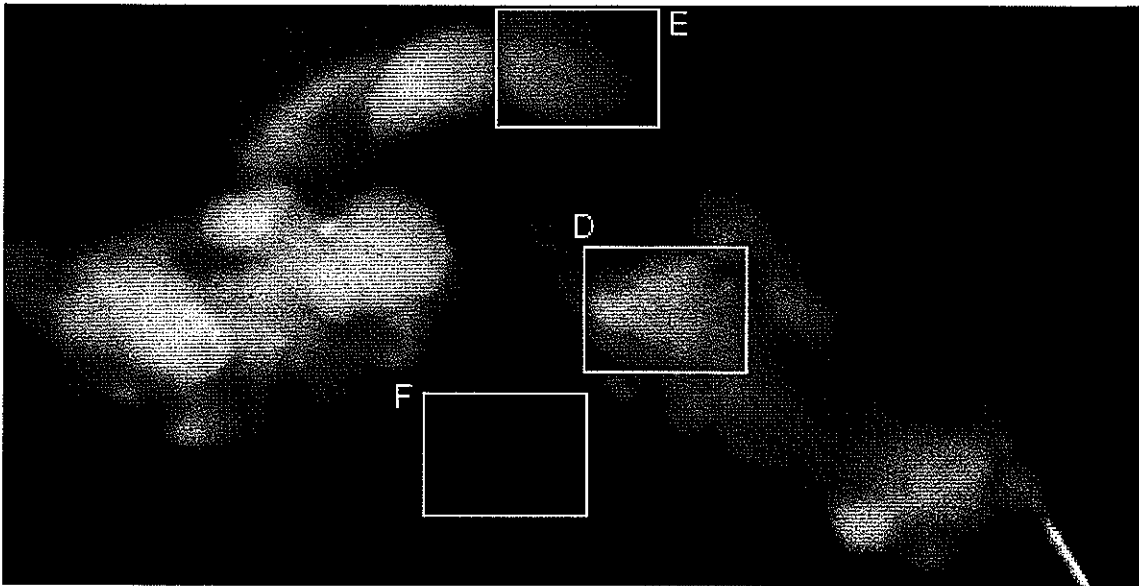


FIGURE 4A

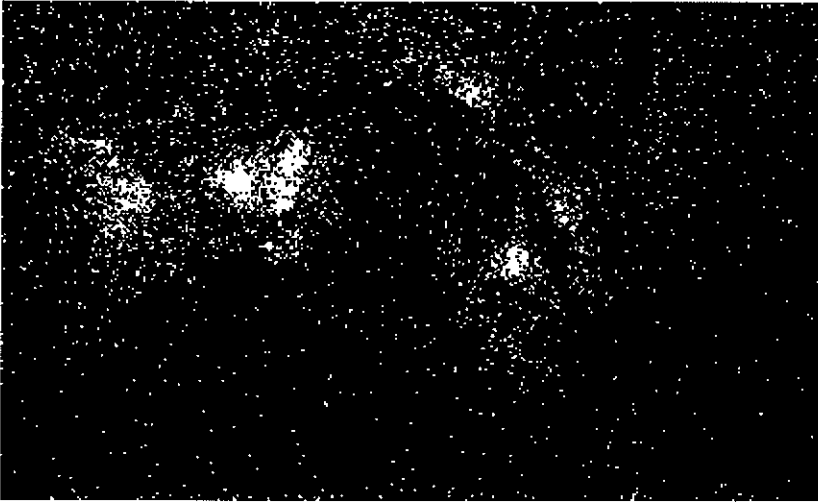


FIGURE 4B

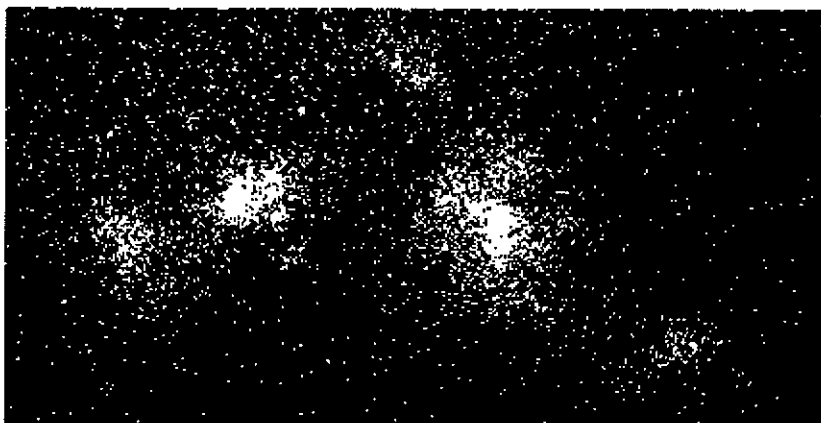


FIGURE 4C

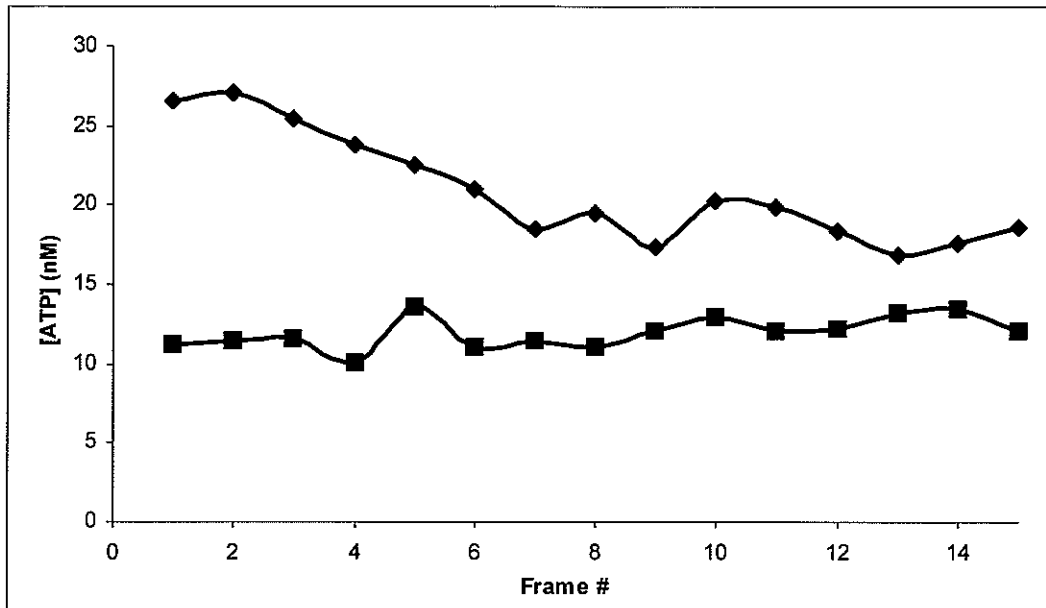


FIGURE 4D

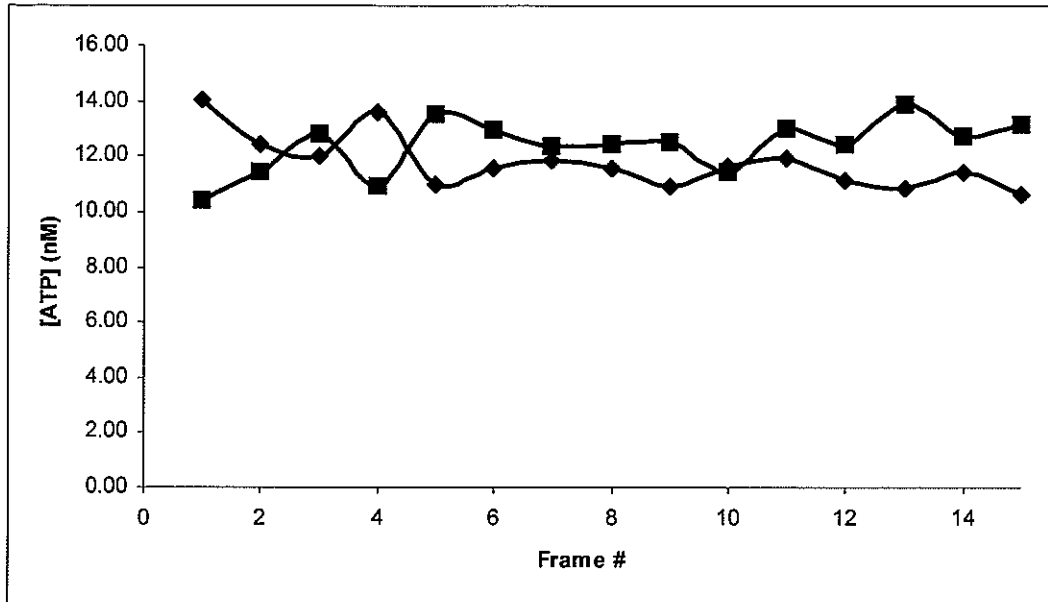


FIGURE 4E

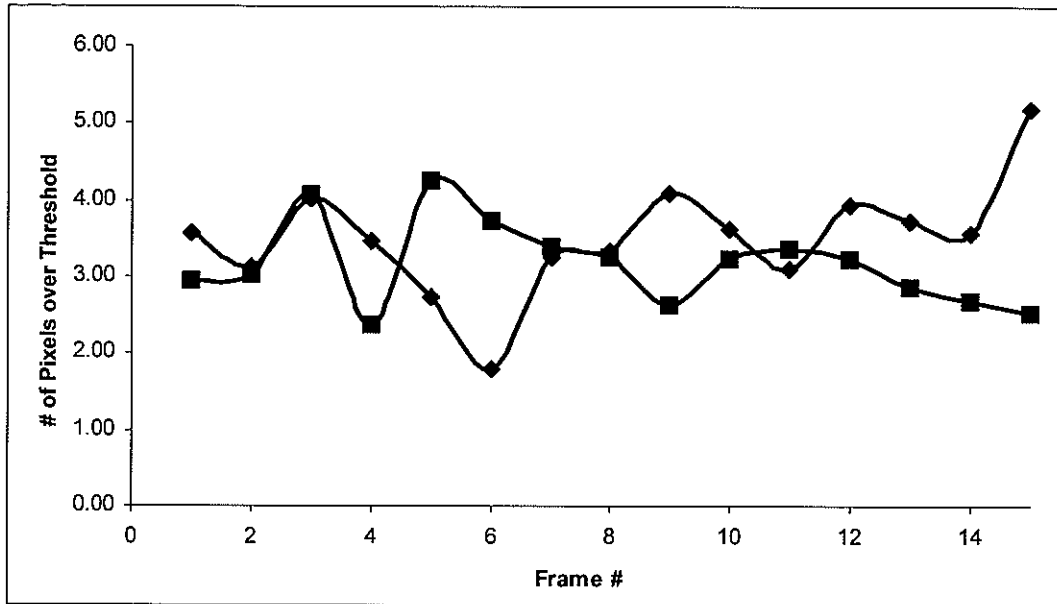


FIGURE 4F

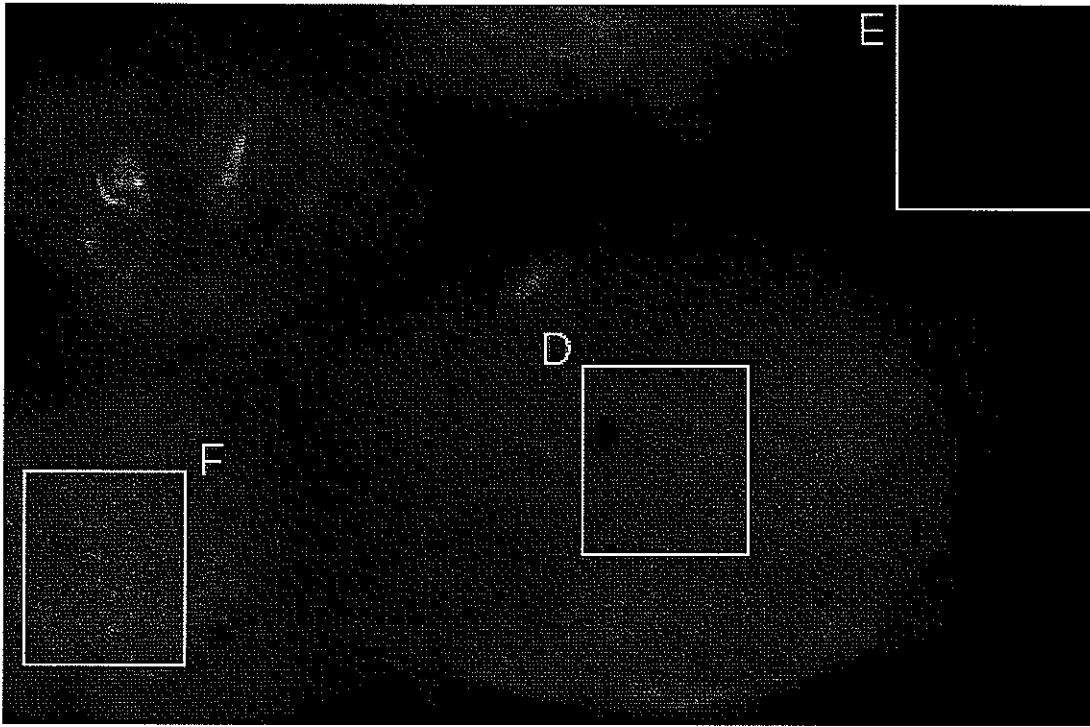


FIGURE 5A

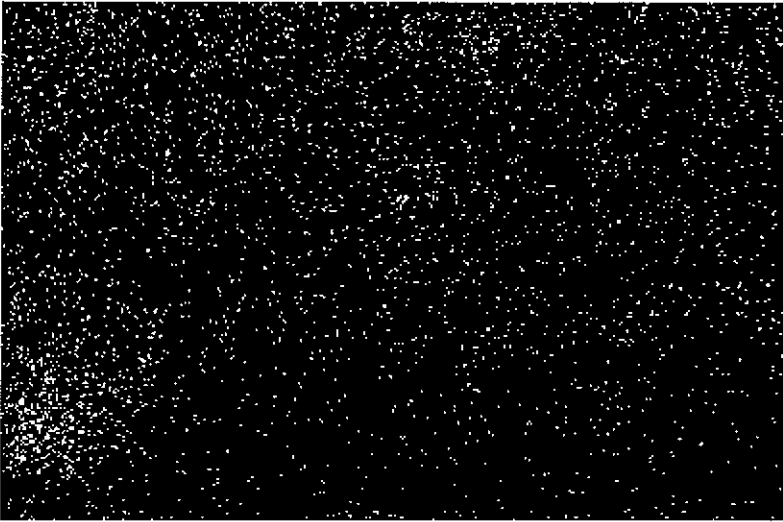


FIGURE 5B

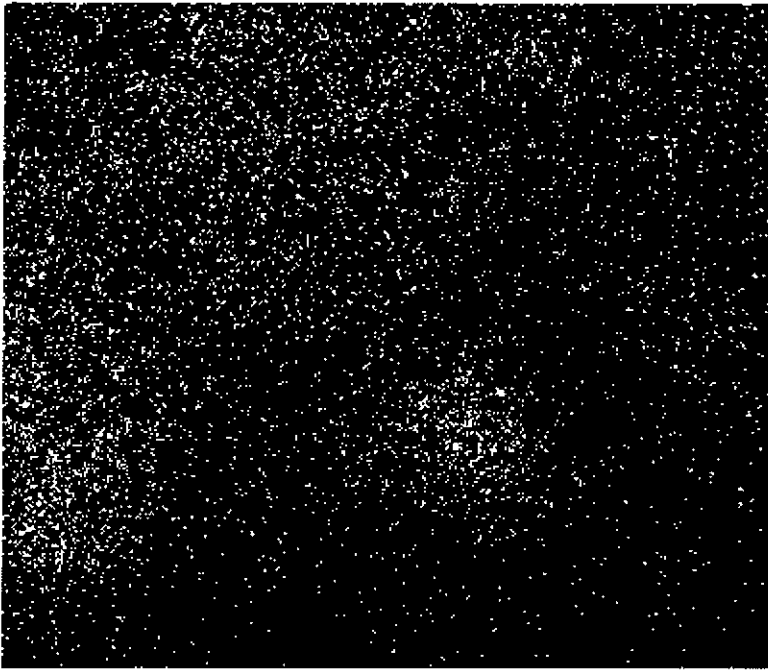


FIGURE 5C

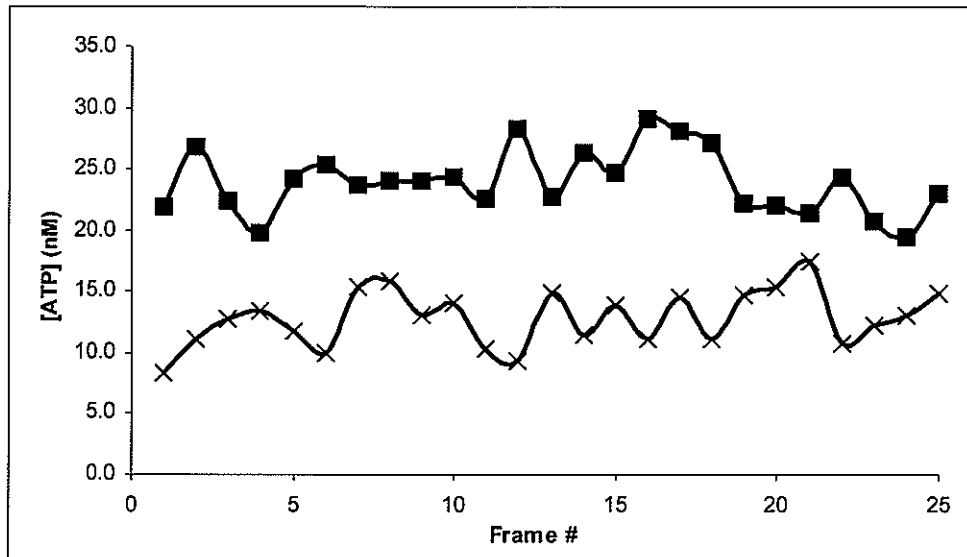


FIGURE 5D

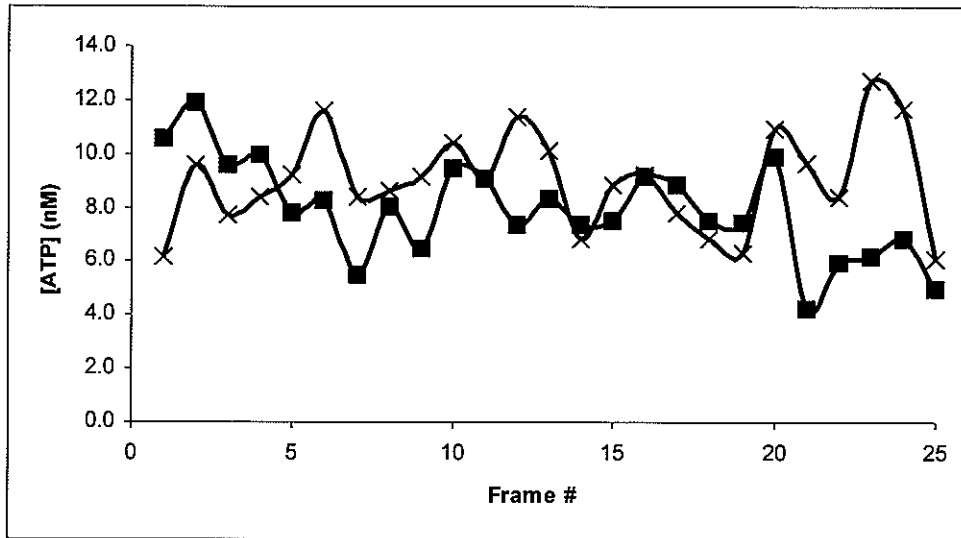


FIGURE 5E

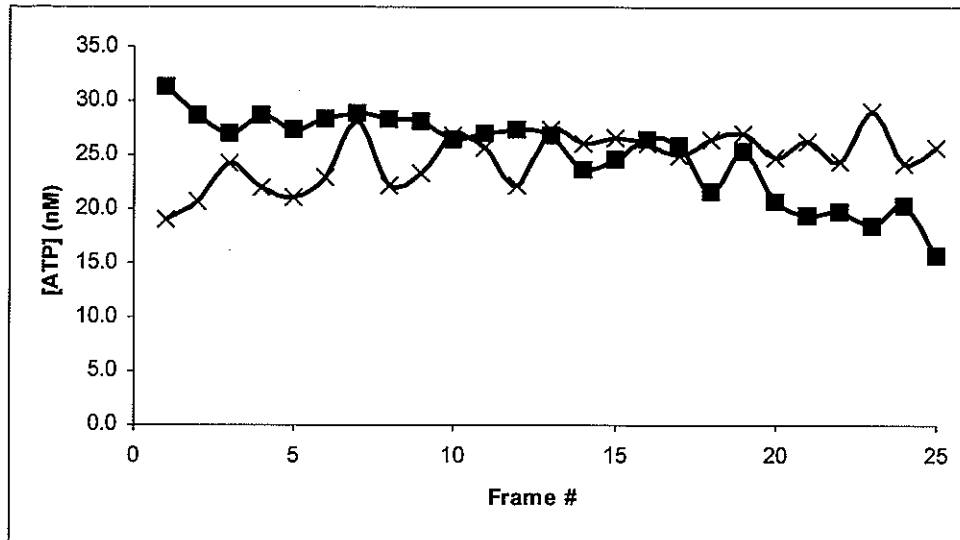


FIGURE 5F

CHAPTER 4. REAL-TIME IMAGING OF RELEASE OF ENCAPSULATED ATP FROM MCM-41-TYPE MESOPOROUS NANOSPHERES

A manuscript prepared for submission to Analytical Chemistry

Jason A. Gruenhagen^{*}, Cheng-Yu Lai, Victor S.-Y. Lin and Edward S. Yeung

^{*} Primary researcher and author

ABSTRACT

As the field of nanotechnology continues to expand at an astounding rate, the need for techniques for the analysis and characterization of nanoparticles is emerging. This challenge can be met through both the development of new techniques and the reapplication of existing methods to new systems. We employed adenosine 5'-triphosphate (ATP)/luciferase chemiluminescence imaging to study the release of ATP from end-capped mesoporous nanospheres. Mesoporous silica nanospheres of the MCM-41 type were bathed in a solution of ATP and were end-capped encasing the ATP. The particles were collected and thoroughly washed to remove any physisorbed ATP. We monitored the uncapping of these particles with disulfide-reducing agents and the subsequent release of the encased ATP via firefly luciferase chemiluminescence. Release profiles were compared amongst various capping themes and disulfide-reducing agent concentrations.

INTRODUCTION

The field of nanotechnology remains one of the hottest areas in science. Nanoscience refers to the ability to build molecular systems, termed nanostructures, on an atom by atom basis. A more general definition of nanotechnology is the synthesis and analysis of structures that can be understood on the nanometer scale¹. Nanoscience has shown great potential in the fields of microscale electronics²⁻⁴, electro-optics⁵, biosensors⁶⁻⁹, etc. One particularly interesting application of nanostructures is the development of novel drug delivery systems. Traditionally, responsive polymer systems have been designed as such devices. Hydrogel polymers are synthesized in the presence of the drug molecule of interest. The polymer, with the drug encapsulated within, usually exhibits very little release of the drug under normal conditions. The polymers are designed to be permeable to small molecules, but impermeable to the higher molecular weight drug compounds. However, upon stimulation, the hydrogels swell and drug flows through the enlarged pores in the polymer. Drug delivery polymers have been synthesized to respond to numerous types of stimulants. External stimulants include exposure of the polymers to a magnetic field, ultrasound, elevated temperature, and electric field. Other self-regulated polymers respond to their local environment with increased or decreased rates of drug release (see references 10 & 11 for thorough reviews of all of these delivery systems). For instance, Horbett and colleagues coupled a glucose sensor with a pH-sensitive insulin release mechanism. When the concentration of glucose in the blood increases, so does its concentration within the polymer. The glucose is broken down to gluconic acid by glucose oxidase immobilized within the polymer. The gluconic acid lowers the pH of the solution causing swelling of the polymer. Insulin encapsulated within the polymer is released through the swelled pores¹².

A unique type of drug delivery system was developed recently by our collaborators¹³. They synthesized mesoporous silica nanospheres of the MCM-41-type and CdS nanocrystals for containing the drug and capping the nanosphere pores, respectively. Model drug molecules loaded into the nanosphere pores were released by addition of disulfide bond-reducing molecules. This type of drug delivery system has numerous advantages over the responsive polymers systems. Prior to uncapping, the particles exhibit negligible release of the drug because the drug is trapped within the pores of the nanospheres. This feature is doubly advantageous: release of the drug would be more site-specific, and just as importantly, the drug would be protected from the external environment by the nanosphere. Exposure to the air or to antibodies within the body could conceivably damage the drug molecule. More recently, new removable caps were synthesized based on dendrimer technology. Generation 2.5 and generation 4.5 carboxyl-terminated PAMAM dendrimers, which are spherical, are the appropriate size to bind to the pores of the nanospheres and trap loaded drug molecules¹⁴.

With the significant advances in drug delivery systems, significant research has been conducted on the release mechanisms and kinetics. For example, Lai and colleagues monitored the release of encapsulated ATP from their MCM-41-type mesoporous nanospheres utilizing high performance liquid chromatography (HPLC)¹³⁻¹⁴. They assayed release of ATP prior to and following addition of DTT. While successful, the HPLC method was only sensitive enough to detect ATP release on the hour timescale. Alternatively, they deposited their nanospheres on a bed of cultured astrocytes. Upon addition of mercaptoethanol (ME), ATP was released from the particles and activated Ca^{2+} signaling in the astrocytes. These experiments demonstrated that the nanospheres were biocompatible

and that ATP was released in high enough concentrations to activate the purinergic receptors of the astrocytes ($EC_{50} \sim 40 \text{ nM}$)¹⁵. However, determination of the exact concentration of ATP released and the temporal profile of release were not possible by this method either.

Detection of release in polymeric systems is commonly accomplished by monitoring the response of the organism in which it is implanted¹¹. For instance, insulin release polymers can be analyzed by monitoring blood glucose levels. Glucose is injected into diabetic and non-diabetic test organisms, usually rats, with and without implanted insulin release polymers. The glucose levels are monitored after injection of glucose into the test organisms¹⁶. However, monitoring release from drug delivery systems on a shorter time scale is also of interest. To attain the desired effect of the drug with minimal total drug necessary would necessitate complete release of the drug on the millisecond or second timescale. Alternatively, other release systems may require continuous release of the drug. Thus, methods for the detection of the drug in real-time are indeed desirable.

ATP detection on a real-time scale is one possible method for just these types of analyses. Luciferase catalyzed bioluminescence is a highly sensitive and selective method for the detection of ATP. In its assay form, this detection scheme has been widely applied in biological fields¹⁷. Through use of an intensified charge coupled device (iCCD) attached to a microscope, Wang and colleagues demonstrated real-time imaging of release of ATP from glial cells with luciferase chemiluminescence detection¹⁸. Detection limits of 10^{-8} M were attained for standard solutions of ATP. They detected release of ATP from physically stimulated astrocytes. Through simultaneous imaging of intracellular Ca^{2+} levels along with ATP, they were able to study intercellular communication among the cells. More recently, real-time ATP imaging has been applied to the investigation of *E. coli* cell death¹⁹, ATP

release mechanisms in astrocytes²⁰ and endothelial cells²¹, and the role of ATP in neurotransmission in molluscan neural systems²². This imaging technique possesses numerous attributes which would be beneficial for analysis of drug delivery systems: high specificity, high sensitivity, excellent temporal response, etc.

Here we present the utilization of ATP chemiluminescence imaging for monitoring the release of ATP from encapsulated MCM-type mesoporous nanospheres. Real-time imaging was employed for investigating the magnitude and kinetics of release from the particles.

EXPERIMENTAL SECTION

Chemicals. Firefly luciferase (from *Photinus pyralis*) was obtained from R & D Systems (Minneapolis, MN). ME and tris(2-carboxyethyl)phosphine (TCEP) was purchased from Aldrich (Milwaukee, WI). All other chemicals were from Sigma (St. Louis, MO). Low ionic strength HEPES buffer contained 10 mM 4-(2-hydroxyethyl)-1-piperazineethanesulfonic acid (HEPES), 5 mM KCl, and 5 mM NaCl (pH = 7.75). Bioluminescence imaging solution was comprised of low ionic strength HEPES buffer with 100 µg/ml firefly luciferase and 205 µM D-luciferin. Half-generation poly(amidoamine) (G4.5 PAMAM, supplied as 5 wt.% in methanol) dendrimer was obtained from Aldrich. 3-mercaptopropyltrimethoxysilane (MPTMS), *n*-cetyltrimethylammonium bromide (CTAB), tetraethyl orthosilicate (TEOS), 2-aminoethanethiol hydrochloride (MEA), 1-[3-(dimethylamino)propyl]-3-ethylcarbodiimide hydrochloride (EDC), mercaptoethanol (ME), tris(2-carboxyethyl) phosphine hydrochloride (TCEP) and aldrithiol-2 were purchased (Aldrich) and used as received. Adenosine triphosphate disodium salt (ATP) were obtained

from Sigma and used without further purification. Nanopure water (18.1 MHz) prepared from a Barnstead E-pure water purification system was employed throughout. PBS buffer (10.00 mM, pH 7.4) solutions with the total ionic strength of 0.06 M were prepared and used as the solvent for all the loading and release experiments of ATP.

Loading and Washing of ATP into the Mesoporous Framework of Linker-MSN and the Capping of the Mesopores with Mercaptoacetic Acid-Functionalized CdS Nanoparticles. MCM-41-type mesoporous silica nanospheres with 2-(propyldisulfanyl)ethylamine functionality, mercaptoacetic acid-derivatized cadmium sulfide (CdS) nanoparticles, and carboxyl-terminated PAMAM dendrimers were synthesized as described previously¹³⁻¹⁴. For loading of the particles, the purified linker-MSN material (100.00 mg) was incubated in phosphate-buffered saline (PBS) solution (0.60 mL, pH 7.4) of 3.00 μ mol ATP for 24 h. The mercaptoacetic acid-functionalized CdS nanoparticles (0.15 mmol) were dissolved in 2.00 mL of PBS buffer with ATP (0.01 mmol in both cases). 1-[3-(dimethylamino)propyl]-3-ethylcarbodiimide hydrochloride (57.50 mg, 0.30 mmol) was added to the CdS/drug solution. The reaction mixture was allowed to stir for 24 h, followed by centrifuging the suspension at 12 000 rpm for 3 min. The resulting precipitates (ATP-loaded, CdS-capped MSNs) were isolated and dried under vacuum. The CdS-capped MSN with ATP (10.00 mg) material was dispersed in 1.50 mL of PBS buffer (pH 7.4), followed by repeating wash/sonication/centrifugation cycles for five times to remove physisorbed ATP molecules from the exterior surface of the material. Following these washes, the particles were again dried under vacuum.

Loading of ATP into the Mesoporous Framework of Linker-MSN and the Capping of the Mesopores with G4.5 PAMAM Dendrimers. The purified linker-MSN

material (100.00 mg) was incubated in the aforementioned PBS buffer solution (0.7 mL, pH 7.4) of ATP (3.00 μ mol) for 24 h. 2 mL of G4.5 Starburst dendrimer solution (supplied as 5% w/w in methanol) was evaporated and transferred to 1 mL aqueous solution in the buffer. 1-[3-(Dimethylamino)propyl]-3-ethylcarbodiimide hydrochloride (EDC) (30 mg) was added to the G4.5/drug solution. The reaction mixture was allowed to stir for 24 h. Any remaining unreacted dendrimers and by-products were removed by subsequent washing via centrifugation, and redispersion of the suspension using water. The resulting precipitates (ATP- loaded, G4.5-capped MSNs) were isolated and dried under vacuum.

Scanning and Transmission Electron Microscopy. Particle morphology of these materials was determined by scanning electron microscopy (SEM) using a JEOL 840A scanning electron microscope with 10 kV accelerating voltage and 0.005 nA of beam current for imaging. For transmission electron microscopy (TEM) studies, a small aliquot was removed and placed between two clean glass slides. Slides were rubbed back and forth to break up larger clumps. The resulting powder was washed into a Petri dish with acetone. The mixture was stirred and ultrasonically agitated. While still in suspension, a lacey carbon-coated TEM grid was pulled through the suspension. The grid was allowed to dry in air and then examined in an Amray 1845 FE-SEM followed by examination with a Philips model CM-30 TEM operated at 300 kV. The specimen was given no further treatment, as it appeared stable under beam bombardment. The preparation for the microtomed samples included embedding into a derivation of EPON epoxy resin using EmBed 812. This mixture was centrifuged and cured for 24 h at 60 °C. The embedded block was microtomed to obtain thin sections of 60-80-nm thickness by using a Reichert Ultracut S ultramicrotome with a diamond knife (Diatome). The floated sections were mounted on a 400 mesh Pd-

coated Cu grid. The TEM images of these microtomed samples were recorded using a Philips model CM-30 TEM operated at 300 kV at 69 000 to 340 000 electron optical magnification.

ATP Imaging. ATP imaging was performed on the stage of an inverted microscope (Axiovert 100 TV, Zeiss, Germany). Chemiluminescence signal was collected with a Zeiss Apochromat 20X microscope objective (NA = 0.75) and detected with an iCCD (EEV 576 x 384 pixels CCD chip, Roper Scientific, Trenton, NJ) attached to the camera mount of the microscope. Nanosphere bulk samples were incubated in imaging solution for at least four hours prior to conducting experiments. The nanospheres were centrifuged down and the supernatant was replaced with fresh imaging solution. Images were collected at a frequency of 0.80 Hz with 1000 ms exposure times. All experiments were performed at room temperature. Stimulant was applied to the cells via a micropipettor.

Data Presentation/Analysis. Chemiluminescence signal was obtained and processed with Winview32 software (Roper Scientific). The number of pixels over a threshold value was tabulated for each particle and each frame of data. The ATP concentrations were calculated from a calibration curve obtained with the exact same imaging parameters. Displayed images are the average of 50 frames.

RESULTS AND DISCUSSION

Characteristics of MCM-41-type Nanospheres. The synthesized MCM-41-type nanospheres employed in this study were identical to those examined in previous reports¹³⁻¹⁴. As shown in Figure 1A, the particles have an average diameter of 200 nm. One unique feature of this particular type of nanosphere preparation is their excellent uniformity. The

nanospheres, as depicted in Figure 1 (B and C), have linear pores 2.3 nm in diameter traversing their entire length. Few chemical techniques afford the parameters necessary to examine release of encapsulated drugs from these particles on the second timescale. Extreme sensitivity is essential since very small amounts of drug are released from the particles. Moreover, an imaging technique would be preferred because release could be observed for single or small aggregates of nanospheres. Fluorescence imaging of release of a model compound would be one method that meets these criteria. However, as observed in previous studies¹³, the nanospheres capped with CdS are highly fluorescent throughout the visible spectrum. Alternatively, chemiluminescence imaging is nearly as sensitive as fluorescence imaging. Furthermore, since no light source is utilized in this case, the fluorescent nanoparticles would not be problematic. Chemiluminescent imaging of ATP release was chosen for a number of reasons. 1) The method is extremely sensitive since firefly luciferase has an extremely high luminescence efficiency of 0.88²³. 2) The reaction kinetics of firefly luciferase catalyzed ATP chemiluminescence are exceedingly rapid²⁴. 3) The luciferase enzyme employed in ATP imaging measures approximately 5.5 X 6.5 X 8.1 nm in size²⁵ and therefore cannot enter the uncapped pores of the nanospheres. This ensures that any detected chemiluminescence must result from release of ATP from the nanospheres. 4) Since previous experiments were conducted on ATP release from this system¹³, comparisons can be drawn between the investigations.

Compatibility of ATP Imaging and MCM-type Nanosphere Drug Release.

Though detection of ATP via firefly luciferase-catalyzed chemiluminescence is highly specific for ATP, experiments were conducted to ensure that the uncapping molecules did not interfere with the detection scheme. Disulfide bond cleaving molecules are commonly added

to protein solutions to maintain proper disulfide bonding. However, excessive concentrations of these agents could diminish the activity of firefly luciferase. This appeared to be the case for ME and DTT. As depicted in Figure 2A, the chemiluminescence from injection of a 66 nM ATP standard was four times lower for luciferase containing 500 μ M ME than for luciferase without ME. In previous experiments, 1 mM ME was employed to remove the CdS caps from their nanospheres. Thus, it was not a suitable uncapping agent for use with our detection scheme. As also illustrated in Figure 2A, addition of 10 mM DTT to luciferase imaging solution also caused a significant reduction in chemiluminescence from injected ATP standards. In this case, however, the reduction in signal was only by a factor of 2. Previous experiments demonstrated that DTT concentrations of 0.1 – 10 mM were effective in uncapping the CdS-capped nanospheres¹³. Therefore, further experiments were conducted to determine if lower concentrations of DTT also interfered with detection of ATP. Figure 2B depicts the results of these experiments. DTT concentrations of 20 mM, 10 mM, and 5 mM showed progressively less interference with our detection of ATP chemiluminescence. Finally, 1 mM DTT did not interfere with our detection scheme significantly, compared to imaging solution only. Thus, DTT was employed as the uncapping agent in our initial experiments. Based on work by Whitesides and coworkers, TCEP was also examined as a possible uncapping agent. TCEP was developed as a softer disulfide bond-cleaving molecule²⁶ and thus might be a more suitable uncapping agent than DTT for our experiments. As shown in Figure 2A, 5 mM TCEP did not cause any significant interference with detection of injected ATP standards. Since only 100 μ M TCEP was necessary to induce significant uncapping of the nanospheres¹⁴, this compound was applicable for our experiments. In Figure 2A, the control (no uncapping agent present) data serves as a

calibration curve for the detection of ATP from luciferase-catalyzed chemiluminescence. The limit of detection was calculated to be 0.5 nM ATP, and the signal was linear over three orders of magnitude (0.5 – 66 nM ATP; $R^2 = 0.9997$).

Detection of Release of Encapsulated ATP from CdS-capped MCM-41-type Mesoporous Nanospheres. Upon addition of nanospheres containing encapsulated ATP to imaging solution, very large chemiluminescence levels were observed. This was a result of physisorbed ATP on the surface of the particles, rather than release or leakage from inside the pores. The surface of the nanospheres is functionalized with positively-charged 2-(propyl)disulfanyl)ethylamine groups, which likely forms strong electrostatic complexes with negatively-charged ATP molecules. Rinsing the particles with a high ionic strength buffer resulted in removal of a large portion of the physisorbed ATP (data not shown). This corroborated our hypothesis, since higher ionic strength solutions would destabilize the electrostatic interactions between ATP and the surface amines. By bathing the nanospheres in imaging solution for an extended amount of time (~4 hrs), any remaining physisorbed ATP was broken down enzymatically into ADP and phosphate.

Prior to uncapping with DTT, nanospheres generated no significant ATP release. However, upon addition of DTT, significant levels of ATP were released from the particles. Figure 3A depicts nine frames of chemiluminescence data obtained from a representative experiment. The optical image shows an aggregate of nanospheres in the lower right region of the image. In this case, the maximal ATP release was observed 93 sec after stimulation, as illustrated in the signal profile in Figure 3B. The magnitude of the ATP signal rose quickly in an initial burst and then quickly decreased again. The rate of signal decline slowed greatly approximately 3 – 4 min after stimulation, and the magnitude of release approached pre-

stimulation levels 8-10 min after stimulation. From this release profile, many observations can be drawn. First, as previously observed via HPLC, the majority of the ATP which is released is detected in the first hour after stimulation with DTT¹³. Our results suggest that, in fact, the majority of release occurs in the first few min after uncapping. The initial peak in the signal likely represents release of a pool of free ATP near the “mouths” of the pores. Additionally, the release following the initial burst (3 – 10 min) is likely associated with diffusion of free ATP from the center of the particle through the pores to the extracellular solution. Finally, the very low-level release detected by Lai and colleagues over a period of days would correspond to release of physisorbed ATP from within the pores. The pores, like the nanosphere external surface, are functionalized with 2-(propylsulfanylamino)ethylamine groups. Thus, the strong adsorption of ATP within the pores can be expected.

Comparison of Uncapping of Nanospheres by DTT and TCEP. As TCEP was the most compatible reducing agent for use with our detection system, it was also utilized for uncapping ATP-loaded nanospheres. While ATP was released in this case as well, surprisingly the release magnitude was attenuated while the temporal maximum of release was extended compared to stimulation of identical particles with DTT. Table 1 illustrates these observations for stimulation of release by 5 mM TCEP and 5 mM DTT. These results indicate that TCEP cannot cleave the disulfides bonds securing the CdS endcaps to the nanospheres as quickly as can DTT. Many possible explanations can be proposed for this phenomenon. First and foremost, the reducing power of DTT is greater than that of TCEP²⁶. The rate of disulfide cleavage for the linkers is likely slower for TCEP than DTT. Thus the rate of nanocrystal release and the ATP release would be delayed. Another possible explanation of this phenomenon is the charge of TCEP. The CdS nanocrystals are derivitized

with carboxylic acid moieties and are thus negatively-charged across their entire surface. TCEP is also negatively-charged while DTT is neutral. Therefore, DTT can more easily diffuse into the nanosphere structure to reach and cleave the disulfide linkers. Also, since TCEP is larger than DTT, its diffusion through the CdS nanocrystal caps could be sterically hindered. The actual basis for the attenuated release of ATP in the case of TCEP stimulation likely is a combination of the above plus additional unidentified reasons. A further investigation of the stimulant diffusion and reaction kinetics would be necessary to fully explain our observations.

Effect of DTT Concentration on Release of Encapsulated ATP from Nanospheres. Experiments were conducted to examine the effect of varying the concentration of uncapping agent on the kinetics and magnitude of release. DTT concentrations from 5 μ M to 5 mM were added to CdS end-capped mesoporous nanospheres. The 5 mM DTT was employed to ensure complete uncapping of the nanospheres, though it decreased the luminescence efficiency as demonstrated in Figure 2B. This was compensated for by using the calibration curve for imaging solution containing 5 mM DTT to calculate ATP concentration. As depicted in Figure 4A, the temporal maximum of ATP release was delayed for lower concentrations of DTT. Intuitively, for high concentrations, a large number of DTT molecules are present near the CdS disulfide linkages. However, for low concentrations, the free DTT molecules must diffuse to the particles to cause uncapping. Figure 4B shows the magnitude of ATP release was also altered with the various concentrations of DTT. 5 mM DTT induced release of 32.9 \pm 1.6 nM ATP compared to only 8.0 \pm 2.9 nM ATP for 5 μ M DTT. Thus the lower concentrations of DTT were unable to completely uncap all of the nanosphere pores or, at least, were unable to uncap all of the

pores nearly simultaneously. These results corroborate those obtained previously with HPLC¹³.

Release of ATP from Dendrimer-capped Nanospheres. Release of ATP from MCM-41-type mesoporous nanospheres with dendrimer caps was also assessed. Two types of PAMAM-based dendrimers (generations 2.5 and 4.5) have been successfully attached to the pores of the nanospheres¹⁴. When stimulated with 5 mM DTT, release of ATP was detected from both nanospheres. The release profiles are displayed in Figure 5 for generation 2.5 and generation 4.5 dendrimer-capped particles along with the profile previously shown in Figure 3B for DTT stimulation. The release profiles for the dendrimer capped particles are obviously quite distinct from those of CdS nanocrystal caps. Upon stimulation with DTT, the generation 2.5 dendrimer-capped particles showed no immediate release of ATP. Only after 20-30 min was a small amount of release observed from the nanospheres. This ATP release slowly increased to a maximum approximately 1.5 hours after stimulation and slowly decreased back towards baseline levels. For nanospheres with generation 4.5 dendrimer caps, release occurred more quickly. ATP signal began 5 min after the addition of DTT, and maximum release was observed 11 min after stimulation. For both types of dendrimer-capped nanospheres, the maximum release of ATP was smaller and the time for the maximum release was longer than that of CdS-capped particles. The dendrimer caps are more flexible than the CdS nanocrystal caps. After forming one link to the nanosphere, a dendrimer can flex slightly and form additional bonds to the mouth of the nanosphere pore. Alternatively, the CdS nanocrystals cannot flex and will form fewer bonds to the nanosphere. Therefore, more disulfide bonds would need to be broken in order to release the dendrimer caps from the nanospheres upon stimulation. Additionally, with more bonds formed, the

dendrimer caps would be held tighter to the nanosphere allowing less room for the reducing agents to diffuse into the pores to reach the disulfide linkers. In the case of the generation 2.5 dendrimers, the dendrimers are actually smaller than the 2.3 nm diameter pores of the nanospheres. Therefore, these dendrimers could diffuse into and bind to the nanospheres. Thus, the pores of nanospheres capped with generation 2.5 dendrimers would be bound by more than one capping molecule. This too would decrease the rate of ATP release the nanospheres. Upon further examination of Figure 5, it appears that the total released ATP from the dendrimer-capped nanospheres is actually greater than that of the CdS-capped particles. As observed via TEM images in earlier report¹³, the capping efficiency for CdS nanocrystal caps is much less than 100%. Alternatively, the dendrimer-capped particles have a capping efficiency of nearly 100%. This indicates that though the nanospheres were loaded with the same concentration of ATP, the dendrimer-capped particles contain more ATP than the CdS-capped particles. Thus, more ATP is present to be released upon stimulation with DTT.

CONCLUSIONS

Real-time imaging of ATP release via luciferase-catalyzed chemiluminescence is a highly sensitive and selective method. This technique is widely applicable in biological systems because of the widespread distribution of ATP. We have now applied this imaging technique to the study of nanoparticles. Drug release from mesoporous nanospheres end-capped with CdS nanocrystals and PAMAM dendrimers were monitored by loading the nanospheres with ATP and inducing its release. The kinetics of release were investigated and revealed a pulse-type release from CdS-capped particles upon uncapping. Alternatively,

the dendrimer-capped nanospheres release ATP in a more gradual and plateau-like profile. Understanding the release mechanisms and release kinetics of these systems will aid in the development of more advanced particle designs. The capping molecules can be tuned to whether a high concentration, one-time drug release or a lower level, continuous drug release treatment is desired. As additional capping molecules and nanosphere drug containers are developed, more advanced, applicable, and tunable drug delivery systems will become available.

ACKNOWLEDGEMENTS

The authors would like to thank Brian G. Trewyn and Daniela R. Radu for their assistance in sample preparations and their helpful discussions. The Ames Laboratory is operated for the U. S. Department of Energy by Iowa State University under Contract No. W-7405-Eng-82. This work is supported by the Director of Science, Office of Basic Energy Sciences, Division of Chemical Sciences.

REFERENCES

1. Wilson, M., Kannangara, K., Smith, G., Simmons, M., Raguse, B. *Nanotechnology: Basic Science and Emerging Technologies*; Chapman and Hall/CRC: Boca Raton, FL, 2002.
2. Macucci, M., Iannaccone, G., Greer, J., Martorell, J., Sprung, D. W. L., Schenk, A., Yakimenko, I. I., Berggren, K.-F., Stokbro, K., Gippius, N. *Nanotechnology* **2001**, *12*, 136-142.

3. Dai, L. In *Perspectives of Fullerene Nanotechnology*; Ed. Osawa, E., Kluwer Academic Publishers: Dordrecht, Netherlands, 2002, 93-111.
4. Allan, G., Delerue, C., Krzeminski, C., Lannoo, M. In *Nanostructured Materials*; Eds. Knauth, P., Schoonman, J., Kluwer Academic Publishers: Norwell, MA, 2002, 161-183.
5. Krenn, J. R. *Nature Materials* **2003**, *2*, 210-211.
6. Cullum, B. M., Vo-Dinh, T. *Biomedical Photonics Handbook*; CRC Press LLC: Boca Raton, FL, 2003.
7. Lin, V. S. Y.; Lai, C.-Y.; Huang, J.; Song, S.-A.; Xu, S. *J. Am. Chem. Soc.* **2001**, *123*, 11510-11511.
8. Lai, C.-Y.; Trewyn, B. G.; Jeftinija, D. M.; Jeftinija, K.; Xu, S.; Jeftinija, S.; Lin, V. S. Y. *J. Am. Chem. Soc.* **2003**, *125*, 4451-4459.
9. Livage, J., Coradin, T., Roux, C. *J. of Physics: Condensed Matter* **2001**, *13*, R673-R691.
10. Peppas, N. A., Huang, Y., Torres-Lugo, M., Ward, J. H., Zhang, J. *Annu. Rev. Biomed. Eng.* **2000**, *2*, 9-29.
11. Kost, J., Langer, R. *Advanced Drug Delivery Reviews* **2001**, *46*, 125-148.
12. Ishihara, K., Kobayashi, M., Ishimaru, N., Shonohara, I. *Polym. J.*, **1984**, *16*, 625-631.
13. Lai, C.-Y., Trewyn, B. G., Jeftinija, D. M., Jeftinija, K., Xu, S., Jeftinija, S., Lin, V. S.-Y. *J. Am. Chem. Soc.* **2003**, *125*, 4451-4459.
14. Lai, C.-Y., Radu, D., Jeftinija, K., Jeftinija, S., Lin, V. S.-Y. In preparation.

15. King, B. F., Neary, J. T., Zhu, Q., Wang, S., Norenberg, M. D., Burnstock, G. *Neuroscience* **1996**, *74*, 1187-96.
16. Fischel-Ghodsian, F., Brown, L., Mathiowitz, E., Brandenburg, D., Langer, R. *Proc. Natl. Acad. Sci. U. S. A.* **1988**, *85*, 2403-2406.
17. Gould, S. J., Subramani, S. *Anal. Biochem.* **1988**, *175*, 5-13.
18. Wang, Z., Haydon, P. G., Yeung, E. S. *Anal. Chem.* **2000**, *72*, 2001-2007.
19. Gruenhagen, J. A., Aspinwall, C. A., Yeung, E. S. Unpublished results.
20. Yeung, E. S., Gruenhagen, J. A., Aspinwall, C. A. In preparation.
21. Gruenhagen, J. A., Yeung, E. S. In preparation.
22. Gruenhagen, J. A., Lovell, P., Moroz, L. L., Yeung, E. S. In preparation
23. Chiu, N. H. L., Christopoulos, T. K. *Clinical Chemistry* **1999**, *45*, 1954-1959.
24. McElroy, W. D., DeLuca, M. *Bioluminescence and Chemiluminescence: Basic Chemistry and Analytical Applications*; Academic Press: New York, 1981, 179-196.
25. Franks, N. Personal Correspondence
26. Burns, J. A., Butler, J. C., Moran, J., Whitesides, G. M. *J. Org. Chem.* **1991**, *56*, 2648-2650.

Table 1. Characteristics of release of encapsulated ATP from CdS-capped MCM-type mesoporous nanospheres for various reducing agents.

Uncapping Agent	Release Maximum (min)	Release Maximum (nM ATP)
5 mM DTT	1.8 +/- 0.8	32.1 +/- 9.8
5 mM TCEP	8.0 +/- 2.3	4.5 +/- 0.8

FIGURE CAPTIONS

- Figure 1. MCM-type mesoporous nanosphere images. SEM (A) and TEM (B, C) micrographs of the linker-MSN. The MCM-41 type of mesoporous channel structure of the nanospheres is visualized with the hexagonally packed light dots shown in B. The white lines traversing the entire particle in C are the pores, as viewed perpendicular to the pore axis. Also visible is the CdS coating the entire perimeter of the particle. The TEM micrographs (300 kV) were measured on an ultramicrotomed sample with a section thickness of 60-80 nm.
- Figure 2. Effect of disulfide-cleaving molecules on chemiluminescence signal. Chemiluminescence signal from ATP standards was collected as detailed in the experimental section. (A) ATP standards were injected into imaging solution containing 5 mM TCEP (X), 10 mM DTT (▲), 1 mM ME (◆), and imaging solution only (■). (B) ATP standards were injected into imaging solution containing DTT concentrations of 20 mM (■), 10 mM (▲), 5 mM (◆), 1 mM (□), and 0 mM (X).
- Figure 3. Release of encapsulated ATP from MCM-type mesoporous nanospheres. Chemiluminescence signal from ATP release was collected as detailed in the experimental section. (A) 1st frame – Optical image of CdS-capped MCM-type mesoporous nanosphere aggregate. Other frames - Frames of data

depicting release of encapsulated ATP from the nanospheres stimulated with 5 mM DTT at time zero. (B) Time course for release of ATP from (A).

Figure 4. Effect of uncapping agent concentration on release of encapsulated ATP from MCM-type mesoporous nanospheres. Chemiluminescence signal from ATP release was collected as detailed in the experimental section. The temporal maximum (A) and maximum magnitude (B) of release of encapsulated ATP with various concentrations of DTT.

Figure 5. Release of encapsulated ATP from dendrimer-capped MCM-41-type mesoporous nanospheres. Chemiluminescence signal from ATP release was collected as detailed in the experimental section. Plots depict release of encapsulated ATP from the nanospheres stimulated with 5 mM DTT at time = 2 min for generation 2.5 PAMAM dendrimer-capped particles (\square), generation 4.5 PAMAM dendrimer-capped particles (Δ) and CdS nanocrystal-capped particles.

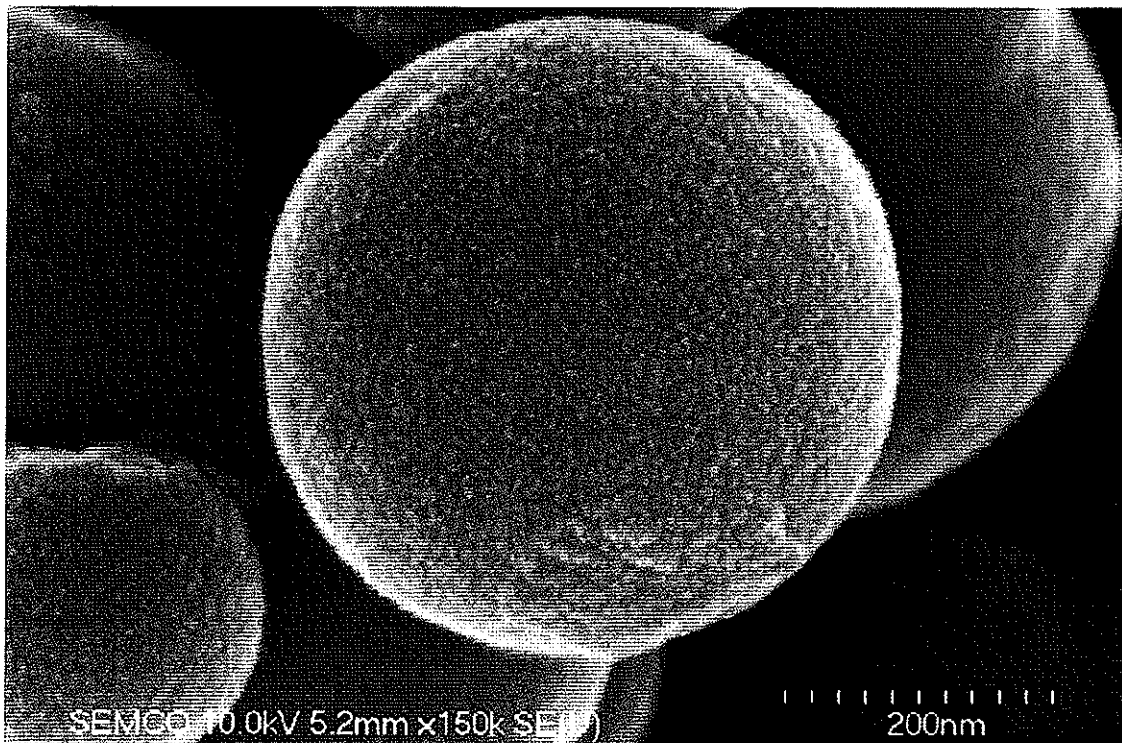


FIGURE 1A

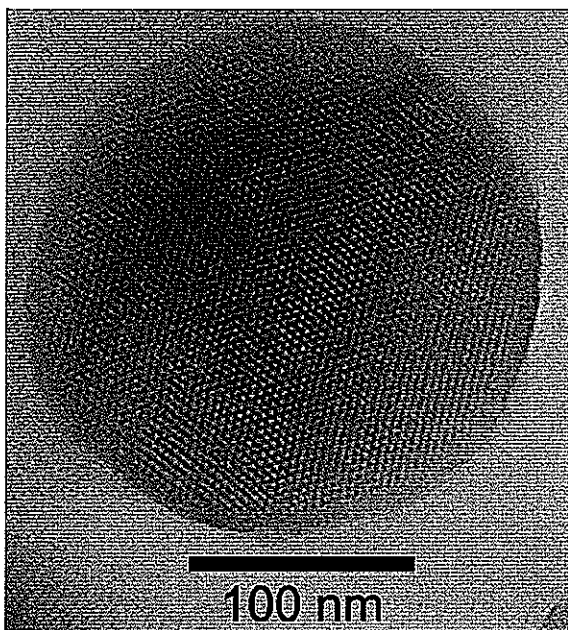


FIGURE 1B

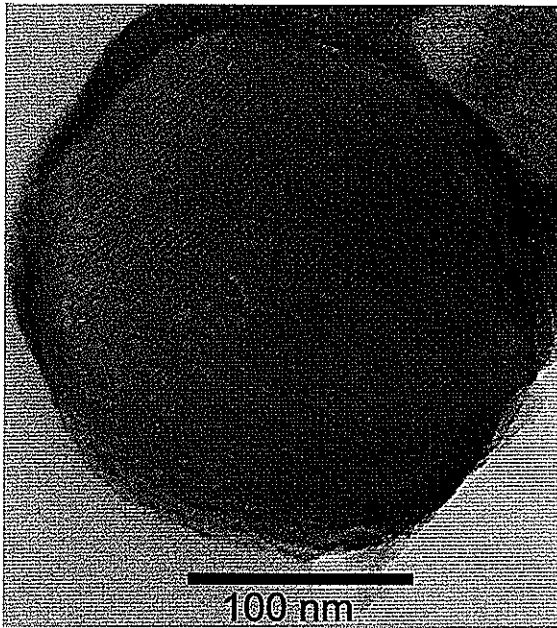


FIGURE 1C

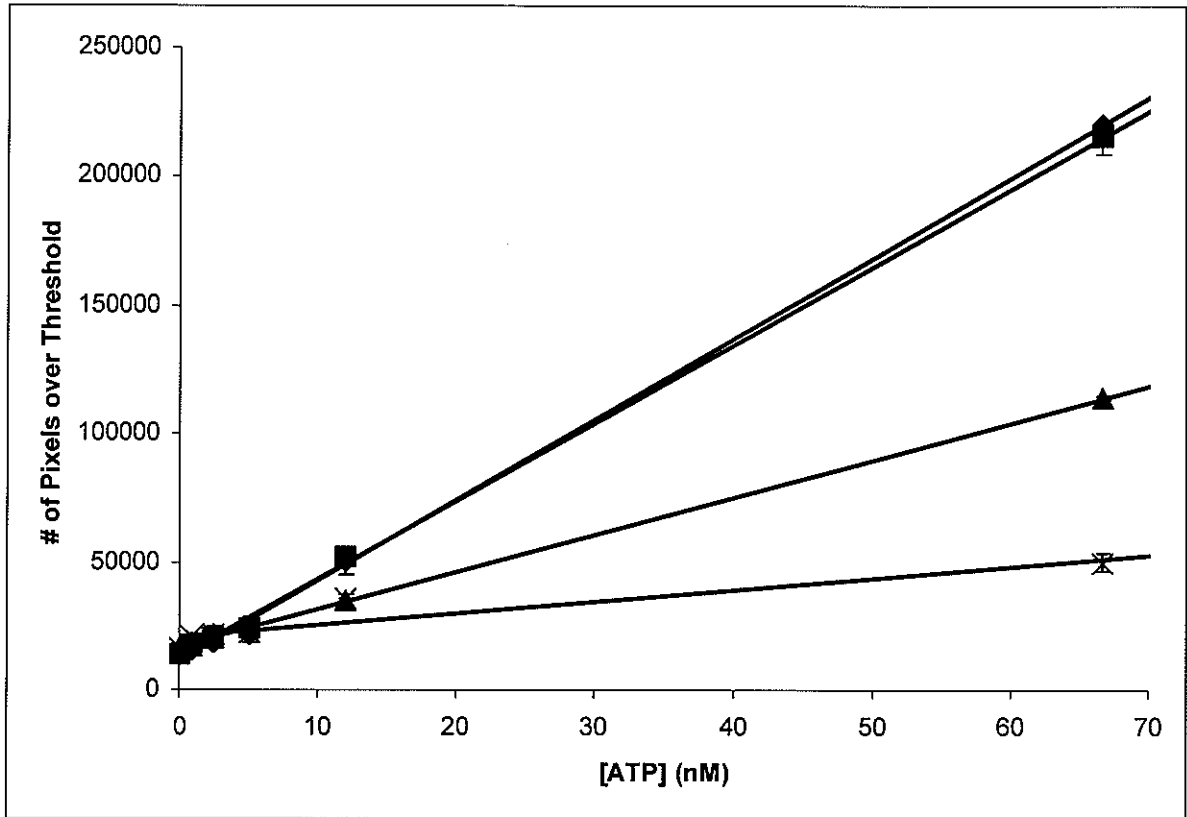


FIGURE 2A

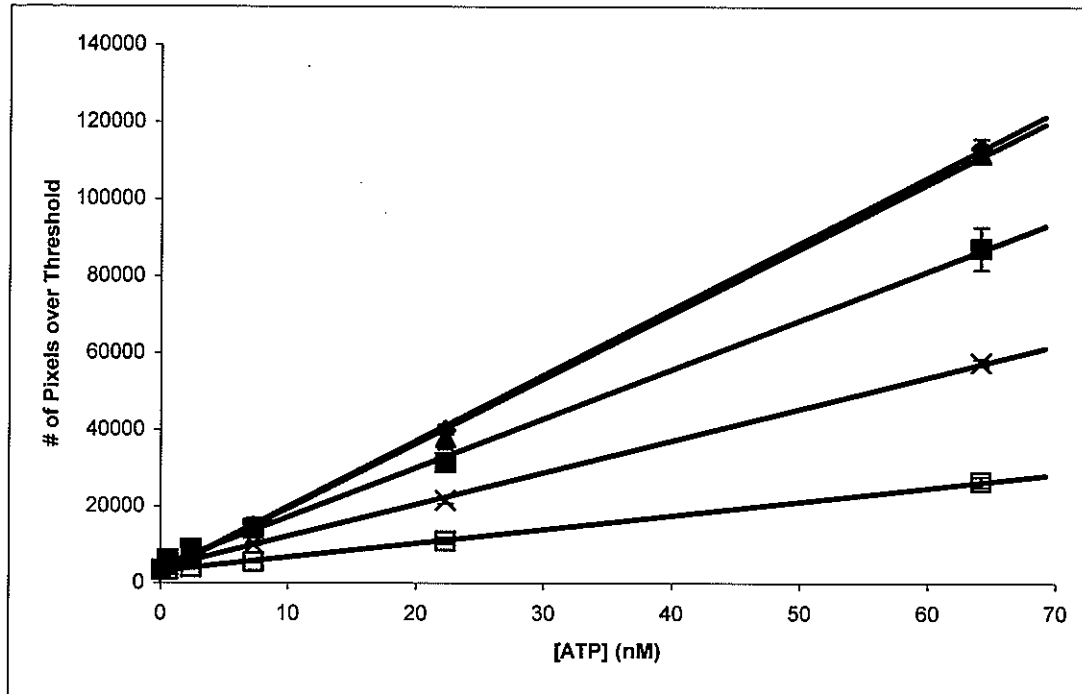


FIGURE 2B

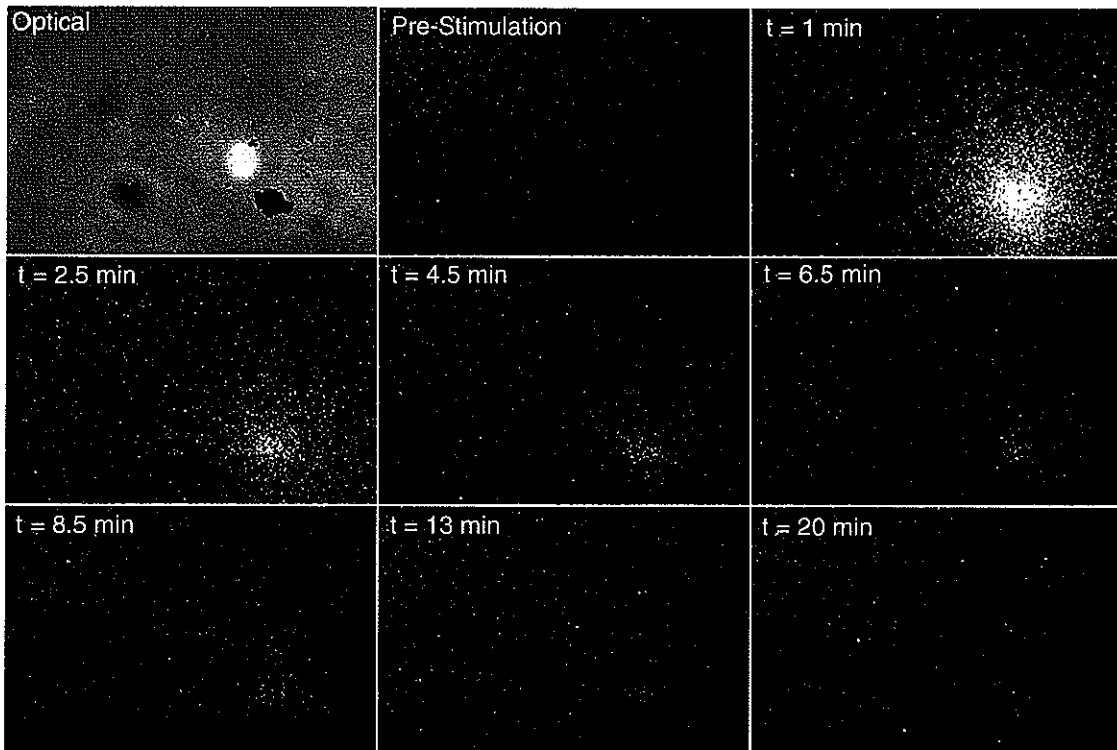
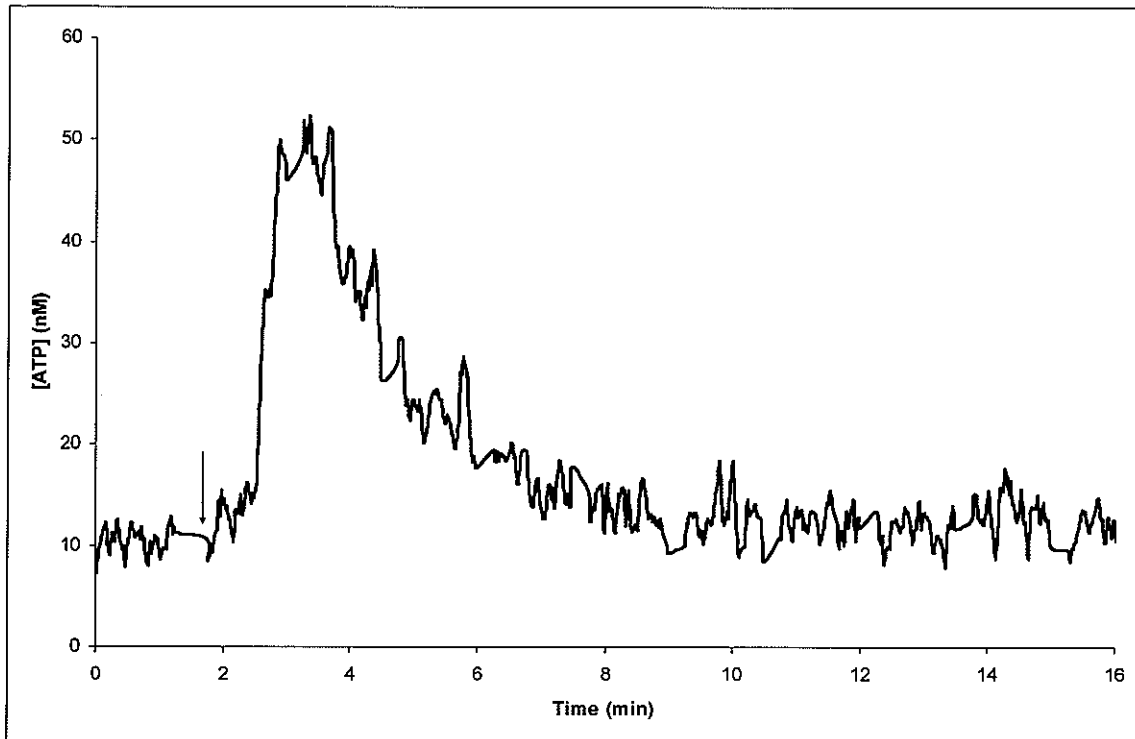


FIGURE 3A

**FIGURE 3B**

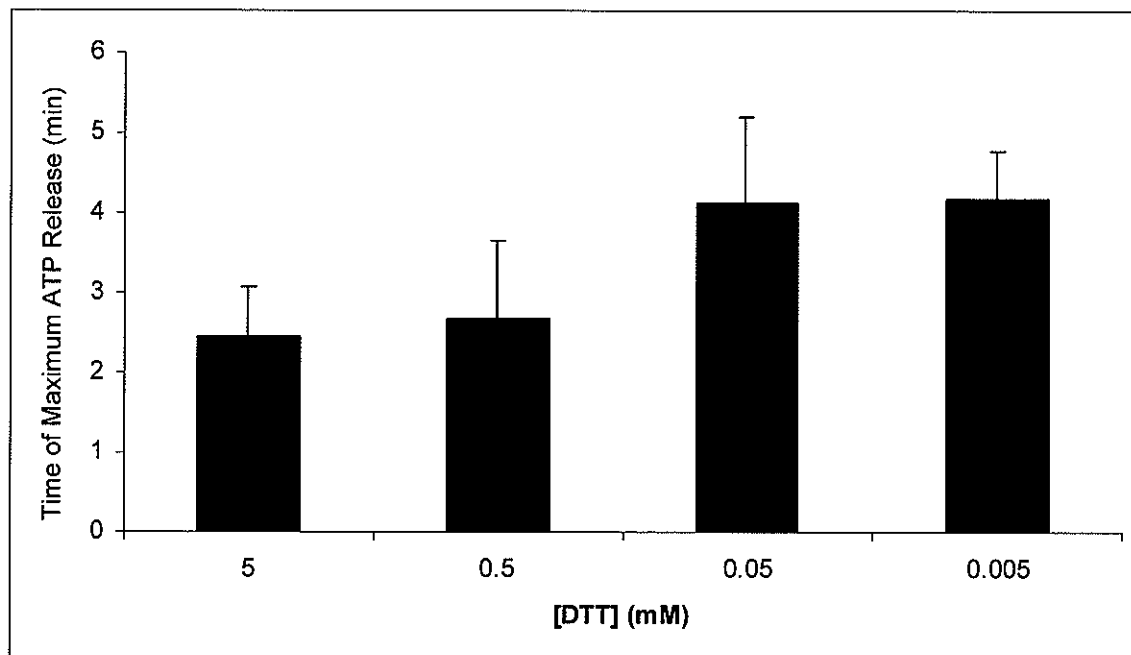


FIGURE 4A

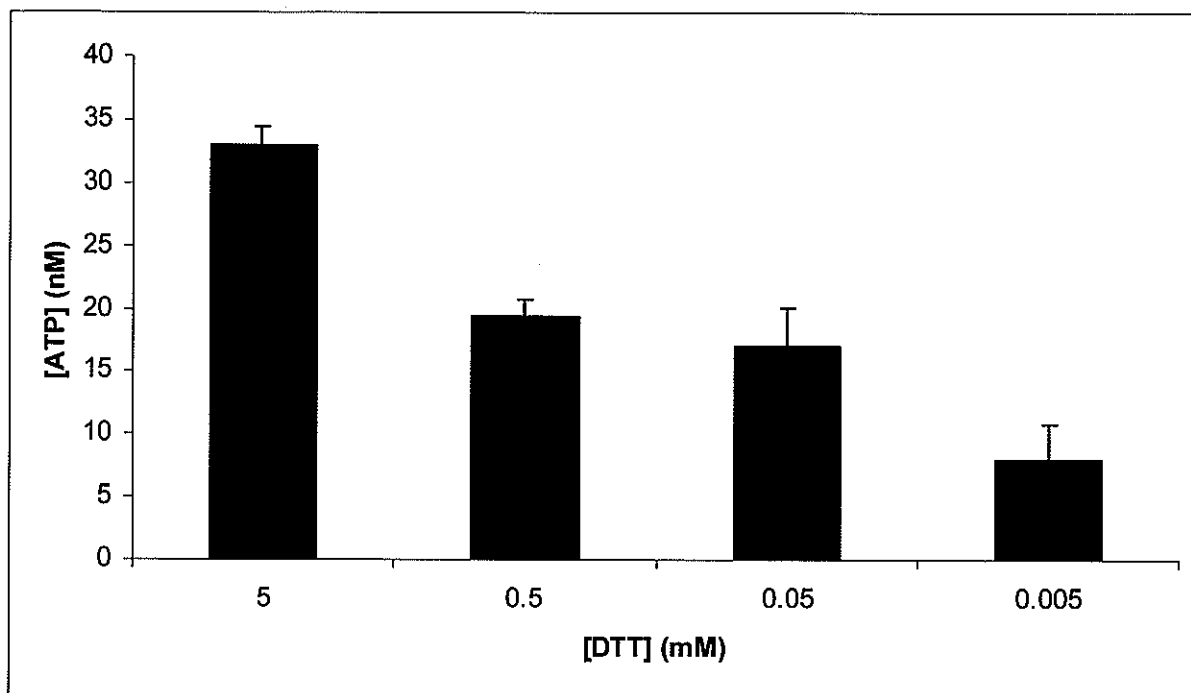


FIGURE 4B

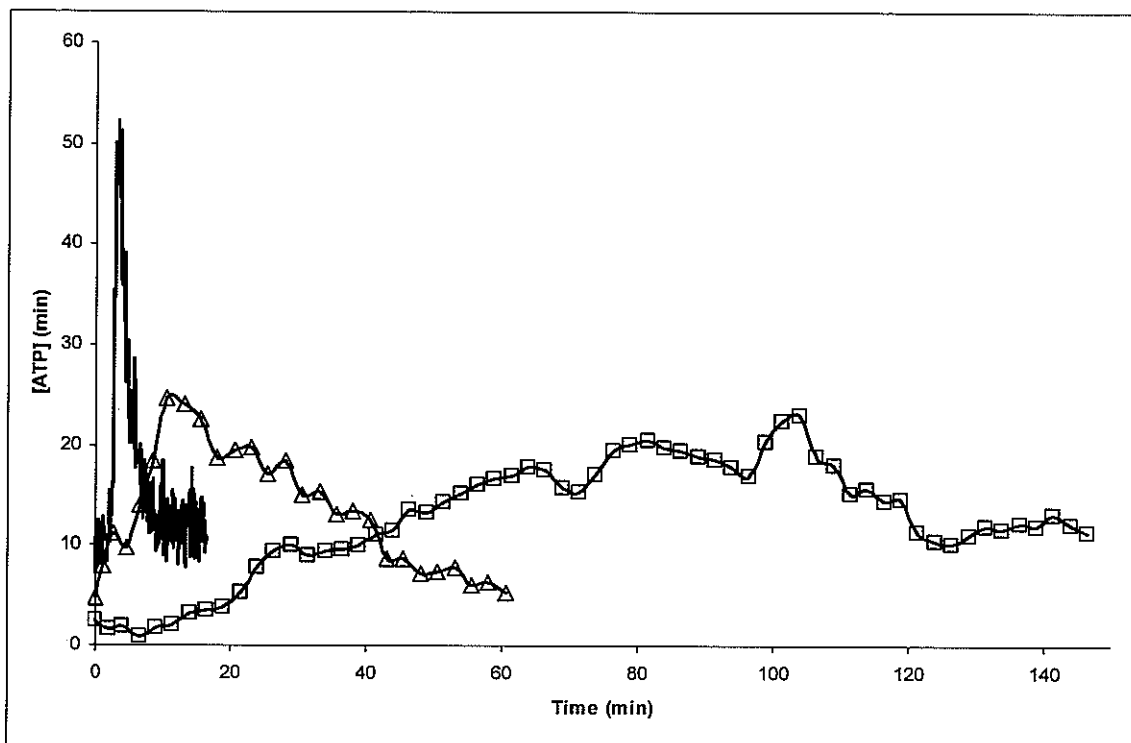


FIGURE 5

CHAPTER 5. GENERAL CONCLUSIONS

Innumerable potential research opportunities for analysis of ATP exist due to the widespread distribution of ATP in biological systems. Bioluminescence imaging of ATP exhibits numerous advantages for ATP analysis, including exceptional sensitivity, tremendous selectivity for ATP, excellent temporal resolution, and outstanding spatial capabilities. This technique is potentially applicable in examining countless biological and chemical systems, three of which were discussed within this dissertation.

First, the mechanism by which the compound 48/80 induces release of ATP from human umbilical vein endothelial cells (HUVECs) was elucidated. The various cellular pathways were probed with ATP and Ca^{2+} imaging to understand their involvement in release of ATP. The identified mechanism involved the activation of a G_q -type protein and phospholipase C and an increase in intracellular Ca^{2+} . The actual release of ATP appeared to proceed through the opening of a non-specific cytoplasmic channel.

The involvement of ATP in cellular communication in the nervous system was also investigated. The ganglia of the freshwater snail *Lymnaea stagnalis* continuously released ATP without neuronal stimulation. This release varied amongst the different ganglia and within an individual ganglion. Moreover, ATP levels were amplified upon stimulation of the ganglia with common neurotransmitters.

Finally, the release kinetics of model drug delivery systems were examined with bioluminescent ATP imaging. ATP was loaded into the pores of CdS-encapped mesoporous nanospheres to act as a model drug. It was released upon uncapping the nanospheres with disulfide bond-cleaving molecules. The drug release occurred within the

first few minutes after addition of the uncapping agents and declined significantly over the following 10-15 minutes. However, the magnitude of the initial burst of ATP was reduced and the release kinetics were delayed with lower concentrations of applied uncapping agent.

Future possible applications of this method include its continued application to drug delivery studies. This includes not only more advanced end-capped nanosphere systems, but also to responsive polymer systems and sol-gels. In biochemistry, the active role of ATP as a cell messenger is still under investigation in numerous cell and tissue types. ATP imaging can provide insight into the most ambiguous area of these analyses: the sources of extracellular ATP. This would be especially important in neuroscience. Our preliminary findings in the freshwater snail *Lymanea* suggest that ATP is actively being released in the central nervous system. This release could occur from synaptic vesicles containing only ATP or is ATP copackaged with other neurotransmitters. Alternatively, the release is not necessarily synaptic. Instead, it could be cytoplasmic as was observed in HUVECs. In that case, ATP release could be occurring from the neurons, the astrocytes surrounding them or the other cell types (including endothelial cells) within the CNS. As discussed briefly in chapter 2, ATP is copackaged with other cellular messengers in exocytotic vesicles. ATP imaging could thus be employed as a general technique to monitor exocytosis. This application would advance our understanding of synaptic transmission, muscular contraction, immune response, and innumerable other cellular processes. The most important role of ATP in biological systems is its involvement in cellular energy homeostasis. Thus, imaging intracellular ATP levels would yield information on the metabolic state of cells. This could yield information in numerous areas, including the effect of infection and the effect of natural

and artificial hormones on cellular homeostasis. ATP imaging is a potentially valuable technique for investigations in any of these areas.

ACKNOWLEDGEMENTS

First and foremost, I would like to thank my major professor, Dr. Edward S. Yeung, for all of his guidance over my career at Iowa State University. Dr. Yeung exemplifies everything a major professor and a scientist should be. His intelligence, his desire to succeed, his creativity, and his dedication to his work are but a few of his qualities that he passes on to the students in his group. He has mentored me in my development from a student to a researcher to, finally, a true scientist. Knowing and working for Dr. Yeung has been a pleasure on all levels.

I would also like to offer my personal thanks to my past and present committee members, Dr. Beitz, Dr. Houk, Dr. Lin, Dr. Ng, and Dr. Porter, for their precious time and advise.

I am also grateful to have worked with such wonderful collaborators: Dr. Leonid Moroz, Dr. Peter Lovell, Sami Jezzini, Thomas Ha, Michaela Bodnarova, Jim Netherton, and Andreas Høglund from the Whitney Lab at the University of Florida; Cheng-Yu Lai, Brian Trewyn, and Daniela Radu of Dr. Victor Lin's group; Dr. Bob Doyle of the Carver Lab; and numerous others.

I would also like to thank all of my group members, past and present: Dr. Wei Wei, Dr. Yan He, Dr. Yan He (II), Dr. Michael Shortreed, Dr. Xiaoyi Gong, Dr. Yonghua Zhang, Dr. Smiley Zhang, Dr. Gang Xue, Dr. Hanlin Li, Dr. Hui Su, Dr. Jinjian Zheng, Dr. Ho-Ming Pang, Dr. Young Park, Michael Christodoulou, Minjie Dai, Wenwan Zhong, Frank Li, Dragan Isailovic, Ji-Youn Li, and various others. Thank you all for the assistance in research and friendship that you all have given me.

I would also like to thank Dr. Yinfa Ma and Dr. Craig Aspinwall who, along with Dr. Yeung, have mentored throughout my career as a chemist. All that I have learned and all that I have accomplished I owe to them. They have guided me and encouraged me to become a better scientist and a better person. For their friendship and inspiration, I am forever indebted.

Finally, I would like to dedicate this dissertation to my family. My parents deserve more credit than words can describe. Throughout my life, they have supported and encouraged me in all of my endeavors. Furthermore, they have instilled in me all of the qualities that have allowed me to reach where I am today. Likewise, to my beautiful wife, I owe unending gratitude. She inspires and encourages me in my research and in life in general. Without her undying love and devotion, the future would never look so bright.

This work was performed at Ames Laboratory under Contract No. W-7405-Eng-82 with the U.S. Department of Energy. The United States government has assigned the DOE Report number IS-T ~~2604~~ to this thesis.